

Lawrence Berkeley National Laboratory

Recent Work

Title

PRECISION MEASUREMENT OF THE g_J -FACTOR OF HE4 IN THE 23S1, METASTABLE STATE

Permalink

<https://escholarship.org/uc/item/9ww0q70g>

Author

Aygun, Erol.

Publication Date

1973-08-01

PRECISION MEASUREMENT OF THE g_J -FACTOR
OF He^4 IN THE 2^3S_1 METASTABLE STATE

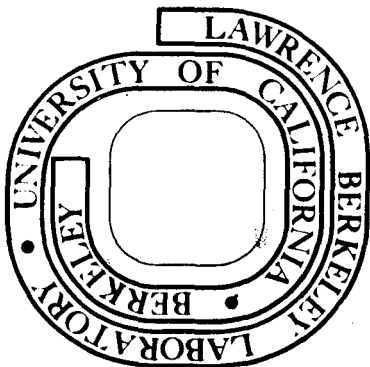
Erol Aygün
(Ph. D. thesis)

August 1973

Prepared for the U.S. Atomic Energy Commission
under Contract W-7405-ENG-48

For Reference

Not to be taken from this room



DISCLAIMER

This document was prepared as an account of work sponsored by the United States Government. While this document is believed to contain correct information, neither the United States Government nor any agency thereof, nor the Regents of the University of California, nor any of their employees, makes any warranty, express or implied, or assumes any legal responsibility for the accuracy, completeness, or usefulness of any information, apparatus, product, or process disclosed, or represents that its use would not infringe privately owned rights. Reference herein to any specific commercial product, process, or service by its trade name, trademark, manufacturer, or otherwise, does not necessarily constitute or imply its endorsement, recommendation, or favoring by the United States Government or any agency thereof, or the Regents of the University of California. The views and opinions of authors expressed herein do not necessarily state or reflect those of the United States Government or any agency thereof or the Regents of the University of California.

ABSTRACT

The objective of the measurements reported here was to deduce a more precise value for the ratio $g_J(\text{He}, ^3S_1)/g_J(\text{H}, ^2S_{1/2})$ and for the Landé g_J -factor of helium in the $1s2s, ^3S_1$ metastable state. This is done by combining the atomic-beam magnetic resonance measurements of $g_J(\text{He}, ^3S_1)/g_J(\text{Rb}^{85}, ^2S_{1/2})$ and of $g_J(\text{He}, ^3S_1)/g_J(\text{Cs}^{133}, ^2S_{1/2})$ with extremely precise, published results by others for $g_J(\text{Rb})/g_J(\text{H})$, $g_J(\text{Cs})/g_J(\text{Rb})$ and $g_J(\text{H})/g_S(e)$.

Obtaining over 600 resonances in total, we find the g_J ratios to be

$$\begin{aligned}g_J(\text{He}, ^3S_1)/g_J(\text{Rb}^{85}, ^2S_{1/2}) &= 1 - 46.83(30) \times 10^{-6} \\g_J(\text{He}, ^3S_1)/g_J(\text{Cs}^{133}, ^2S_{1/2}) &= 1 - 151.28(30) \times 10^{-6}.\end{aligned}$$

Combining these with the results given in refs. 1, 2, and 3 we find

$$g_J(\text{He}, ^3S_1)/g_J(\text{H}, ^2S_{1/2}) = 1 - 23.25(30) \times 10^{-6}$$

and combining this with the results given in refs. 4 and 5 we find

$$g_J(\text{He}, ^3S_1) = -2.002\ 237\ 35(60).$$

We give an outline of the theoretical calculation of the Landé g_J -factor for the 3S_1 metastable state of helium and a resume of the practical work in Ankara, with a description of the main characteristics of the atomic-beam machine, including the first Stern-Gerlach patterns obtained there.

ACKNOWLEDGEMENT

My Ph.D. studies included participation in the construction of the atomic beam machine in Ankara, Turkey, and the precision experiment performed in Berkeley, California, USA. So, I had strong interactions with two groups of people and from them I learned many things.

For the studies in Ankara I want to thank the personnel of the workshop in the Physics Department at METU. Assistant Technician Mr. Faik Pekyılmaz, Technician Mr. İsmail Doğru and Chief Technician Mr. Hasan T. Ataizi have shown excellent performance in manufacturing the machine components from the drawings, and proved their skills in doing fine and precision work.

I want to thank my coworkers in the beam group, Mr. Atilla Özmen, Mr. Ateş Tezer, Mr. Tuncay İncesu, and the former supervisor of the group, Professor Dr. Adnan Şaplakoglu for their participation in the construction of the machine and in the establishment of the atomic beams laboratory. Professor Şaplakoglu's combining of different designs should be especially mentioned here.

Among the Berkeley group I want to thank Mr. Pat Yarnold for his patient help during field-shimmings and many other services he performed, and Mr. Warren Harnden for drafting the figures for this thesis.

The cooperation between Berkeley and Ankara, as far as the Atomic Beams Project in Ankara is concerned, is gratefully acknowledged here.

In this sense, very special thanks go to the Engineering Coordinator Doug McDonald for his help with the engineering problems during the constructional phase and for his assistance in drafting the figures in this thesis.

I want to thank Dr. Charles E. Johnson for his many helpful suggestions concerning the experimental problems.

I especially want to thank Dr. Bernard D. Zak for his participation in the early days of the experiment and his constant concern in every phase of this study.

Most of all, I want to give my profound thanks to my research advisor, Professor Dr. Howard A. Shugart for his constant encouragement, his guidance, continuous contact, and devoting the laboratory exclusively to this experiment. His valuable comments are contained throughout the pages of this thesis. I also want to acknowledge the interest of Professor Shugart in the problems of the atomic beams laboratory at METU, Ankara. His cooperation has been invaluable in the development of our laboratory.

I appreciate the assistance of Mr. Donald Paxson who made many helpful editorial suggestions.

I want to express my thanks to the beam group secretary Ms. Peggy Gore, for her excellent typing of this thesis.

Finally I want to thank my wife and my son for their lovely companionship and patience during the lonely evenings while this experiment was being performed.

Financial support of the Ford Foundation, administered by METU, and of the Lawrence Berkeley Laboratory is gratefully acknowledged.

TABLE OF CONTENTS

	<u>Page</u>
ABSTRACT.....	iv
ACKNOWLEDGEMENT.....	v
INTRODUCTION.....	1
I. THEORY	
A. Outline of QED calculation of g_J -Factors.....	7
B. Theory Pertinent to the Experiment.....	19
C. Hyperfine Structure Interactions for Alkali Atoms.....	22
II. APPARATUS AND THE EXPERIMENTAL TECHNIQUE	
A. Apparatus in Ankara.....	31
B. The Feature of the Experiment.....	41
C. The Apparatus and the Experiment in Berkeley.....	50
1. The Sources.....	50
2. Lifetime of the Metastable State of Helium.....	55
3. The Detectors and the Data Collection System.....	57
4. C-Field: Locking and Shimming.....	61
5. Radio-Frequency System.....	71
6. Experimental Procedure.....	79
III. DATA, ANALYSIS, AND RESULTS	
1. Introduction.....	83

	<u>Page</u>
2. 5-Parameter Analysis.....	83
3. 4-Parameter Analysis.....	85
4. Results.....	94
5. Sources of Error and Attempts to Eliminate Them.....	94
a. Systematic Errors.....	94
b. Random Errors.....	97
6. Confirmation by Another Program.....	97
7. Discussion of the Results.....	99
 APPENDICES	
APPENDIX A1, Dr. H. Grotch's Letter.....	102
APPENDIX A2, Prof. J. Brossel's Letter.....	103
APPENDIX A3, Prof. H. Shugart's Letter.....	104
APPENDIX A4, Prof. Moos' Letter.....	105
 APPENDIX B, OUTLINE OF THE COMPUTER ROUTINE	
1. Least Squares Fitting to the Lorentzian Line-Shape.....	106
2. Calculation of Center Frequencies.....	108
3. Calculation of the Magnetic Field.....	109
4. Calculation of g_J , g_J -ratios and Statistics.....	110
 APPENDIX C, CONSTANTS USED IN THE COMPUTATION.....	 114
 REFERENCES.....	 116

INTRODUCTION

The experimental verification of the quantum electrodynamic (QED) theory of atoms in an external magnetic field is being carried out by measuring certain atomic constants. Precision measurements are needed to check the precise theoretical calculations which include higher order correction terms, such as relativistic bound state contributions of the order of α^2 ($\approx 50 \times 10^{-6}$), bound state radiative corrections of the order of α^3 ($\approx 0.1 \times 10^{-6}$) and nuclear finite mass corrections of the order of $\alpha^2 \frac{m}{M}$ ($\approx 0.01 \frac{M_p}{M} \times 10^{-6}$), where α is the fine structure constant given by $\alpha = e^2/\hbar c$, m is the electron mass, M_p is the proton mass, and M is the nuclear mass. Besides the desire to perform an important precision experiment, the discrepancy between the two experimental results published in 1958 and 1972 was the motivation of the study presented in this thesis. The former experiment has better agreement with theory than the latter, but the latter carries more precision than the former, and it is speculated that the disagreement might be due to the neglected terms in QED calculations. Two theoretical studies^{17,18} have also been motivated by the discrepancy.

Some of the atomic constants which are subjects for experimental measurements are the magnetic dipole moment μ , the Landé g_J -factors, the magnetic dipole-dipole interaction constant a , the electric quadrupole interaction constant b , the magnetic octupole interaction constant c ,

the hyperfine separation $\Delta\nu$, the hyperfine structure (HFS) anomaly ${}_1\Delta_2$, and the Lamb shift. Experimenters first started with the simplest atoms such as hydrogen⁶ and ionized helium⁷, and measured the Lamb shift and the spin magnetic moment⁸ of the electron to check the present QED theory.

The Dirac theory results in a value of one Bohr magneton for the spin magnetic moment of a free electron and -2 for the spin gyromagnetic ratio of it. Spectroscopic measurement⁹ of the Zeeman effect of one-electron atoms have shown that the precise value of the spin gyromagnetic ratio of a free electron is not equal to -2. The difference in gyromagnetic ratio is termed the anomaly. The electron anomaly is defined by

$$\frac{1}{2} (|g_S| - 2) = a, \quad (1)$$

where "a" is the anomaly which is one half of the deviation from the Dirac value. The reasons for these deviations from the Dirac values are the quantum electrodynamic effects such as the "virtual radiative process" (or "quantization of electromagnetic field"), "vacuum polarization" in various orders, and "photon-photon scattering" which are not included in the Dirac theory. The explanation of these interactions with S-matrix theory and Feynman diagrams yielded precise theoretical values for the anomalous magnetic moment of a free electron and also for the free electron anomaly. The anomaly can be calculated from quantum electrodynamics in the form of an expansion in powers of the fine structure constant α .

$$a(e) = A\alpha + B\alpha^2 + C\alpha^3 + \dots \quad (2)$$

The latest QED calculation of the free electron anomaly was done by Kinoshita and Cvitanovic¹⁰ in 1972. The latest measurement of the anomaly was done by Wesley and Rich¹¹ in 1971 and their result was corrected by Granger and Ford⁵ in 1972 after reanalyzing their data. So the best available values are:

$$\begin{array}{l} a(e) \\ \text{THEO.} \end{array} = 0.0011596529 (24)^{10} \quad (3)$$

$$\begin{array}{l} a(e) \\ \text{EXP.} \end{array} = 0.0011596567 (35)^5 \quad (3a)$$

When the electron is bound in an atomic system, the spin gyromagnetic ratio g_S differs from the free electron value due to the presence of the other atomic constituents. Also present are corrections to the orbital gyromagnetic ratio g_L , for which Dirac theory gives unity. In contrast to free electron corrections, these corrections are called bound state corrections.

The simplest two-electron system to check the quantum electrodynamic theory is positronium. The ground state HFS of positronium has been measured¹² to check the theory of mutually interacting electrons. The next simplest two-electron system to check the quantum electrodynamic theory of the two electron system is the helium atom.

The g_J ratio of $1s2s, ^3S_1$ metastable state of He to the g_J of H in its ground state was measured first by V. W. Hughes¹³ and his collaborators in 1953, using the atomic-beam magnetic-resonance technique. The ratio was found to be

$$\left[\frac{g_J(\text{He}, {}^3S_1)}{g_J(\text{H}, {}^2S_{\frac{1}{2}})} \right]_{\text{EXP.}} = 1 - (11 \pm 16) \times 10^{-6}. \quad (4)$$

At the same time, Perl and Hughes¹⁴ made a precision calculation of this ratio and the result came out as

$$\left[\frac{g_J(\text{He}, {}^3S_1)}{g_J(\text{H}, {}^2S_{\frac{1}{2}})} \right]_{\text{THEO.}} = 1 - (23.3 \pm 1.0) \times 10^{-6}. \quad (5)$$

Drake and Hughes¹⁵ measured the ratio in 1958 with an increase in accuracy of a factor of 20. The result was found to be

$$\left[\frac{g_J(\text{He}, {}^3S_1)}{g_J(\text{H}, {}^2S_{\frac{1}{2}})} \right]_{\text{EXP.}} = 1 - (23.3 \pm 0.8) \times 10^{-6}. \quad (6)$$

M. Leduc, F. Lalöe, and J. Brossel¹⁶ measured the same ratio to a higher precision with the optical pumping technique in 1972, and found

$$\left[\frac{g_J(\text{He}, {}^3S_1)}{g_J(\text{H}, {}^2S_{\frac{1}{2}})} \right]_{\text{EXP.}} = 1 - (21.6 \pm 0.5) \times 10^{-6}. \quad (7)$$

The discrepancy between the last result and all previous results drew our attention to the subject. As a result, two theoretical calculations are being published besides our experimental measurement in 1973. One of the new theoretical results is being published by H. Grotch and R. A. Hegstrom.¹⁷ Their results are

$$\left[\frac{g_J(\text{He}, ^3S_1)}{g_J(\text{H}, ^2S_{1/2})} \right]_{\text{THEO.}} = 1 - 23.212 \times 10^{-6}, \quad (8)$$

$$g_J(\text{He}, ^3S_1)_{\text{THEO.}} = -2.002\ 237\ 363 \quad (8a)$$

The other new theoretical study was done by V. W. Hughes and M. L. Lewis.¹⁸

Their result is

$$\left[\frac{g_J(\text{He}, ^3S_1)}{g_J(\text{H}, ^2S_{1/2})} \right]_{\text{THEO.}} = 1 - 23.29 \times 10^{-6}. \quad (9)$$

Finally, with the highest experimental accuracy so far, our results are

$$\left[\frac{g_J(\text{He}, ^3S_1)}{g_J(\text{H}, ^2S_{1/2})} \right]_{\text{EXP.}} = 1 - (23.25 \pm 0.30) \times 10^{-6}, \quad (10)$$

$$g_J(\text{He}, ^3S_1)_{\text{EXP.}} = -2.002\ 237\ 35(60). \quad (10a)$$

This thesis is composed mainly of three chapters. In the first chapter we outline the quantum electrodynamic theory of the Landé- g_J factor calculation, especially emphasizing the corrections applied to the Zeeman levels. Besides QED theory, we also outline the theory pertinent to the experiment, that is, quantum mechanical (QM) calculations of Zeeman splittings, mainly concentrating on Landé- g_J and Breit-Rabi formulas which are directly related to the experiment. The weak field coupling scheme, which is the case for the fields we have used, is employed. In the second chapter we present details of the apparatus. Meanwhile, we give the main characteristics (dimensions and the first Stern-Gerlach patterns) of the beam machine in Ankara, Turkey. We believe that the inclusion of the practical study in Ankara is worthwhile, since the author took part in

the construction of the beam machine and spent quite a long time in the atomic beams laboratory there. Then we emphasize the features of the experiment in Berkeley and the construction of the two NMR systems to lock and map the C-field, in order to increase our precision to the desired level. Field shimming is specifically explained as being one of the important features of the experiment. A new hairpin was designed and used to obtain a better π -transition field configuration in the rf region. The properties and problems of the new stripline hairpin are mentioned. In the third chapter, we give the analyses of data and results. The sources of error and the attempts to eliminate them are specifically emphasized. An outline of the computational technique is given in Appendix B. Finally the results we obtained are criticized in comparison with the previous and the simultaneous studies on the same quantity, both theoretical and experimental.

To reflect the scientific concern about the result of the experiment, we have included some of the correspondence regarding the problem in Appendix A.

I. THEORY

We present a precision experiment in this thesis; and we do not attempt to explain well-known principles of atomic theory. Instead, we intend to emphasize the bound state corrections which affect the result of our precision measurement. In the second part of this chapter we outline the elements of the theory pertinent to the experiment. We do not go into detail since we have previously completed a pre-doctorate study on $g_J(\text{Na}, ^2S_{\frac{1}{2}})$; the elementary principles of the theory of atomic resonance are surveyed in that publication.^{19,20}

The increase in the precision of experimental measurements of atomic constants has frequently stimulated theoretical calculations of equivalent precision. For the g_J -factor in helium the present precision is about third order in the fine structure constant α , ($\alpha^3 \approx 1$ part in 10^7). The terms of the order of α^3 are now on the border of today's atomic-beam magnetic-resonance studies.

A. The Outline of QED Calculations of g_J -Factors

Our problem is the Zeeman Effect on atomic systems in an external magnetic field. Quantum electrodynamic calculation assumes that the atomic system is in an electromagnetic field, and constructs the total Hamiltonian of the atom. One then separates the magnetic field-dependent terms to evaluate the Zeeman levels.

The total Hamiltonian of an atom in an external field can be written as

$$\mathcal{H} = \mathcal{H}_{\text{Atomic}} + \mathcal{H}_{\text{HFS}} + \mathcal{H}_{\text{EXT}} , \quad (11)$$

where the first term is the classical Schrodinger Hamiltonian plus all other interaction terms within an isolated atom - such as fine structure (FS) and Breit interaction terms. The second term stands for the hyperfine structure (HFS) interactions, and the last term is the interaction of the atomic electrons and the nucleus with the external field.

The QED calculations of atomic energy levels should start with a fully covariant field theory, but this is not the case yet because of the complexity of atomic structure. Present calculations are perturbative approximations - such as the Rayleigh,²¹ Ritz,²² and WKB²³ techniques.

The Dirac equation, which represents a one electron system, is not applicable to many electron systems, but it is the fundamental equation written for an atom in an external field. The Dirac Hamiltonian for a one-electron atom in a stationary state of total energy E is (Ref.24, page 47)

$$\mathcal{H} = \beta E_0 + \vec{\alpha}(\vec{c}\vec{p} + e\vec{A}) - e\phi , \quad (12)$$

where ϕ and \vec{A} are the scalar and vector potentials of the given external magnetic field, E_0 and \vec{p} are the rest mass energy and the momentum operator for the electron, $\vec{\alpha}$ is a vector operator which has the cartesian components $(\alpha_1, \alpha_2, \alpha_3)$ and $\beta = \alpha_4$. These are so-called Dirac operators that satisfy the following commutation relation

$$\alpha_i \alpha_k + \alpha_k \alpha_i = 2\delta_{ik} \quad (i, k = 1, 2, 3, 4) . \quad (13)$$

The Dirac operators α_i have the explicit form of 4x4 matrices as follows

$$\alpha_i = \begin{pmatrix} 0 & \sigma_i \\ \sigma_i & 0 \end{pmatrix}, \beta = \begin{pmatrix} I & 0 \\ 0 & -I \end{pmatrix}, \quad (14)$$

where σ_i are the well known Pauli matrices and I is the 2x2 identity matrix.

G. Breit²⁵ developed a Hamiltonian for two-electron systems. It was the first step forward in the construction of the many-electron Hamiltonian. Breit included the mutual interactions of electrons in the Dirac Hamiltonian. These mutual interactions include orbit-orbit, spin-spin and spin-other-orbit terms. For the helium atom the Breit interaction terms can be written as²⁴

$$B' = - \frac{e^2}{2m^2 c^2 r_{12}} \left[\vec{\alpha}_1 \cdot \vec{\alpha}_2 + \frac{(\vec{\alpha}_1 \cdot \vec{r}_{12})(\vec{\alpha}_2 \cdot \vec{r}_{12})}{r_{12}^2} \right], \quad (15)$$

where r_{12} is the distance between the two electrons, and other quantities have the same meaning as in the Dirac Hamiltonian.

Drake²⁶ expressed the Breit interaction terms in the Pauli approximation as follows:

$$B' = - \frac{e^2}{2m^2 c^2 r_{12}} \left(\vec{\Pi}_1 \cdot \vec{\Pi}_2 + \frac{\vec{r}_{12} \cdot (\vec{r}_{12} \cdot \vec{\Pi}_1) \vec{\Pi}_2}{r_{12}^2} \right) + \frac{\mu_0 e}{m c r_{12}^3} (\vec{r}_{12} \times \vec{\Pi}_2 \cdot \vec{\sigma}_1 + \vec{r}_{12} \times \vec{\Pi}_1 \cdot \vec{\sigma}_2) + \mu_0^2 \left[-(8/3) \Pi(\vec{\sigma}_1 \cdot \vec{\sigma}_2) \delta^{(3)}(\vec{r}_{12}) + \frac{1}{r_{12}^3} (\vec{\sigma}_1 \cdot \vec{\sigma}_2 - \frac{3(\vec{\sigma}_1 \cdot \vec{r}_{12})(\vec{\sigma}_2 \cdot \vec{r}_{12})}{r_{12}^2}) \right] \quad (16)$$

where the first term represents orbit-orbit, the second term spin-other-orbit, and the third term spin-spin interactions between the two electrons of helium. Here the Π_i ($i=1,2$) are the canonical momenta given in Eq.(17) when an external magnetic field is present.

$$\begin{aligned} \vec{\Pi}_i &= \vec{p}_i - e\vec{A}_i/c \\ \vec{A}_i &= (1/2)\vec{H} \times \vec{r}_i \end{aligned} \quad (17)$$

Since the Breit Hamiltonian is the sum of the Dirac Hamiltonian and the Breit interactions terms, it will have the following form for an n-electron atom in an external magnetic field:

$$\begin{aligned} \mathcal{H}_{\text{Breit}} = & \sum_i^n \left[\vec{\alpha}_i \cdot (\vec{p}_i + \frac{e}{c} \vec{A}_i) + \beta_i mc^2 - \frac{Ze^2}{r_i} \right] + e^2 \sum_{i < k}^n \frac{1}{r_{ik}} \\ & - \frac{e^2}{2} \sum_{i < k}^n \left[\frac{\vec{\alpha}_i \cdot \vec{\alpha}_k}{r_{ik}} + \frac{(\vec{\alpha}_i \cdot \vec{r}_{ik})(\vec{\alpha}_k \cdot \vec{r}_{ik})}{r_{ik}^3} \right] . \end{aligned} \quad (18)$$

Here the characters and the terms have the same meaning as in previous equations and the second term stands for inter-electrons Coulomb interaction.

The g_J -calculation of quantum electrodynamic theory starts with the Breit Hamiltonian given in Eq.(18). The Breit Hamiltonian is reduced to Schrödinger-Pauli form and developed in terms. In addition to the Dirac and Breit terms, the following higher order correction terms are included in the Hamiltonian of an atom:

1) Relativistic bound state corrections which account for the change of kinetic energy and the mass of the bound electron with velocity. This correction term is represented by Eq.(22) in the Zeeman Hamiltonian of helium. It is of magnitude $\alpha^2 = 50$ ppm (parts per million).

2) The bound-state radiative correction (also called the anomalous electron moment correction) is of magnitude $\alpha^3 = 0.1$ ppm. In the Breit Hamiltonian, the interaction of the electron with its own (virtual) radiation field is not included. This so-called radiative **correction** includes the quantization of the electromagnetic radiation field. This interaction is explained using S-matrix theory and Feynman diagrams. A method of calculation is to convert the Feynman diagrams, which represent

the interaction, to integral equations. Kinoshita and Cvitanovic¹⁰ completed this calculation in detail for the free electron in 1972. Grotch and Hegstrom¹⁷, and Hughes and Lewis¹⁸ included anomalous moment corrections, by using Kinoshita¹⁰ expression for g_S free electron, in their calculation.

3) The finite nuclear mass correction is the effect of the motion of the nucleus on the orbital angular momentum of the electrons. In the original Breit Hamiltonian the nucleus is supposed to be immobile - equivalent to having an infinite mass. At first sight this may be a good approximation for heavy nuclei, but for helium it is not satisfactory. In general, considering the nucleus in motion around the center-of-mass, the orbital angular momentum of the "system" is shared by the nucleus and the electron. Then the orbital gyromagnetic ratio g_L of the electron (non-S electron) is reduced from 1 to $(1 - m/M)$ by the motion of the nucleus. For S electrons, as in our case, $L = 0$. That means there is no tangential velocity component. Thinking of the radial motion of the nucleus and the S-electron with respect to the center-of-mass, one still needs a correction due to the motion of the nucleus. Grotch and Hegstrom¹⁷ have calculated this correction for the 3S_1 state of helium. They replace the electronic mass m by $m_{red.} = mM/(m+M) \approx m(1 - m/M)$. Their estimated value of this correction to the g_J of helium in the 3S_1 metastable state is $g_S(e) \times 10^{-9}$, which is neglected in their calculation. Here $g_S(e)$ is the intrinsic gyromagnetic ratio of the free electron. The magnitude of the nuclear finite mass correction is formally $\alpha^2 m/M \approx (.01)M_p/M$ ppm.

The diamagnetic correction is due to the reduction of the external magnetic field at the site of a given electron because of the external magnetic field-induced moments in the other electrons. The order of

magnitude of this term is α^2 . The diamagnetic correction term is derivable from Breit interaction terms; for S electrons it is the spin dependent part¹⁴ of the Breit interaction contribution.

The development of the Breit Hamiltonian was done by W. Perl²⁷, A. Abragam and J. H. Van Vleck²⁸, and Kambe and Van Vleck²⁹. Finite nuclear mass and anomalous moment corrections have been discussed in detail more recently by R. A. Hegstrom³⁰ for the many-electron atom.

Grotch and Hegstrom¹⁷, and Hughes and Lewis¹⁸ have considered the above corrections to the Breit Hamiltonian in calculating the g_J -helium in the $1s2s, {}^3S_1$ metastable state this year.

The Landé g-factor is defined by¹⁷

$$g_J = \frac{\langle 2^3S_1 | \mathcal{H} | 2^3S_1 \rangle}{\mu_0 H}, \quad (19)$$

where \mathcal{H} is the sum of all magnetic field-dependent terms in the reduced Breit Hamiltonian, H is the external magnetic field and μ_0 is the Bohr magneton. For the experimentalist the value of the matrix element is simply $h\Delta\nu$ or $h\nu$. Therefore, the equation for the experimentalist becomes

$$g_J = \frac{\nu}{(\mu_0/h)H}, \quad (19a)$$

where ν is the transition frequency and h is Planck's constant.

Theoreticians calculate the value of the matrix element by including all possible magnetic field-dependent interaction terms up to the accuracy desired. Hughes and Lewis¹⁸ give the magnetic field-dependent parts of the reduced Breit Hamiltonian as shown in equations (21) through (26). The sum of those terms constitutes the Zeeman Hamiltonian which can be written as

$$\mathcal{H}_Z = \sum_{n=0}^6 \mathcal{H}_n \quad (20)$$

$$\mathcal{H}_0 = \mu_0 \vec{H} \cdot (\vec{L} + g_S \vec{S}) \quad (21)$$

$$\mathcal{H}_1 = -\alpha^2 \mu_0 \vec{H} \cdot \sum_i (\ell_i + 2s_i) T_i \quad (22)$$

$$\mathcal{H}_2 = \frac{1}{2} Z \alpha^2 \mu_0 \vec{H} \cdot \sum_i [\vec{s}_i \times \nabla_i (r_i^{-1})] \times \vec{r}_i \quad (23)$$

$$\mathcal{H}_3 + \mathcal{H}_4 = -\alpha^2 \mu_0 \vec{H} \cdot \sum_{i < j} [(\vec{s}_i + 2\vec{s}_j) \times \vec{v}_i (r_{ij}^{-1})] \times \vec{r}_i \quad (24)$$

$$\begin{aligned} \mathcal{H}_5 = & -\alpha^2 \mu_0 \vec{H} \cdot \sum_{i < j} [r_{ij}^{-1} (\vec{r}_i \times \vec{p}_j) \\ & + r_{ij}^{-3} (\vec{r}_i \times \vec{r}_j) (\vec{r}_{ij} \cdot \vec{p}_j)] \end{aligned} \quad (25)$$

$$\mathcal{H}_6 = -\frac{m}{M} \mu_0 \vec{H} \cdot [\vec{L} + \sum_{i \neq j} (\vec{r}_i \times \vec{p}_j)] \quad (26)$$

In the Hamiltonian, \mathcal{H}_0 is the lowest order Zeeman effect. This term represents the non-relativistic interaction between the magnetic dipole moment of the 3S_1 state and the external magnetic field. This is the largest term in magnitude. Neglecting all other terms but \mathcal{H}_0 , one obtains $g_J = g_S = -2$ from Eq.(19) because $\vec{L} = \sum_i \vec{\ell}_i = 0$, $\vec{S} = \sum_i \vec{s}_i$ and $g_S = -2$ for the electron in this approximation. The coupling scheme just mentioned is known as the LS coupling or Russell-Saunders coupling which is appropriate for the magnetic field range we used.

\mathcal{H}_1 represents the correction due to the relativistic increase in mass with velocity. This term is obtained from \mathcal{H}_0 after replacing m by its relativistic value given by

$$m = m_0 [1 - (v/c)^2]^{-1/2} \quad (27)$$

In Eq.(22) T_i is the kinetic energy of the i^{th} electron given by

$$T_i = mc^2 - m_0c^2 \quad . \quad (28)$$

\mathcal{H}_2^{C} is the spin-orbit interaction term in the presence of an external field. This term is obtained replacing p_i by Π_i (See Eq.(17)) in the spin-orbit interaction term. Relativistic and spin-orbit corrections are known as the Breit Margenau correction.^{31,32} $\mathcal{H}_3^{\text{C}} + \mathcal{H}_4^{\text{C}}$ are the spin-other-orbit interaction terms between the two electrons in the external magnetic field.

\mathcal{H}_5 is the orbit-orbit interaction term between the electrons in the external magnetic field.

\mathcal{H}_6 is the correction for the motion of the nucleus.

Hughes and Lewis¹⁸ include the self-radiative corrections by using Kinoshita and Cvitanovic¹⁰ expression for $g_S(e)$, which is calculated up to the order of α^3 .

Thus far we have considered the corrections to the Hamiltonian operator of the 3S_1 state of helium. In order to calculate the matrix element of the Zeeman Hamiltonian given in Eq.(21) through Eq.(26) for the 3S_1 state, we need the wavefunction of the state in question. Because of the complexity of atomic structure, it is difficult to find a wavefunction which represents the state exactly. Consequently, one has to make some approximations for the wavefunction, which is therefore yet another source of error. For the ground state of helium, the Ritz variational technique^{33,34} with a hydrogen-like trial wavefunction gives satisfactory results, but we are dealing with an excited (metastable) state of helium. Even for the excited states of helium some analytic and numerical approximate wavefunctions have been used.

The wavefunction of the 3S_1 state of He is the product of an orbital function $U(r_1, r_2)$ and a triplet spin function $\chi^{35,36,37}$ so that

$$\psi({}^3S_1) = U(r_1, r_2)\chi, \quad (29)$$

where χ is given by

$$\begin{aligned} \chi_+ &= |++\rangle \\ \chi_- &= |--\rangle \\ \chi_0 &= \frac{1}{\sqrt{2}} (|+-\rangle + |-+\rangle) \end{aligned} \quad (30)$$

for the triplet state and

$$\chi_{\text{Singlet}} = \frac{1}{\sqrt{2}} (|+-\rangle - |-+\rangle) \quad (31)$$

for the singlet state.

For the orbital part of the wavefunction of helium in the 3S_1 state, Eckart³⁸ used hydrogen-like trial functions with the two nuclear charge parameters for the inner and outer electrons. Later on, Hylleraas and Undheim³⁹ used a similar trial function with six parameters in it. Those six Hylleraas parameters are the polar coordinates of the two electrons. For S-electrons, U does not depend on the Euler angles, so it is a function only of r_1 , r_2 and r_{12} (Ref.24, page 147). Various forms of the test functions are given in references 17, 18, and 40.

Grotch and Hegstrom¹⁷ used a 715-term numerical wavefunction obtained by Pekeris⁴⁰ for the 3S_1 state of helium. They followed the first order perturbation technique and evaluated the matrix elements in the "stretched" state ($J = m_J = 1$). Hughes and Lewis¹⁸ used a Hylleraas³⁹ -like numerical

wavefunction in their perturbative calculations. The properties of those wavefunctions are given in the mentioned references and the references contained therein.

The matrix elements of the Zeeman Hamiltonian in Eqs.(21) through (26) for the 3S_1 state wavefunction of helium are¹⁸

$$\langle ^3S_1 | \mathcal{H}_0 | ^3S_1 \rangle = \mu_0 H g_S \quad (32)$$

$$\langle ^3S_1 | \mathcal{H}_1 | ^3S_1 \rangle = -\alpha^2 \mu_0 H \langle T \rangle \quad (33)$$

$$\langle ^3S_1 | \mathcal{H}_2 | ^3S_1 \rangle = \frac{1}{3} \alpha^2 \mu_0 H \left[\left\langle \frac{1}{r_1} \right\rangle + \left\langle \frac{1}{r_2} \right\rangle \right] \quad (34)$$

$$\langle ^3S_1 | \mathcal{H}_3 + \mathcal{H}_4 | ^3S_1 \rangle = -\frac{1}{2} \alpha^2 \mu_0 H \left\langle \frac{1}{r_{12}} \right\rangle \quad (35)$$

$$\langle ^3S_1 | \mathcal{H}_5 | ^3S_1 \rangle = 0 \quad (36)$$

$$\langle ^3S_1 | \mathcal{H}_6 | ^3S_1 \rangle = 0 \quad (37)$$

where

$$T = T_1 + T_2 \quad (38)$$

is the total kinetic energy of both electrons. The electronic configuration of metastable helium is $1s2s$; both electrons are in S states, so they do not have orbital magnetic moments; consequently the orbit-orbit interaction Hamiltonian \mathcal{H}_Q has a zero matrix element for the S states.

\mathcal{H}_Q is the correction due to the motion of the nucleus. In general, this motion effects the orbital g_L of the electron (non-S electrons), but

for the S states, since there is not any tangential velocity component, one expects the expectation value (matrix element) of \mathcal{H}'_6 to be zero. As we have mentioned earlier, one can replace electronic mass by the reduced mass to include a center-of-mass correction. Even this effect is negligible,¹⁷ so the Zeeman levels of the 3S_1 state of helium consist of a spin-external field term \mathcal{H}'_6 (the most dominant term), a relativistic mass correction \mathcal{H}'_1 , a spin-orbit \mathcal{H}'_2 , and a spin-other-orbit $\mathcal{H}'_3 + \mathcal{H}'_4$, which are coupling terms to the precision required to explain the current experiment.

Once the matrix elements of the Zeeman Hamiltonian are found, using some other theorems such as the "virial theorem" all the terms in the expression are expressed in terms of $g_S(\mathbf{e})$, the fine structure constant α , the energy of the 3S_1 state E , and $\langle \frac{1}{r_{12}} \rangle$. In both papers^{17,18} the Pekeris³⁷ values are used for $\langle \frac{1}{r_{12}} \rangle$ and E . Again, both papers use the recent theoretical expression for $g_S(\mathbf{e})$ ¹⁰ to include the self-radiative effect. The value of the fine structure constant α is taken to be⁴¹

$$\alpha^{-1} = 137.03602 \quad (39)$$

Then the computations continue to find $g_J(\text{He}, ^3S_1)/g_J(\text{H}, ^2S_{1/2})$ ratio.

For the hydrogen Landé-factor, Hughes and Lewis¹⁸ and Grotch and Hegstrom¹⁷ used the theoretical expression obtained by the latter group of authors in a previous study.⁴² They expressed their final ratios in terms of their deviations from unity as

$$\frac{g_J(\text{He}, ^3S_1)}{g_J(\text{H}, ^2S_{1/2})} = 1 - a, \quad (40)$$

where "a" is the deviation.

The two theoretical results obtained by Grotch and Hegstrom, Hughes and Lewis, together with those of our experimental measurement, are given in the Introduction to this thesis.

The value of $g_J(\text{He}, {}^3S_1)$ has been calculated theoretically to the order of α^3 (≈ 0.1 ppm), but the present most precise experimental measurement (our result) falls slightly behind the theory in precision to identify or test the α^3 terms. We believe that the second phase of this experiment which will employ the Ramsey double loop technique, should be capable of testing the contributions of the α^3 terms in the g_J of helium.

B. Theory Pertinent to the Experiment

Now we discuss the elements of the theory that are pertinent to the g_J measurement. In this section we concentrate on the interactions of the atoms with the static external magnetic field. The perturbation produced by a weak magnetic field on the energy level of an atom can be written as

$$\mathcal{H} = -\vec{\mu}_J \cdot \vec{H} = -\mu_0 (g_L \vec{L} + g_S \vec{S}) \cdot \vec{H}, \quad (41)$$

where $g_L = -1$ and $g_S = -2$ for the electron in the zero order approximation, μ_0 is the Bohr magneton, and H is the external static magnetic field. For the Zeeman region, LS coupling (Russell-Saunders coupling) is valid; L , S , J , and m are the good quantum numbers. $|LSJm\rangle$ is a simultaneous eigenfunction of J^2 , L^2 , S^2 , and J_z . Making use of Wigner-Eckart⁴⁴ theorem and vector operator algebra,⁴⁵ it can be shown that the energy shift due to the perturbation \mathcal{H} is

$$\Delta E = \langle \mathcal{H} \rangle = \langle LSJm | \mathcal{H} | LSJm \rangle = -g_J \mu_0 H m, \quad (42)$$

where

$$g_J = g_L \frac{J(J+1)+L(L+1)-S(S+1)}{2J(J+1)} + g_S \frac{J(J+1)+S(S+1)-L(L+1)}{2J(J+1)}. \quad (43)$$

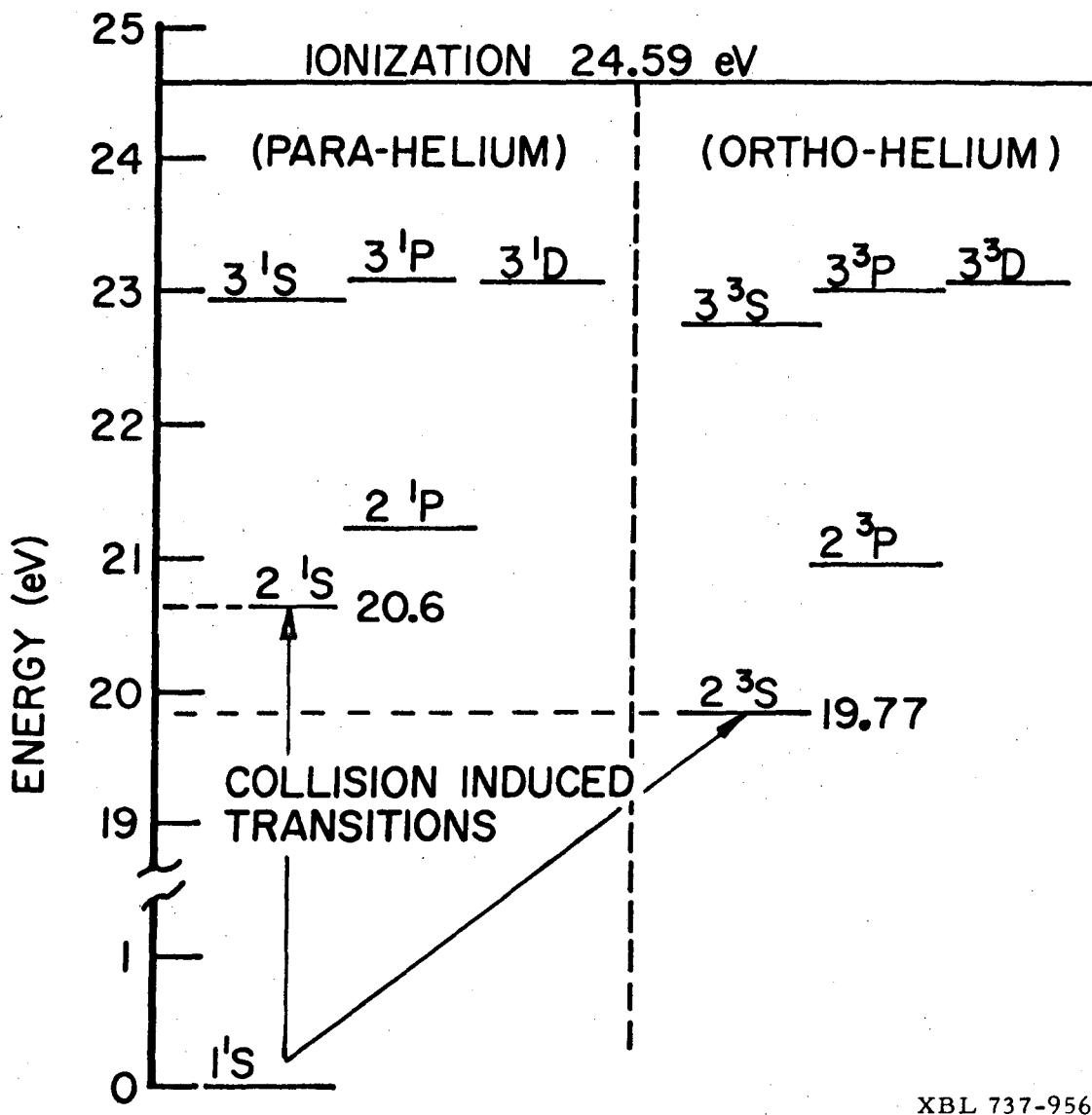
Equation (43) is the Landé- g_J formula. Whenever we study the coupling of atomic angular momenta, we meet with some factors in the derivations that

are functions of the free-electron gyromagnetic ratios g_S , and g_L , and the angular momentum quantum numbers specifying the state in question. These are the so called Landé g -factors, which are dimensionless quantities. Landé g -factors are a measure of the splitting due to the angular momenta coupling.

Since we are dealing with the 2^3S_1 state of He (see Fig.1), the first term in Eq.(43) vanishes and the coefficient of the second term is unity; therefore, one gets $g_J = g_S$. For S-states, there is no orbital contribution to the Landé g_J -factor.

A discussion of the Landé g_J formula seems worthwhile at this point. For non-S states, the value of g_J obtained from the Landé g_J formula is different from the value observed. Thinking of the function $g_J = f(g_L, g_S, L, S, J)$, one can say that the precision of g_J is dependent on the precision in determining the free-electron values g_S , g_L , and the specification of the state. By specification of the state, we mean how well L , S , and J represent the actual state. In addition to bound state radiative corrections on g_S , the impurity in the assumed state (the presence of the other same- J -states, that is, configuration mixing) is the main cause of a change in the Landé g_J value. This means that the coupling scheme that is assumed in the derivation of the Landé g_J formula is an approximation. Of course one should not forget the other correction terms (such as Breit-Margenau corrections) which are mentioned in the preceding section, and are not considered in the derivation of the Landé g_J formula.

Let us see how we can make use of the approximate equation (42) in the experimental measurement. We can write:



XBL 737-956

Fig.1. The energy level scheme of neutral helium, showing the $n=1,2,3$ states only, and the production of metastable states by electron impact.

$$\Delta E = h\nu \quad . \quad (44)$$

Then, assuming g_J as the unknown in Eq.(42), one obtains Eq.(19a), so the precision of g_J depends on the precision with which the transition frequency, ν , and the magnetic field, H , are measured. Consequently, a precision measurement of ν and H will yield a precise experimental value for the Landé g_J -factors.

We obtain the magnetic field H from the transitions between the hyperfine levels of alkali atoms by using the Breit-Rabi formula. Therefore, we next outline briefly the hyperfine interactions of alkali atoms.

C. Hyperfine Structure (HFS) Interactions For Alkali Atoms

For nuclei which have spin $I \neq 0$, the fine structure levels will be further split, due to the interactions between the nuclear spin and electronic magnetic moments. Since we have a coupling between nuclear and atomic angular momenta, we have to define a total angular momentum vector $\vec{F} = \vec{I} + \vec{J}$ for the atom. The number of HFS levels is either $(2I + 1)$, if $I < J$, or $(2J + 1)$, if $J < I$, and the total angular momentum quantum number F obeys the triangular inequality: $|I - J| < F < |I + J|$.

The interactions of a nucleus with its atomic electrons are electrostatic and magnetic in character. The electrostatic interaction can be written as (Ref.43, page 52)

$$\mathcal{H}_E = \int_{\tau_e} \int_{\tau_n} \frac{\rho_e \rho_n}{r_{en}} d\tau_e d\tau_n \quad , \quad (45)$$

where ρ_e and ρ_n are the charge densities at the distances \vec{r}_e and \vec{r}_n from the center of the nucleus, respectively, and $r_{en} = |\vec{r}_e - \vec{r}_n|$. Here $d\tau_e$ and $d\tau_n$ are the volume elements at the end points of the position vectors \vec{r}_e and \vec{r}_n , respectively. In the case of stationary currents, Ramsey³ gives an analogous formula for the magnetic interactions as follows:

$$\mathcal{H}_M = \int_{\tau_e} \int_{\tau_n} \frac{(\nabla_e \cdot \vec{M}_e)(\nabla_n \cdot \vec{M}_n)}{r_{en}} d\tau_e d\tau_n, \quad (46)$$

where \vec{M}_e and \vec{M}_n are the vector potentials from which the current densities j_e and j_n can be derived. So, the nucleus-atomic electrons interaction Hamiltonian has two components, namely electrostatic and magnetic terms.

$$\mathcal{H}_{HFS} = \mathcal{H}_E + \mathcal{H}_M \quad (47)$$

These interactions can be written in the tensor notation as

$$\mathcal{H}_{Ek} = Q^{(k)} \cdot F^{(k)} \quad (48)$$

$$\mathcal{H}_{Mk} = T_e^{(k)} \cdot T_n^{(k)} \quad (48a)$$

where $Q^{(k)}$ and $F^{(k)}$ are electric charge and field tensors of rank k , respectively. $T_e^{(k)}$ and $T_n^{(k)}$ are the spherical tensors of rank k for the magnetic interactions. The Racah tensor formalism^{4,5} is applicable to the HFS interaction formulations, but since we are presenting an experimental study, we will not go into the details of this formalism. All of these interactions are outline by Ramsey

in Chapter III of Ref. 43. On the other hand, the matrix elements we require can also be obtained with usual vector operator technique.

Reviews of the theory pertinent to atomic beam magnetic resonance experiments are given in refs. 46, 47, and 48.

The parities of $Q^{(k)}$ and $F^{(k)}$ are $(-1)^k$ and the parities of $T_e^{(k)}$ and $T_n^{(k)}$ are $(-1)^{k+1}$. The multipolarity is $N_E=2^k$ for nuclear electrostatic interactions, and $N_M=2^{k+1}$ for nuclear magnetic interactions. One can conclude from the parities that, under the conditions of the theorems stated on page 58 (for electrostatic interactions) and on page 70 (for magnetic interactions) in Ref. 43, all odd-k electric multipole and all even-k magnetic multipole moments vanish. Another theoretical restriction on the highest multipolarity of nuclear electric multipole moments for a particular nucleus with spin I is that it is impossible to observe a nuclear electrical multipole moment of order 2^k for $k > 2I$. For example: for Rb^{85} , $I=5/2$, $2I=5$; $(N_E)_{\max} = 2^5 = 32$. In light of theorems mentioned previously, it is possible to explain the nonexistence of magnetic monopoles and nonexistence of any nuclear moment of even-even nuclei. Table I shows the multipolarity of electric and magnetic interactions.

Table I. Electric and magnetic nuclear multipolarities of various ranks.

Multipolarity	k=0	k=1	k=2	k=3	k=4
$N_E=2^k$	1 (monopole)	2 (dipole)	4 (quadrupole)	8 (octupole)	16 (16-pole)
$N_M=2^{k+1}$	2 (dipole)	4 (quadrupole)	8 (octupole)	16 (16-pole)	32 (32-pole)

For an atom in an external magnetic field, the HFS and Zeeman interaction Hamiltonian can be written as follows:

$$\begin{aligned} \mathcal{H} = & a \vec{I} \cdot \vec{J} + \frac{b}{2I(2I-1)J(2J-1)} \{ 3(\vec{I} \cdot \vec{J})^2 + \frac{3}{2} (I \cdot J) \\ & - I(I+1)J(J+1) \} + \frac{c}{I(I-1)(2I-1)J(J-1)(2J-1)} \quad (49) \\ & \{ 10(\vec{I} \cdot \vec{J})^3 + 20(\vec{I} \cdot \vec{J})^2 + 2(\vec{I} \cdot \vec{J}) [-3I(I+1)J(J+1) + I(I+1) + J(J+1) \\ & + 3] - 4I(I+1)J(J+1) \} + \frac{(-g_J + g_I)\mu_0 H J_z}{h} - \frac{g_I \mu_0 H F_z}{h} \end{aligned}$$

where the first term represents magnetic dipole-dipole interaction, the second term stands for the electric quadrupole interaction, the third term represents the magnetic octupole interaction and the last two terms represent the interactions of magnetic dipoles with the external magnetic field H. Here a, b, and c are the coefficients of the respective interactions.

The matrix element of the magnetic dipole-dipole interaction term in the F_m representation is (Ref. 43, page 73):

$$ha \langle F_m | \vec{I} \cdot \vec{J} | F_m \rangle = \frac{ha}{2} [F(F+1) - I(I+1) - J(J+1)] \quad (50)$$

This term splits the J levels by an amount ΔW , which is known as the hyperfine separation. For alkali atoms $J = 1/2$, $I =$ arbitrary, and the hyperfine separation is

$$\Delta W = \frac{ha}{2} (2I + 1) \quad (51)$$

Quadrupole moments are due to the deviations of electrical charge distributions from spherical symmetry. All nuclei with spin equal to or

greater than unity possess an electrical quadrupole moment, and nuclei with spin 3/2 or greater may possess a magnetic octupole moment (Ref. 43, page 52). The effects of quadrupole and octupole terms are negligible for alkali atoms. The last two external field-dependent terms in Eq.(49) can be written as

$$\mathcal{H}'_{EXT} = - \vec{\mu}_J \cdot \vec{H} - \vec{\mu}_I \cdot \vec{H} , \quad (52)$$

where μ_J and μ_I are the electronic and nuclear magnetic dipole moments defined by

$$\vec{\mu}_J = \mu_0 g_J \vec{J} \quad (53)$$

$$\vec{\mu}_I = \mu_0 g_I \vec{I} . \quad (53a)$$

For the alkali atoms the HFS-Zeeman Hamiltonian can be written as (Ref. 43, page 84)

$$\mathcal{H}' = ha \vec{I} \cdot \vec{J} - d I_z - c J_z \quad (54)$$

where $d = (\mu_I/I)H$ and $c = (\mu_J/J)H$. Equation(54) is the perturbation Hamiltonian we have used for the calibration isotopes, Rb^{85} and Cs^{133} .

In Eq.(54) the dot product can be expressed as

$$\vec{I} \cdot \vec{J} = 1/2(I_+ J_- + I_- J_+) + I_z J_z , \quad (55)$$

where (+) subscripts are raising and (-) subscripts are the lowering operators. Substituting Eq.(55) into Eq.(54), and using the F_m representation, one can obtain the HFS energy levels which are the eigenvalues of the perturbation operator \mathcal{H}' . For $J = 1/2$, and I arbitrary, a coupled representation can be written in terms of the uncoupled representation as follows:

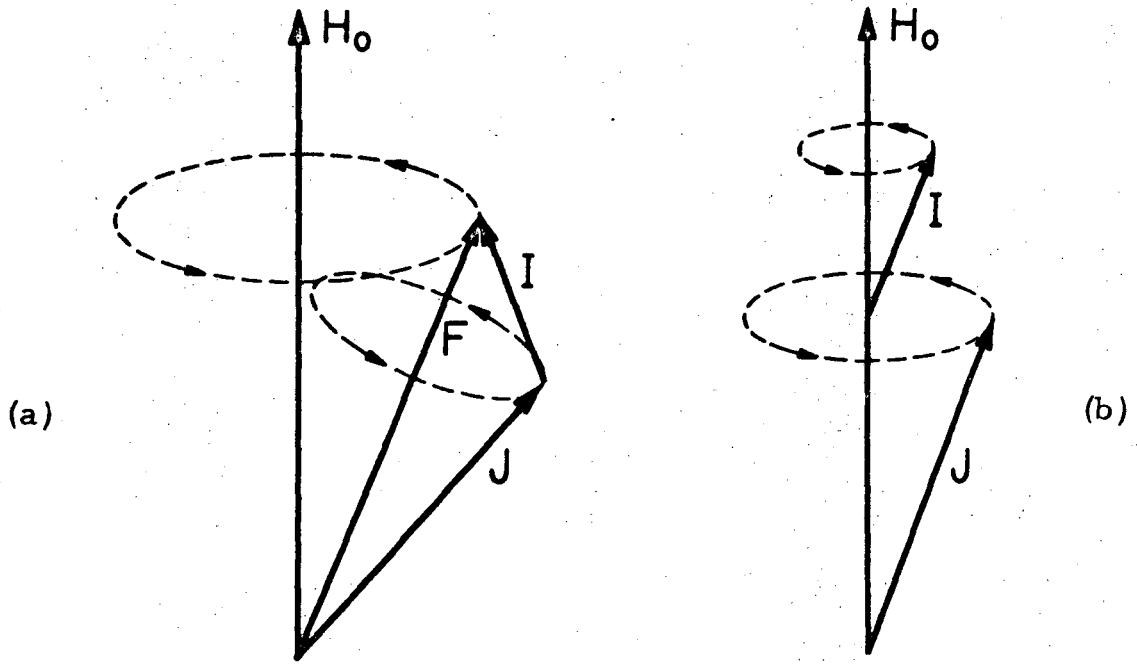
$$|F_m\rangle = a|m - 1/2, 1/2\rangle + b|m + 1/2, -1/2\rangle , \quad (56)$$

where a and b are the Clebsch-Gordan coefficients to be determined. Finding the matrix elements of the perturbation operator \mathcal{H}' in the uncoupled representation, and solving the secular determinant for hyperfine structure energy levels W, Breit and Rabi⁴³ expressed the hyperfine levels as

$$W(F,m) = -\frac{\Delta W}{2(2I+1)} - \frac{\mu_I}{I} mH \pm \frac{\Delta W}{2} \left(1 + \frac{4m}{2I+1} x + x^2\right)^{1/2} \quad (57)$$

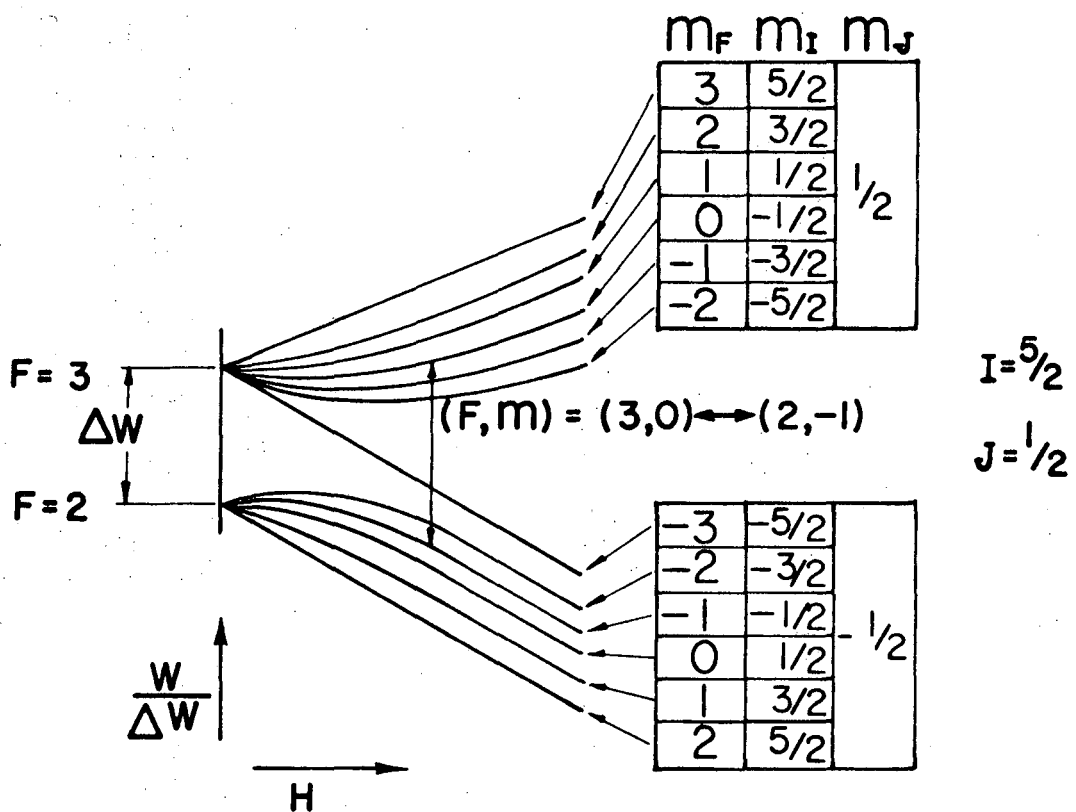
where $x = (g_J - g_I)\mu_0 H / \Delta W$. For the roots of quadratic equation the (+) sign is taken when $F = I+J$ and the (-) sign when $F = I-J$. Equation (57) is the well known Breit-Rabi formula for $J = 1/2$ atoms.

Figure 2 shows the coupling schemes appropriate to the limits of a weak and a strong external magnetic field. Figures 3 and 4 are the schematic plots of the Breit-Rabi formula for Rb^{85} and Cs^{133} , respectively. The transitions we induced are indicated on those figures.



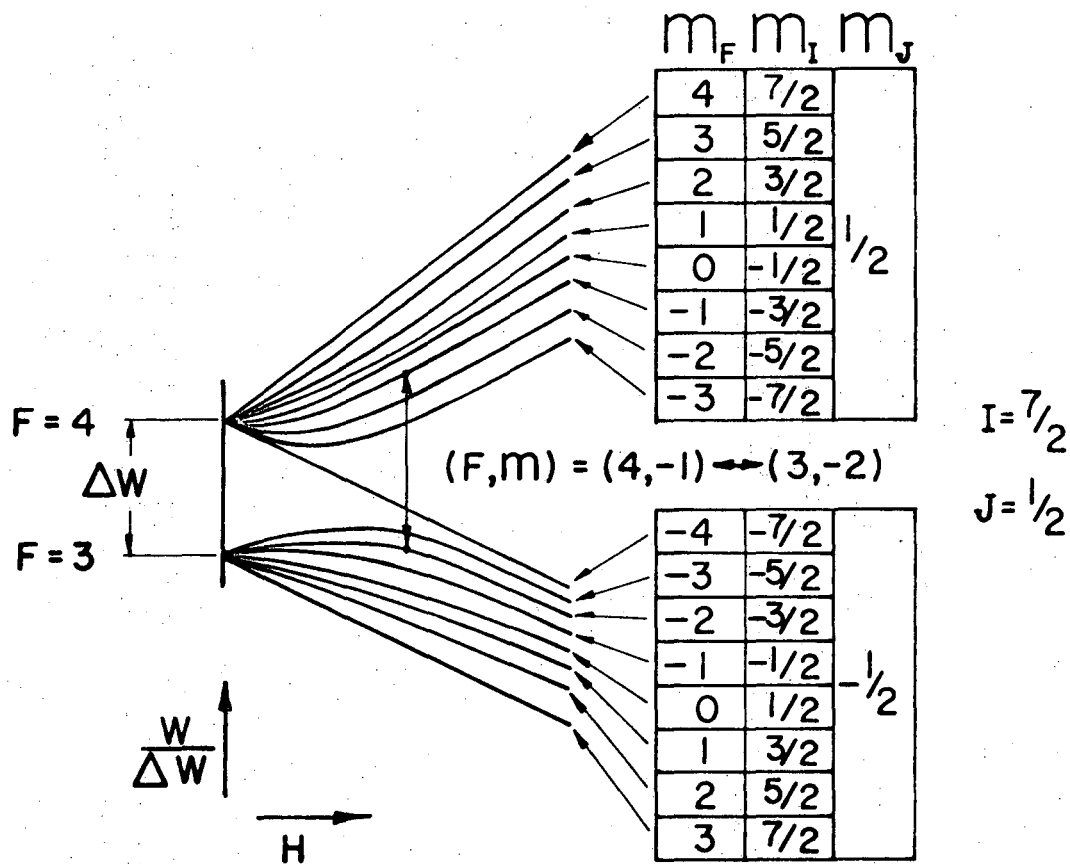
MU-13365

Fig.2. The coupling schemes of (a) weak field, and (b) strong field regions.



XBL 735-556

Fig.3. The Breit-Rabi diagram for Rb^{85} . The transition shown is the one we induced.



XBL 735-552

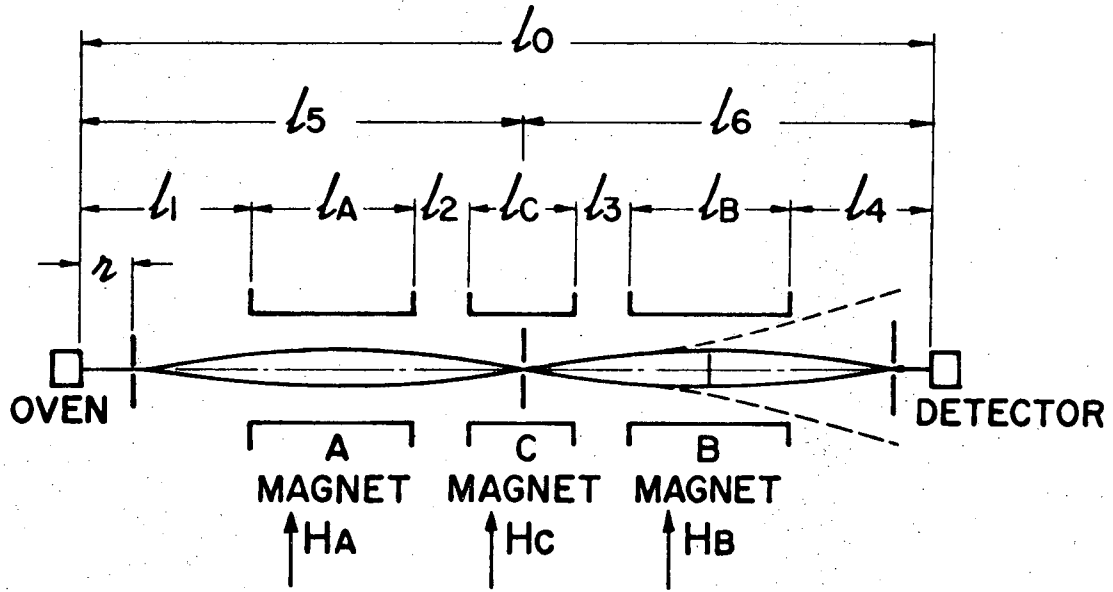
Fig.4. The Breit-Rabi diagram for Cs^{133} . The transition shown is the one we induced.

II. APPARATUS AND EXPERIMENTAL TECHNIQUE

A. Apparatus in Ankara

The apparatus we have used at Berkeley is a flop-in type atomic and molecular beam machine. The basic principles of atomic-beam magnetic-resonance measurements are given by N. F. Ramsey^{4,3} and by P. Kusch and V. W. Hughes^{4,7}. Reminded of the pre-doctorate study^{19,20} completed, we do not need to go back to Stern's, Rabi's, and Purcell's contributions.

As we have mentioned earlier, we took part in the construction of the atomic beam machine in Ankara, Turkey, so we choose to include a resume of that study here. The atomic beam machine at the Middle East Technical University (METU), Ankara, Turkey is very similar to the one at the University of California, Berkeley. The designs, except for the C-magnet were borrowed from Berkeley beam group. Only the C-magnet design is adapted from the beam laboratory at Brookhaven National Laboratory, New York. The Brookhaven C-magnet design provides easier handling of radio frequency loops in the C-region, and probably more homogeneity, because it is 2 inches longer than the Berkeley magnet. Figure 5 shows a flop-in type atomic beam machine with the dimensions of the one at METU. The machine consists mainly of an oven chamber, A, C, and B magnet cans, and a detector chamber. Each chamber is evacuated by mechanical and



$\uparrow \nabla H_A$ $\nabla H_c = 0$ $\uparrow \nabla H_B$

DIMENSIONS (CM.)

- $l_1 = 35.4$ $l_3 = 25.0$
- $l_A = 49.6$ $l_4 = 20.7$
- $l_2 = 21.1$ $l_5 = 123.9$
- $l_B = 49.6$ $l_6 = 113.1$
- $l_C = 35.6$ $l_0 = 237.0$
- $r = 10.7$

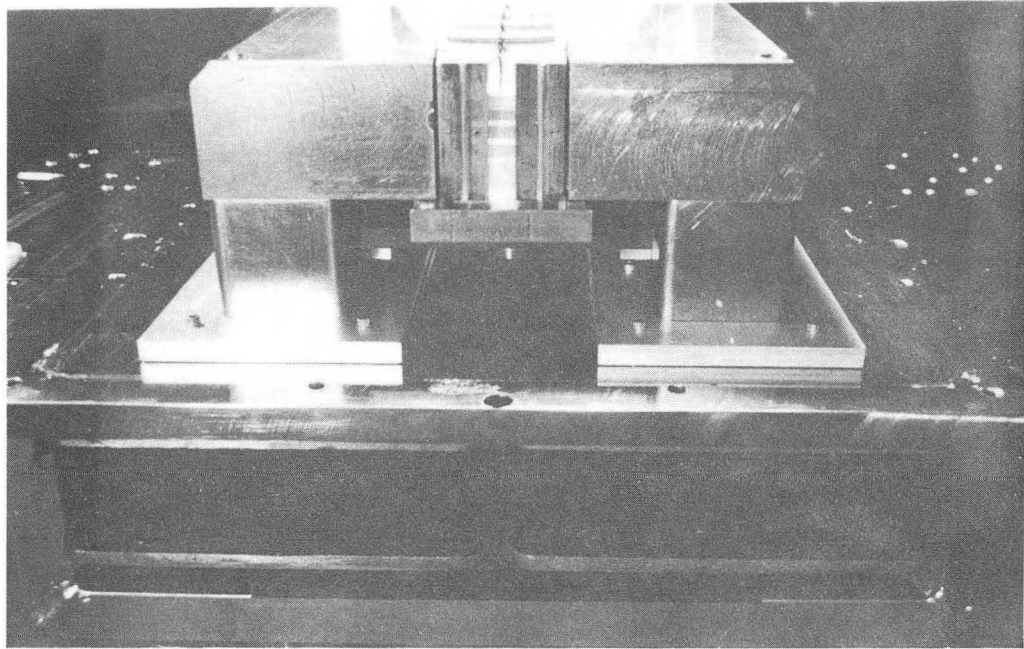
XBL 737-933

Fig.5. Flop-in type atomic-beam machine with the dimensions of the one at MITU-Ankara, Turkey.

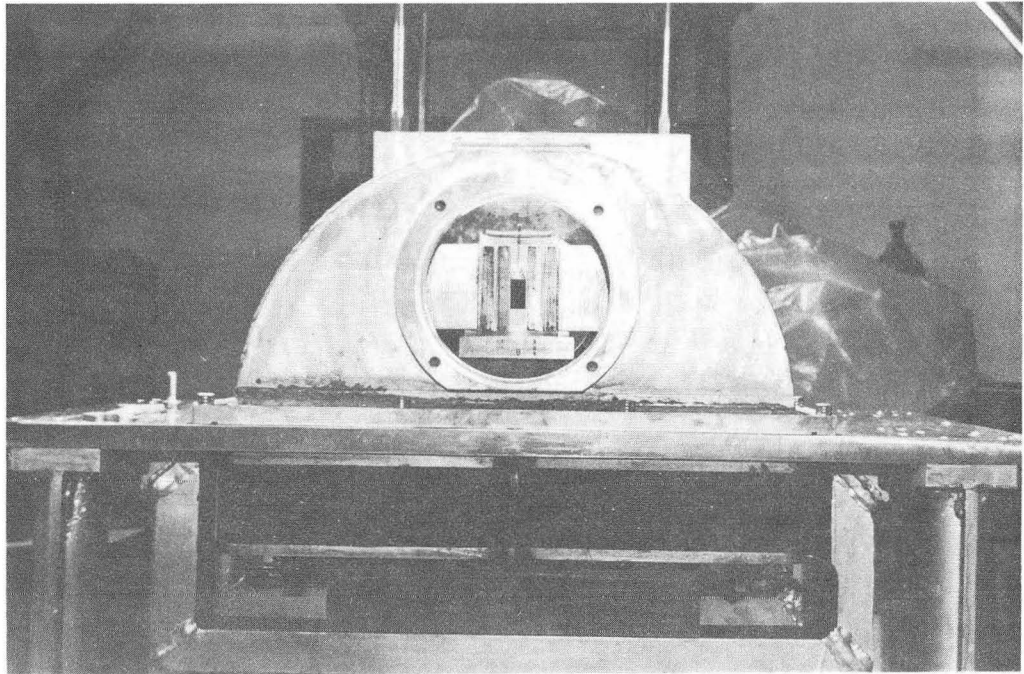
diffusion pumps. The vacuum throughout the machine is in the 10^{-6} torr range. When water and electricity shut-off problems are overcome, the vacuum will become better than 10^{-6} torr because of the long-term running of the vacuum pumps.

The C-magnet in Ankara consists of four rectangular Armco magnetic iron plates with the dimensions 1/2 inch, 3 inch and 14 inch. The C-magnet power supply (50V, 30A by Kepco) is being operated in the external sensing mode, which gives a more stable current to the coils. The A, B, and C magnet coils in Ankara have very low resistance; about $1/4\Omega$ per coil. This is achieved by using Cu-bands for the windings, manufactured especially for this purpose. Low resistance reduces the temperature dependent variations of the fields in the C, A, and B magnets, which are already water cooled. Figure 6 shows the C-magnet sandwich assembly in Ankara, Turkey. The magnet pole plates are separated from each other by quartz spacers whose thicknesses are measured optically. The thicknesses of the quartz are matched accurately to 1 part in 10^4 . The plates are also isolated from the main yoke members by quartz separators. Potentially, this enables one to study the Stark effect also. The gap for the rf loops between the plates is 0.55 inch wide. The saturation field is about 20k gauss in the C-magnet. We also have Kepco (50V, 30A) DC power supplies for the A and B magnets. At 30 amps. the gradient of the field between the Stern-Gerlach pole pieces in the A and B magnets is about 10kgauss/cm. Figure 7 shows the cross-section of the Stern-Gerlach pole pieces in the A and B magnets in Berkeley and Ankara.

In Ankara we have an electron bombardment-heated oven as the source of alkali atoms and a tungsten hot wire as the detector. The ionization potentials of all alkali atoms are less than the work function of tungsten.



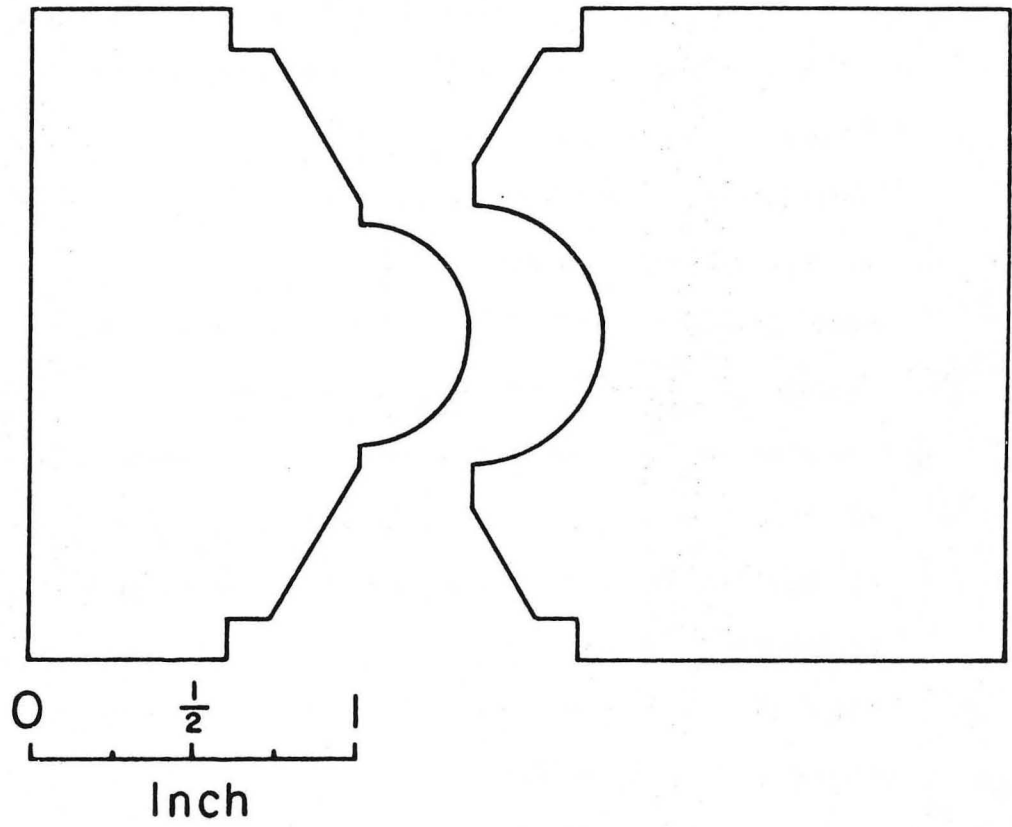
(a)



(b)

XBB 737-4393

Fig.6. C-magnet sandwich assembly while C-can off (a) and on (b)
at METU-Ankara, Turkey.

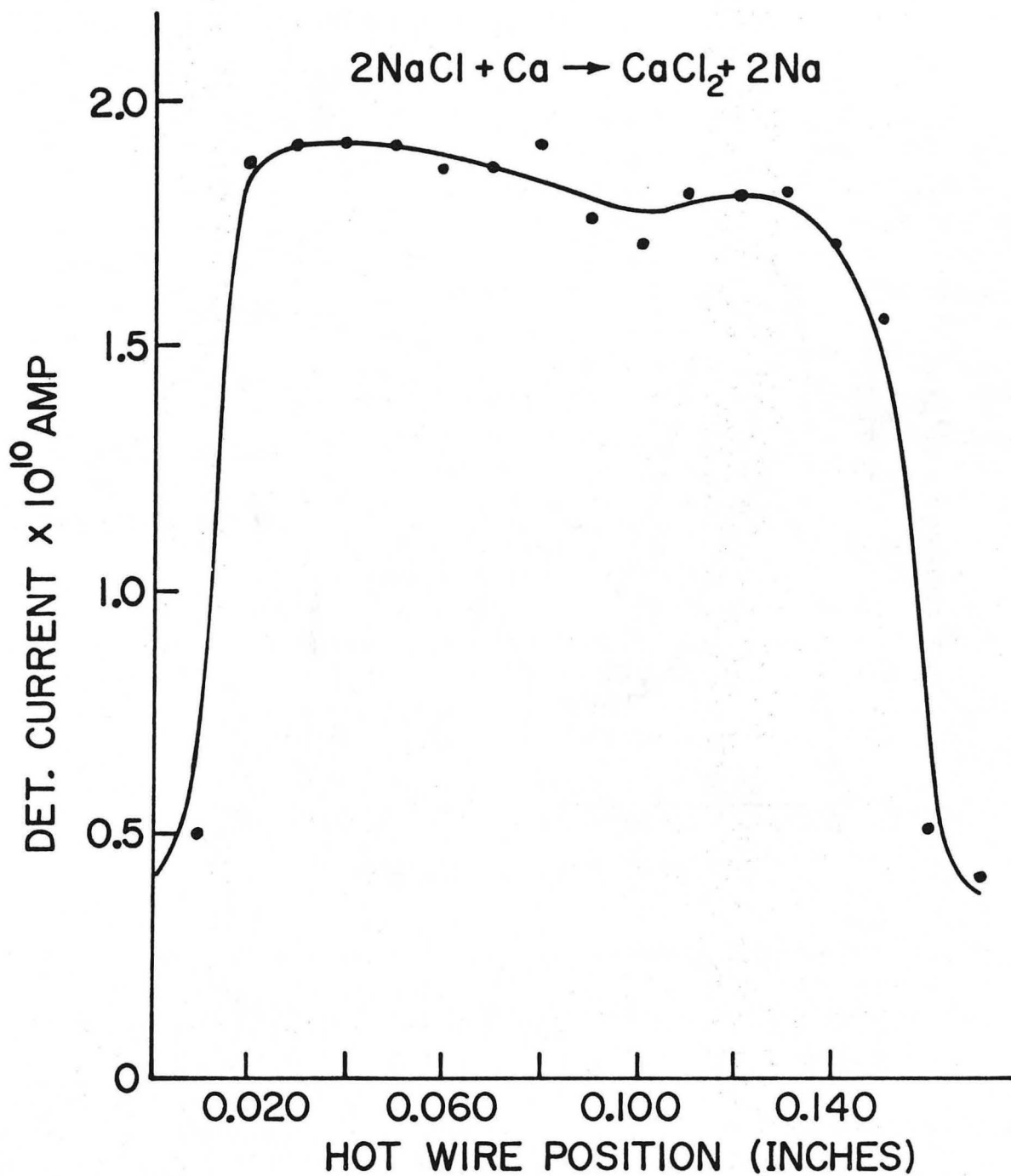


MUB-10145

Fig.7. Cross-section of the Stern-Gerlach pole pieces
of the A and B magnets at Berkeley and Ankara.

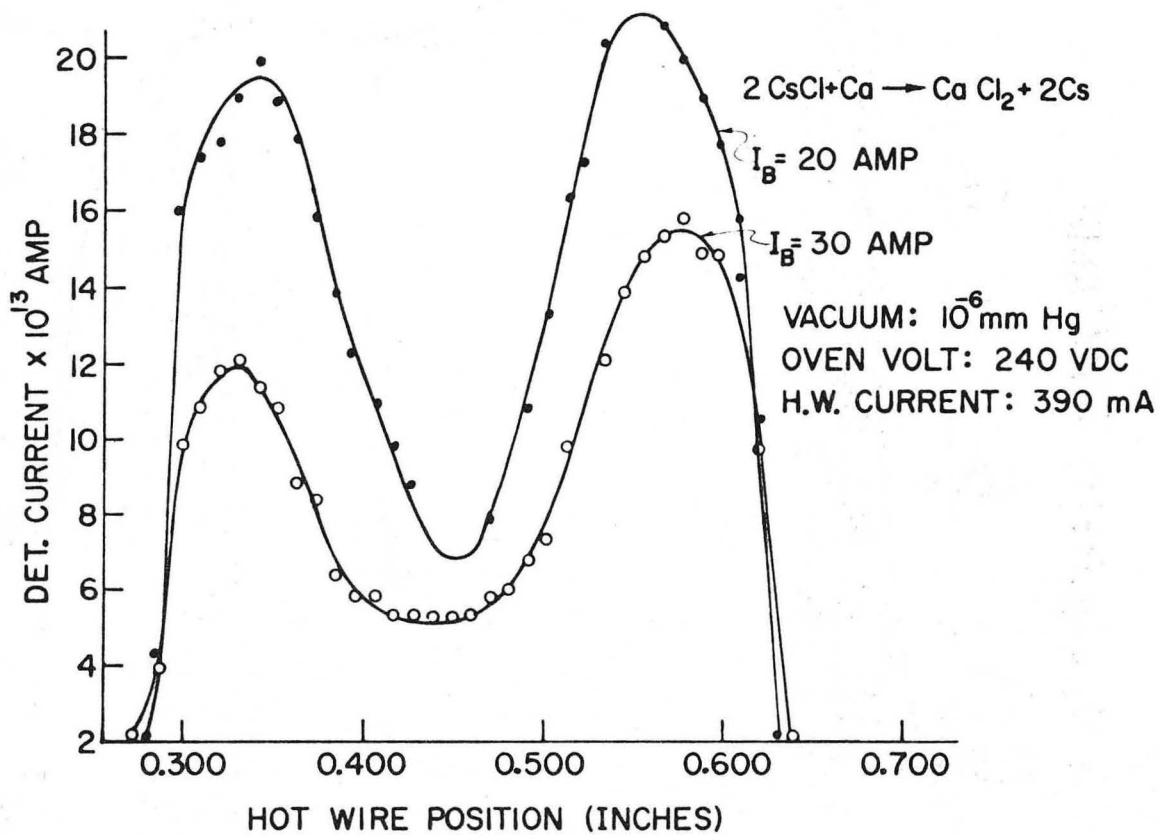
We obtained alkali beams after the vacuum and the alignment problems were solved. Figure 8 shows the first beam obtained in Ankara with the detector slit fully opened. The hot wire (HW) detector is heated with a DC current of about 400 mA, and a negative voltage with respect to the HW is applied to the collector that surrounds the hot wire. The alkali ions formed at the HW are attracted to the collector, and this current is sent to an electrometer which reads down to 10^{-13} amps. The HW detector was moved across the sodium beam and the detector current was recorded as a function of HW position. Then we tried to see the Stern-Gerlach patterns of alkali atoms. Figure 9 shows the first Stern-Gerlach patterns obtained with the atomic beam machine in Ankara. For that particular experiment we produced a Cesium beam and tried two values of B-magnet current while the A-magnet was off. We checked the A-magnet by putting the HW on the beam line and varying the current of the A-magnet power supply while the B-magnet was off. We noticed that as the field gradient in the A-magnet was increased, the detector current decreased, as expected.

The rf system in Ankara is composed mainly of a Schomandl frequency synthesizer, klystrons, magnetrons, and their power supplies. Besides these we have a local 100 KHz crystal oscillator and a Gertsch - VLF phase comparison receiver. The above frequency sources cover the frequency range from zero to 24 GHz. A klystron oscillator is locked on a harmonic of the Schomandl frequency synthesizer which is referenced to a 100 kHz standard signal obtained from a local crystal oscillator. The local crystal oscillator is phase compared with a standard signal (16 kHz) received from Rugby, England. A block diagram of the frequency locking system in Ankara is given elsewhere⁴⁶. Figures 10 and 11 show the atomic beam laboratory in Ankara, Turkey.



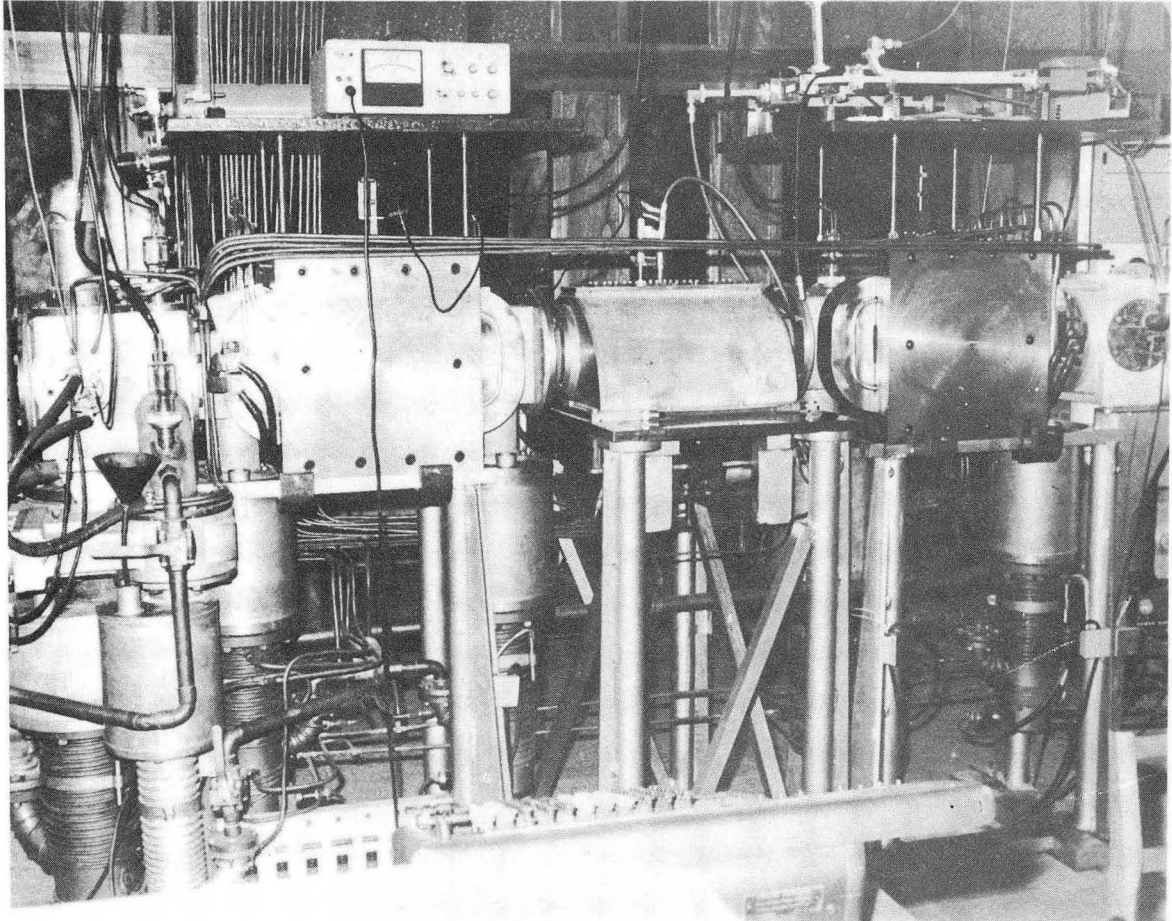
XBL 737-954

Fig.8. First Beam profile obtained with the atomic beam machine in Ankara, Turkey.



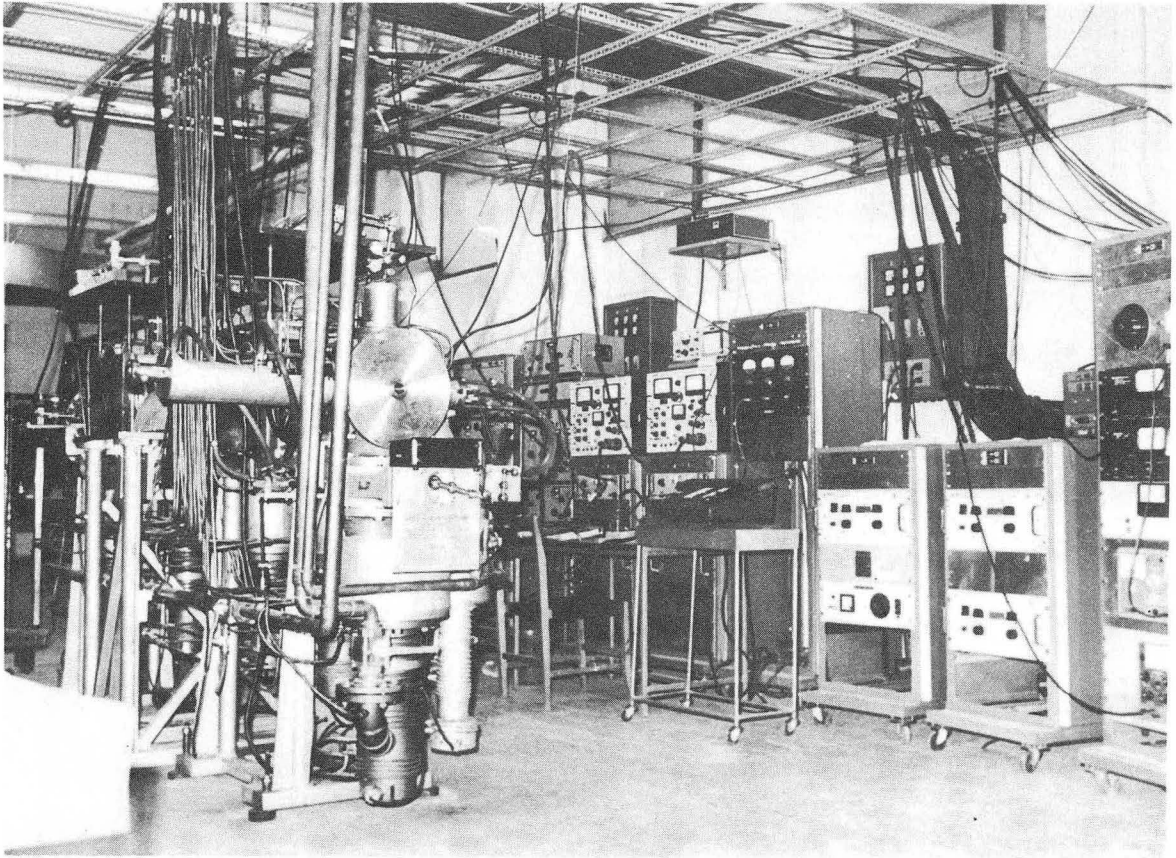
XBL 737-934

Fig.9. First Stern-Gerlach pattern obtained with the atomic beam machine in Ankara, Turkey.



XBB 737-4395

Fig.10. The atomic beam machine in the METU, Ankara, Turkey.



XBB 737-4394

Fig.11. The RF System of the atomic beam laboratory in the METU, Ankara, Turkey.

B. The Feature of the Experiment

From here on we shall present the experiment we performed at Berkeley, California.

Atomic beam magnetic resonance (ABMR) experiments are performed, in general, with isotopes of two different elements. One is the experimental isotope for which some constant or constants are to be determined; the other is the so-called calibration, or reference, isotope. Occasionally, one can induce two or more transitions in the same isotope, first as the field calibration, then for the experimental measurement. (This is the case which V. W. Cohen and his coworkers are doing at Brookhaven for the g_I (Rb^{85}) study). As we have mentioned earlier (see Eq.(19a), we need to know the transition frequency ν and the magnetic field H to make any calculation for the constants mentioned in the introduction. Usually the transition of the experimental isotope is induced at the very same field (ideally) as that of the calibration transition. The value of the magnetic field is calculated from an appropriate formula (such as the Breit-Rabi formula) by using the measured transition frequency and the associated constants of the calibration isotope. Then, using the calculated magnetic field and the measured transition frequency of the experimental isotope in the formula for the constant in question (Eq.(19a) for g_J), the experimental value is determined.

In most previous work, the beamist produces the two beams, and then by switching the frequency to the rf loop back and forth between the calibration and the experimental frequencies, he obtains one resonance for each of the isotopes. This succession of frequency measurements (Runs) is repeated to the number desired. Because of the drift of the C-field for some unknown reason, the average of the preceding and succeeding fields is used for the particular experimental resonance between them. Even this averaging usually includes some error in it. The error arises because each data collection takes about 5 minutes, and a pair of resonances requires at least 15 minutes. Even if the magnetic field drifts uniformly in one direction the calculated average may not correspond to the actual field at the time of the experimental resonance.

In our experiment we partially eliminated this error by inducing the experimental and calibration transitions simultaneously. To arrange this procedure we produced transition frequency tables for the experimental and calibration isotopes as a function of H by using a computer program called FREQ at Berkeley. This program handles any transition in an atom described by the Hamiltonian given in Eq.(49). In this way we produced all possible (allowed by the selection rules) transition frequencies of Rb⁸⁵, Rb⁸⁷, Cs¹³³, and He⁴. Then we plotted all of those frequencies as a function of the magnetic field. The transition we induced in helium was $\Delta F = 0$ and $\Delta m = \pm 1$. Equation(49) implies that the plot will be a straight line for helium, passing through the origin. The plot is a curve for the calibration isotopes we have mentioned. The curvature occurs because of the hyperfine terms in the expression of the Hamiltonian. (See Eq.(49) or Eq.(57)). Doing the plots on the same scale, we have located the crossing point of the helium transition frequency with the calibration transition

frequencies. With the computer program one can locate the crossing point up to a fraction of a milligauss, just by proceeding to progressively finer steps in field. In this way, one can find quite a number of crossings, but one has also to consider the technical limitations such as the frequency sources. Another important factor is the details of the crossing. The smaller the crossing angle, the better. The transitions we have tried are shown on the next three pages. After these considerations, we chose to study the crossing points shown in Table II.

Table II. $\text{He}^4\text{-Rb}^{85}$ and $\text{He}^4\text{-Cs}^{133}$ crossings for the transitions shown:

Isotope	(F,m)Transition	Crossing Point Values	
He^4	(1,0) \leftrightarrow (1,+1)	Magnetic Field (Gauss)	Frequency (GHz)
Rb^{85}	(3,0) \leftrightarrow (2,-1)	3161.53	8.859
Cs^{133}	(4,1) \leftrightarrow (3,-2)	4306.18	12.067

Figure 12 shows the Breit-Rabi diagram of the $^3\text{S}_1$ metastable state of helium with the transition we have induced. Figures 3 and 4 show also the transition which we have induced on the Breit-Rabi diagrams for Rb^{85} and Cs^{133} , respectively. Figures 13 and 14 show the plots to locate the crossing points of the mentioned transitions for Rb^{85} and Cs^{133} , respectively.

Rb⁸⁷ Transitions

$$I=3/2, J=1/2 \rightarrow F=2, 1$$

A) Transitions: $\Delta F = 0, \Delta m = \pm 1$

F = 2		F = 1	
<u>m₁</u>	<u>m₂</u>	<u>m₁</u>	<u>m₂</u>
1)	2 ↔ 1	5)	1 ↔ 0
2)	1 ↔ 0	6)	0 ↔ -1
3)	0 ↔ -1		
4)	-1 ↔ -2		

B) Transitions: $\Delta F = 1, \Delta m = 0$

- 7) 1 ↔ 1
- 8) 0 ↔ 0
- 9) -1 ↔ -1

C) Transitions: $\Delta F = 1, \Delta m = \pm 1$

- | | | | |
|-----|--------|-----|---------|
| 10) | 2 ↔ 1 | 13) | -2 ↔ -1 |
| 11) | 1 ↔ 0 | 14) | -1 ↔ 0 |
| 12) | 0 ↔ -1 | 15) | 0 ↔ 1 |

Rb⁸⁵ Transitions:

$I=5/2, J=1/2 \rightarrow F=3,2$

A) Transitions: $\Delta F = 0, \Delta m = \pm 1$

$F = 3$		$F = 2$	
<u>m_1</u>	<u>m_2</u>	<u>m_1</u>	<u>m_2</u>
1)	$3 \leftrightarrow 2$	7)	$2 \leftrightarrow 1$
2)	$2 \leftrightarrow 1$	8)	$1 \leftrightarrow 0$
3)	$1 \leftrightarrow 0$	9)	$0 \leftrightarrow -1$
4)	$0 \leftrightarrow -1$	10)	$-1 \leftrightarrow -2$
5)	$-1 \leftrightarrow -2$		
6)	$-2 \leftrightarrow -3$		(Standard transition)

B) Transitions: $\Delta F = 1, \Delta m = 0$

- 11) $2 \leftrightarrow 2$
- 12) $1 \leftrightarrow 1$
- 13) $0 \leftrightarrow 0$
- 14) $-1 \leftrightarrow -1$
- 15) $-2 \leftrightarrow -2$

C) Transitions: $\Delta F = 1, \Delta m = \pm 1$

- | | | | |
|------|-------------------------|-----|-------------------------|
| 16) | $3 \leftrightarrow 2$ | 21) | $-3 \leftrightarrow -2$ |
| 17) | $2 \leftrightarrow 1$ | 22) | $-2 \leftrightarrow -1$ |
| 18) | $1 \leftrightarrow 0$ | 23) | $-1 \leftrightarrow 0$ |
| 19)* | $0 \leftrightarrow -1$ | 24) | $0 \leftrightarrow +1$ |
| 20) | $-1 \leftrightarrow -2$ | 25) | $1 \leftrightarrow +2$ |

*This is the transition we induced.

Cs¹³³ Transitions:

$I = 7/2, J = 1/2 \rightarrow F = 4, 3$

A) Transitions: $\Delta F = 0, \Delta m = \pm 1$

$F = 4$			$F = 3$		
$\underline{m_1}$	$\underline{m_2}$		$\underline{m_1}$	$\underline{m_2}$	
1) 4	\leftrightarrow 3	6) -1	\leftrightarrow -2	9) 3	\leftrightarrow 2
2) 3	\leftrightarrow 2	7) -2	\leftrightarrow -3	10) 2	\leftrightarrow 1
3) 2	\leftrightarrow 1	8) -3	\leftrightarrow -4	11) 1	\leftrightarrow 0
4) 1	\leftrightarrow 0			12) 0	\leftrightarrow -1
5) 0	\leftrightarrow -1			13) -1	\leftrightarrow -2

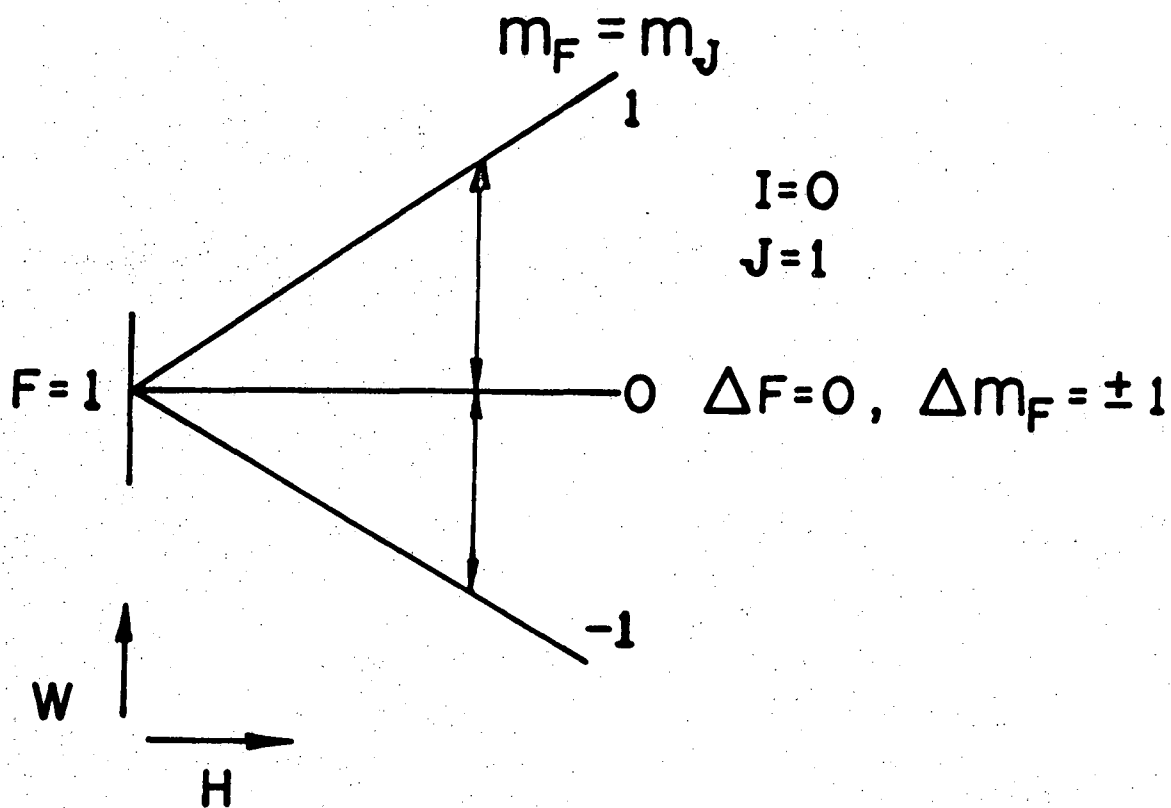
B) Transition: $\Delta F = 1, \Delta m = 0$

- 14) -2 \leftrightarrow -3
- 15) 3 \leftrightarrow 3
- 16) 2 \leftrightarrow 2
- 17) 1 \leftrightarrow 1
- 18) 0 \leftrightarrow 0
- 19) -1 \leftrightarrow -1
- 20) -2 \leftrightarrow -2
- 21) -3 \leftrightarrow -3

C) Transition: $\Delta F = 1, \Delta m = \pm 1$

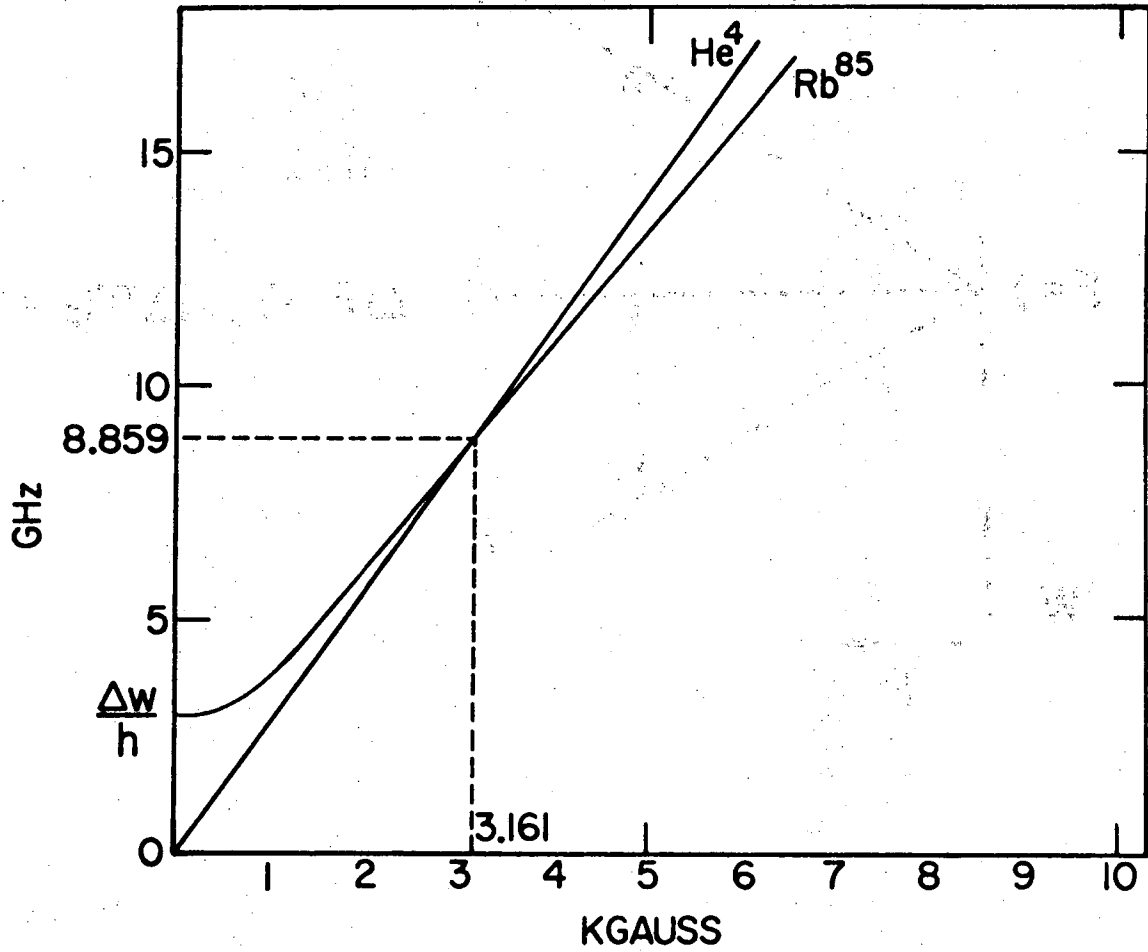
- 22) 4 \leftrightarrow 3
- 23) 3 \leftrightarrow 2
- 24) 2 \leftrightarrow 1
- 25) 1 \leftrightarrow 0
- 26) 0 \leftrightarrow -1
- 27)* -1 \leftrightarrow -2
- 28) -2 \leftrightarrow -3
- 29) -4 \leftrightarrow -3
- 30) -3 \leftrightarrow -2
- 31) -2 \leftrightarrow -1
- 32) -1 \leftrightarrow 0
- 3) 0 \leftrightarrow 1
- 34) 1 \leftrightarrow 2
- 35) 2 \leftrightarrow 3

*This is the transition we induced.



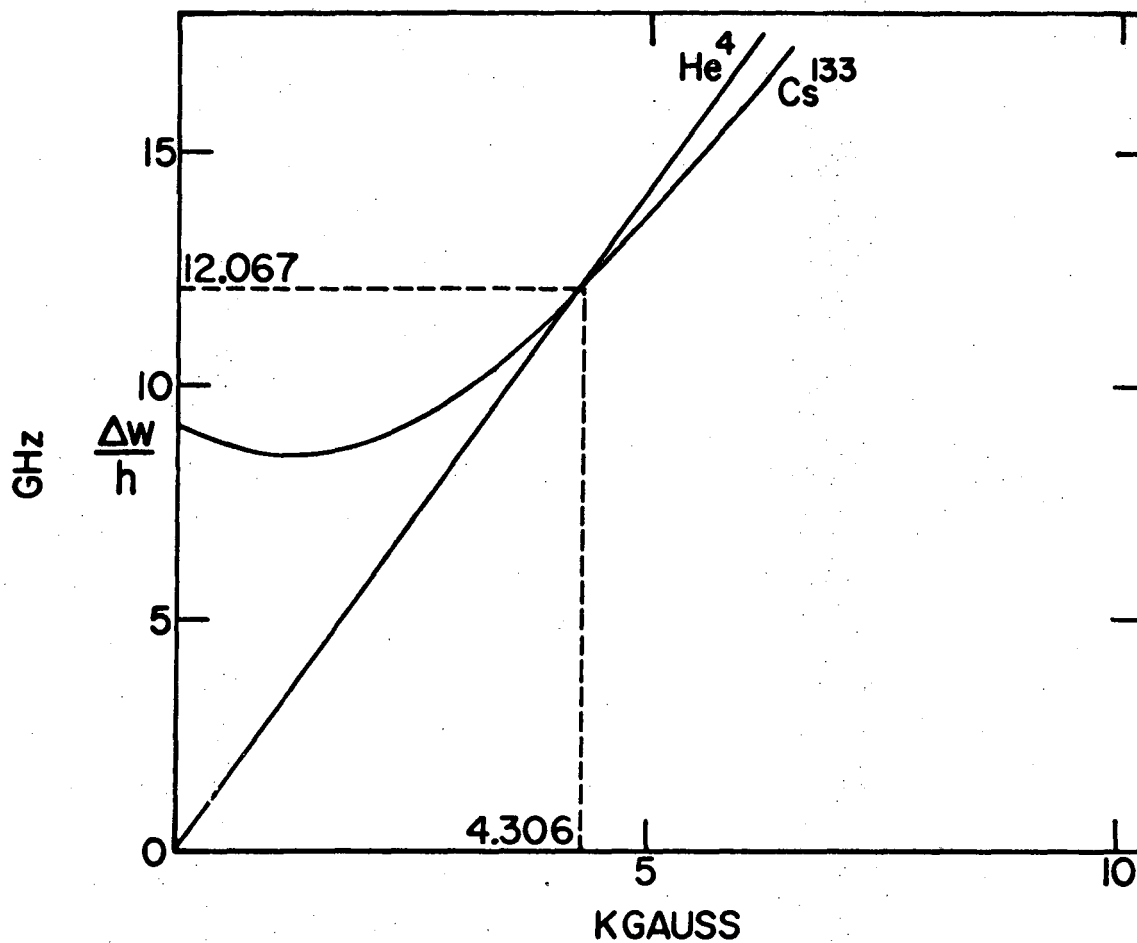
XBL 735-558

Fig.12. The Breit-Rabi diagram of the 3S_1 metastable state of helium. The transition shown is the one we have induced in helium.



XBL 735-549

Fig.13. The crossing point between $\Delta F = 0, \Delta m = \pm 1$ transition in helium and $(F,m) = (3,0) \leftrightarrow (2,-1)$ for Rb⁸⁵.



XBL 735-548

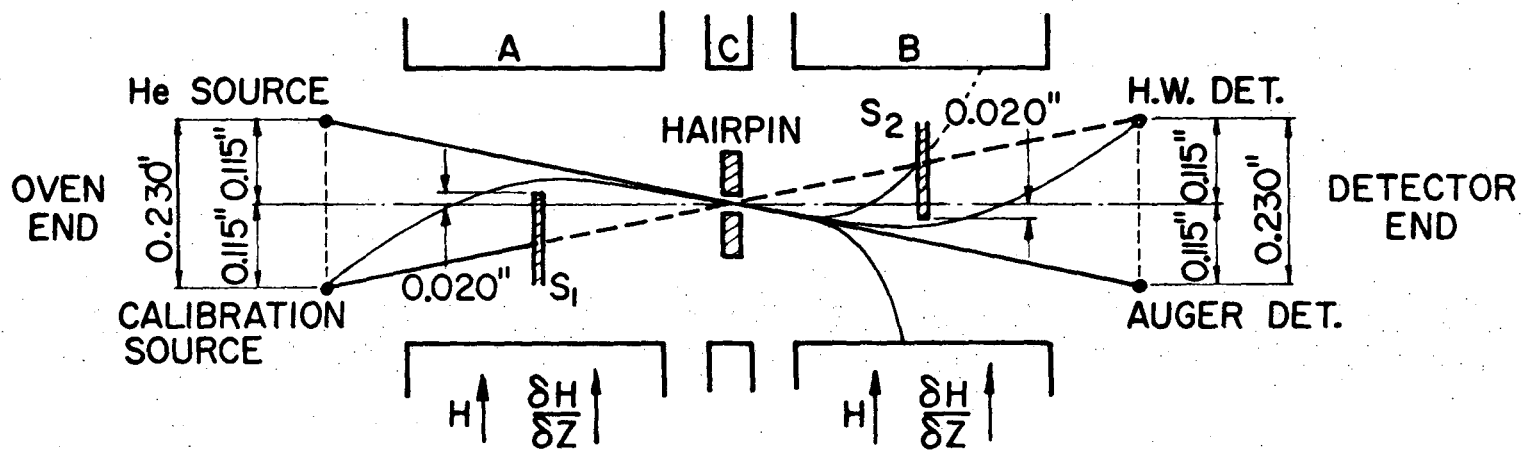
Fig.14. The crossing point between $\Delta F = 0, \Delta m = \pm 1$ transition in helium and $(F,m) = (4,-1) \leftrightarrow (3,-2)$ for Cs^{133} .

C. The Apparatus and the Experiment in Berkeley:

The beam geometry we have used is shown in Fig.15. The beam machine in Berkeley is about 2.5 meters long from the oven to the detector, and consists of an oven, buffer, A, C, and B magnets, and detector chambers. All chambers are separated by valves from the rest of the machine. This gives very easy access for the experimenter in the event of any problem, such as the burn out and replacement of the gun-filament or hot wire, or turning around the hairpin in the C-can. Even for the detection of coarse vacuum leaks, these valves are very handy. The whole system is evacuated by 5 mechanical and 7 diffusion pumps. The mechanical pumps are always on, but the diffusion pumps are turned on and off, depending on the planning and the progress of the experiment. The pressure in the machine was in the 10^{-6} to 10^{-7} torr range for our experiment. At this pressure, the mean free-path is much longer than the length of the machine, and scattering of the beam is not important.

1. The Sources:

The calibration source is a sample in a resistance-heated oven, with a source slit of about 5 mils. The power supply for the calibration oven is a Lawrence Berkeley Laboratory, 20V, 25A, AC source. The calibration sample is put into the oven in chloride form with an admixture of calcium metal grains. A chemical reaction at a temperature of about 450°C gives us the alkali beams. A typical calibration beam intensity is 200 counts



XBL 737-931

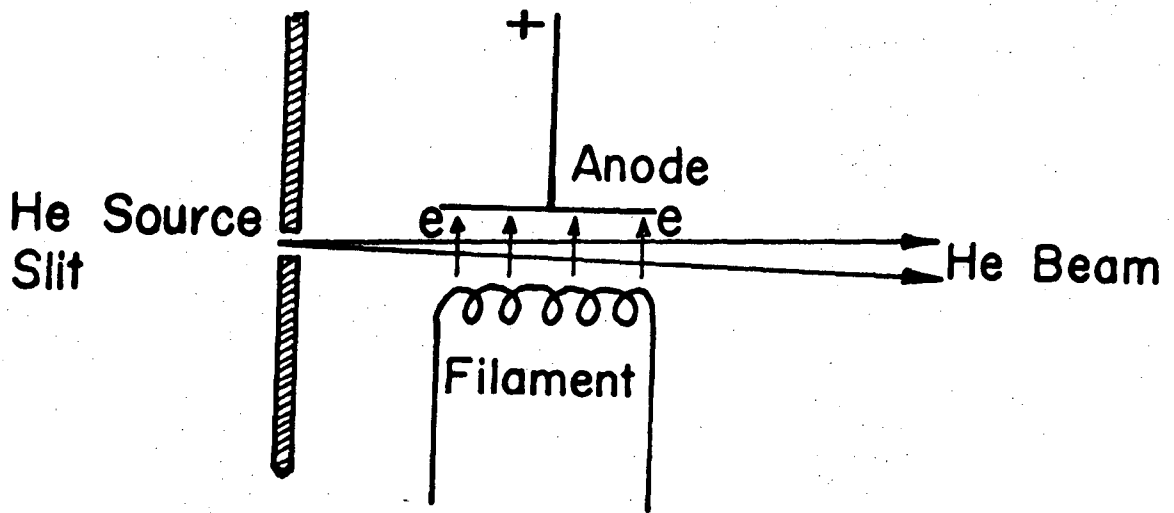
Fig.15. The geometry used for the helium experiment.

per .3 sec. when off resonance and 1500 counts per .3 sec. when on resonance in the scaling system.

The helium source consists of a tank of pressurized helium, gauges, a buffer volume to insure a steady pressure, a manometer to read the pressure, valves, and a tiny hole with a diameter of about 25 microns to the beam machine. The helium beam is cooled down to liquid nitrogen temperature (77°K) to achieve uniform and slow velocities. During the experiment it was noticed that the cooled beam resonance half width (100 KHz) was about 70% of the warm (room temperature) beam resonance half width (150 KHz). We maintained a constant pressure in the buffer volume throughout each run. Typical running pressure in the helium source was 60 torr.

Immediately after the tiny hole, we have the electron-gun to produce the metastable states of helium. The gun is a simple diode which produces an electron beam at right angles to the helium beam. We always worked in the space-charge limited mode of the diode to achieve a steady gun emission current. Typical working conditions are 100V anode voltage, filament current 2.5A, and emission current 80 mA. The filament is heated with a DC supply. The filament is a 3% thoriated-tungsten wire of diameter .004". For our particular design, the anode is in the grid form. It consists of some number of windings of the same tungsten wire used for the filament. Figure 16 shows a simplified scheme of the electron gun.

The metastable state, which is about 20eV above the ground state (see Fig.1), is produced by electron bombardment of the ground state helium beam. He atoms effusing from the tiny hole are crossed with an electron beam of about 100eV energy, immediately after the source slit



XBL 737-932

Fig.16. A simplified scheme of the electron gun to bombard the helium beam.

(see Fig.16). After electron bombardment, the atomic beam then contains metastable helium atoms in both the 2^1S_0 singlet and 2^3S_1 triplet excited states, as well as ground state helium atoms. The beam also may contain nonmetastable excited states, but their lifetime (10^{-8} sec) is smaller than the time of flight in the machine. Then the beam is state-selected in the A-magnet, and some of the $m_J = \pm 1$ states are thrown out, depending on the spin orientation relative to the field gradient in the A-magnet. The others pass on to the rf region at the center of the C-magnet. Therefore, all three Zeeman levels of the triplet besides the singlet and ground states of helium exist in the rf region, where we induce $\Delta m = \pm 1$ transitions (see Fig.15). Applying the appropriate frequency to the rf loop, the helium atoms in the $m_J = 0$ state of the triplet are pumped to the other two Zeeman levels, then are deflected out by the B-magnet. Consequently we get a decrease at the detector output when the resonance condition is fulfilled. The He detector is situated on a straight line with the source slit and collimator in the "C" region. When the metastable helium atom hits the sensitive surface of the electron multiplier, it knocks out an electron from the surface and becomes de-excited. These Auger electrons are multiplied and scaled in the detection system. A typical He-count rate is 20,000 counts/.3 sec.

Another way of producing metastable states of helium is to use discharge tubes. Hughes,¹³ Drake¹⁵, and Leduc¹⁶ applied discharge techniques in their experiments. We can say that the discharge technique adds more impurities to the beam than the electron bombardment technique. Hughes¹³ and his coworkers mention that they had electrons, helium ions, helium molecules, photons, and nonmetastable excited states as the impurities in the beam besides ground and metastable states of He. Among

these impurities we too may have electrons, helium ions and nonmetastable states in our technique. The charged impurities will be deflected out by the A-magnet, and nonmetastable excited states will not be able to reach to the detector because of the shorter lifetime (10^{-8} sec). In another paper Drake¹⁵ and his coworkers mention similar impurities. They say that the photon background is even higher for the DC discharge. They mention that about 1 particle in 7×10^4 particles in the helium beam was in the 3S_1 metastable state. We also have done a similar study during the experiment. Keeping the He count rate constant at 20,000 cnts/.3 sec, we changed the gun voltage and recorded the resonance for various values of anode voltage. Then we calculated signal/background ratios for each resonance. Realizing the metastabilization probability (that is, the collision cross-section of the helium beam with the electrons) is a function of gun voltage, $\sigma = f(V)$, we saw that the probability is roughly a maximum around 100V, for which S/B is 3%, where B is the background count and S is the resonance height in terms of counts.

2. Lifetime of the Metastable State of Helium:

Some of the excited states of certain elements such as hydrogen in $2s^2S_{1/2}$ and helium in $1s2s^3S_1$ and 1S_0 states are said to be metastable, because those states have much longer lifetimes than 10^{-8} sec, which is the typical lifetime for allowed electric dipole transitions from other excited states. The reason for the longer lifetime in metastable states is because angular momentum and parity selection rules prevent the usual electric dipole transitions to lower states. Decay from these metastable states are forbidden by the selection rules. But the metastable atom can decay spontaneously by some higher order radiative processes.

Theoretical calculations and experimental measurements of the decay rate, which is the inverse of the lifetime of a metastable state, show that it is sufficiently slow so that it does not affect our experiment. A recent experimental measurement for $2^1S_0 \rightarrow 1^1S_0$ decay rate was made by R. S. Van Dyck⁴⁹ and his coworkers. They found $\tau(\text{He}, ^1S_0) = 19.7 \pm 1.0$ msec, which is in agreement with $\tau(\text{He}, ^1S_0) = 19.5$ msec by Drake, Victor, and Delgarno⁵⁰. The 3S_1 state is the lowest state of the triplet system (ortho-Helium). G. Drake,⁵¹ theoretically, showed that the forbidden $2^3S_1 \rightarrow 1^1S_0$ transition can take place spontaneously by a single-photon magnetic dipole emission, rather than the two-photon emission proposed by Breit and Teller.⁵² Drake's theoretical result for the transition rate is $1.27 \times 10^{-4} \text{ sec}^{-1}$, which gives a lifetime of $\tau(\text{He}, ^3S_1) = 8000$ sec. So far, no precise experimental value for this quantity is known. But H. W. Moos and J. R. Woodworth⁵³ are attempting to observe the lifetime of the 3S_1 state of helium by using a time-resolved, high resolution spectrophotometric technique. Their experimental value for the transition rate is $2.4 \times 10^{-4} \text{ sec}^{-1}$, which gives $\tau(\text{He}, ^3S_1) = 4000$ sec. They quote a large experimental error of a factor of 3, and also mention that further work will reduce the experimental uncertainty. In any case, the 2^3S_1 metastable state of helium has a lifetime much longer than the time of flight from the source to the detector in the beam machine.

3. The Detectors and the Data Collection System:

Miscellaneous detectors, which are used in the ABMR technique, are discussed by Ramsey in Ref. 43, chapter XIV.3. Among those we have used is a surface ionization detector (usually called a hot wire, HW), for the calibration isotopes and a cold wire technique for the helium beams.

Nearly every alkali atom that strikes a heated pure tungsten wire comes off as a positive ion. The numbers of positive ions that emerges from the HW at temperature T is given by Ramsey (Ref.43, page 379) as

$$N_+ = N_0 e^{-q(\phi_i - \phi_t)/kT} \quad (58)$$

where N_0 is the number of neutral beam atoms reflected from the HW, ϕ_i and ϕ_t are the ionization potential and the work function of the incident and target atoms, respectively, q is the electronic charge, and k is the Boltzmann constant. The work function of pure tungsten is 4.5 V, and the ionization potentials of Rb and Cs are 4.16 V and 3.87 V, respectively. The hot wire we have used is 10 mils in diameter, and a typical running current is 2.8 amp, DC. Then these positive ions are either measured as a current or counted electronically. For the current measurement one can use either a very sensitive electrometer (down to 10^{-13} A, which is the case in Ankara) or accelerate the positive ions onto the sensitive surface of an electron multiplier tube and then measure the output current of the multiplier. Another alternative for this last case is to count the output of the electron multiplier tube, electronically. This is the method we used in our experiment for the detection of the calibration resonances.

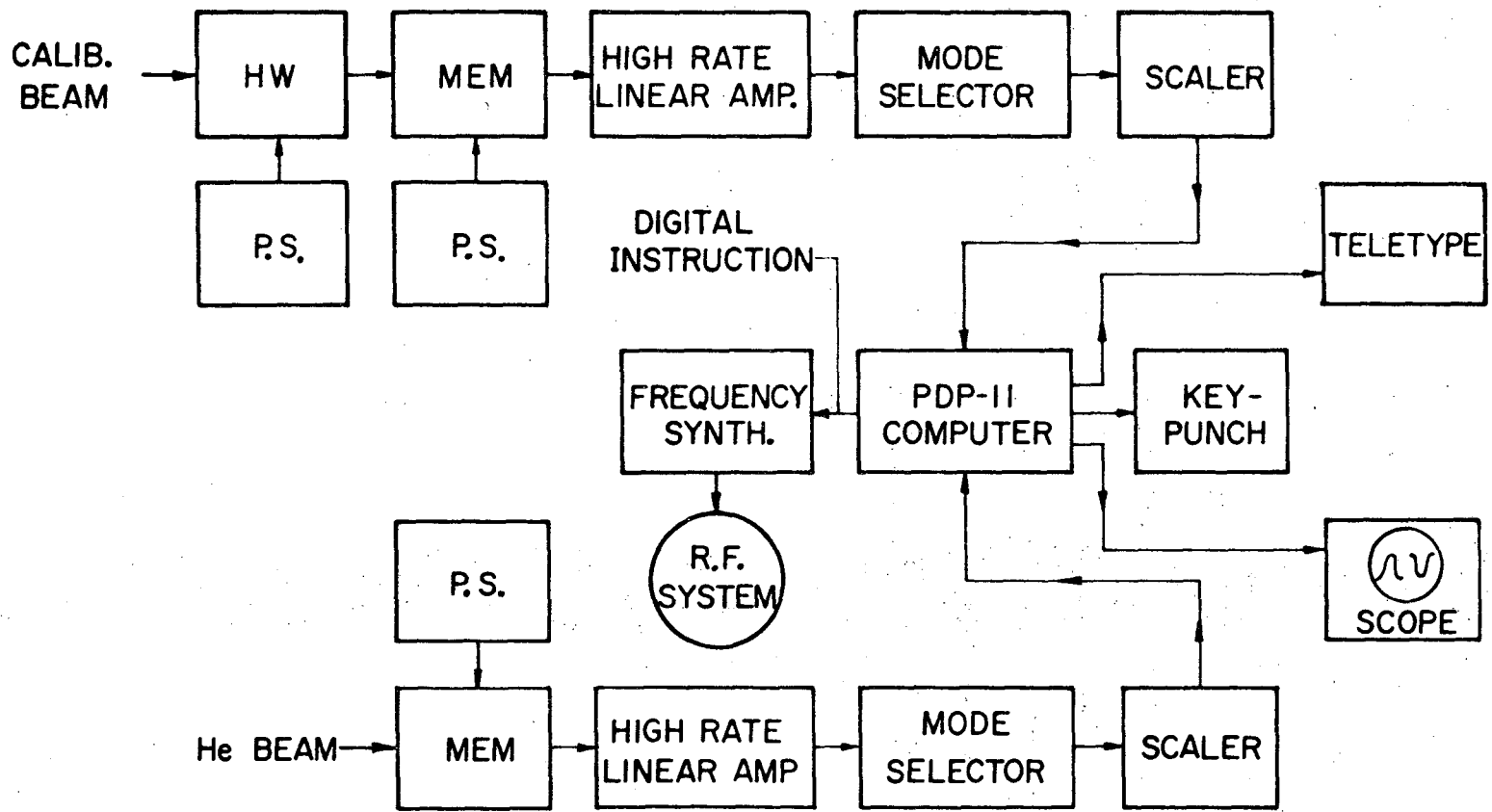
Bendix series 300 magnetic electron multipliers (MEM) were employed in both counting channels. The windowless, MEM can amplify electron

beams by a factor of 10^7 or more. Their operation is based on the secondary electron emission phenomenon. These multipliers use continuous semi-conducting films to form accelerating electric fields and to serve as secondary electron emitters. The value of these multipliers lies in the excellent stability of dynode surfaces while exposed to the atmosphere and their complete lack of photo-sensitivity to visible and near-ultraviolet radiation. More specifications are given in the manufacturer's manual. Figure 17 shows the block diagram of the data collection system.

We think that this experiment is one of the more sophisticated beam experiments performed recently. Due to the computerization involved in the experiment, one person can almost carry out the runs alone. The Digital Equipment Corporation PDP11 computer is shown in Fig.17. It drives the frequency synthesizer back-and-forth across the resonance and collects data in 50 equally spaced channels. The width of a channel (in frequency) can be set, depending on the estimated resonance widths of the samples. Of course, the wider resonance (helium in our case) should be considered while setting the channel width. The frequency synthesizer is a Hewlett-Packard 5105A (0-500MHz), which is a computer-controllable type with push button controls. Any number of digits (3 in our case) in any range of frequency within the limits of the synthesizer can be left to the control of the computer. As our resonance widths are about 100 kHz, we controlled the 99.9 kHz buttons with the PDP11 to scan the frequency back-and-forth over the resonance.

Since the experimental arrangement enables us to record simultaneous transitions the counts coming back to the PDP11 via the calibration-branch of Fig.17 go to one set of 50 memory locations, while the counts coming

via the helium-branch of the same figure go to another set of 50 memory locations. The computer scans the synthesizer frequency back-and-forth over the resonance for about 5 minutes. The memory contents are displayed continuously on the screen of an oscilloscope while the data are being collected. This display enables the experimenter to eliminate bad resonances immediately and start data collecting over again. When the counting is complete for a particular resonance, the memory content is transferred to the key-punch and teletype machines. In this way the counts at 50 equidistant frequency points on each (calibration and helium) resonance are punched on cards in a FORMAT usable by the computer. This OUTPUT of the memory is also printed on the teletype simultaneously. Next the deck of cards is analyzed by a computer program called LFIT. We shall discuss this point again in the section on analysis of data. The teletyped record is kept in the LOG-BOOK for future use in case of need.



XBL 737-961

Fig.17. Data Collection system for the calibration and the helium resonances.

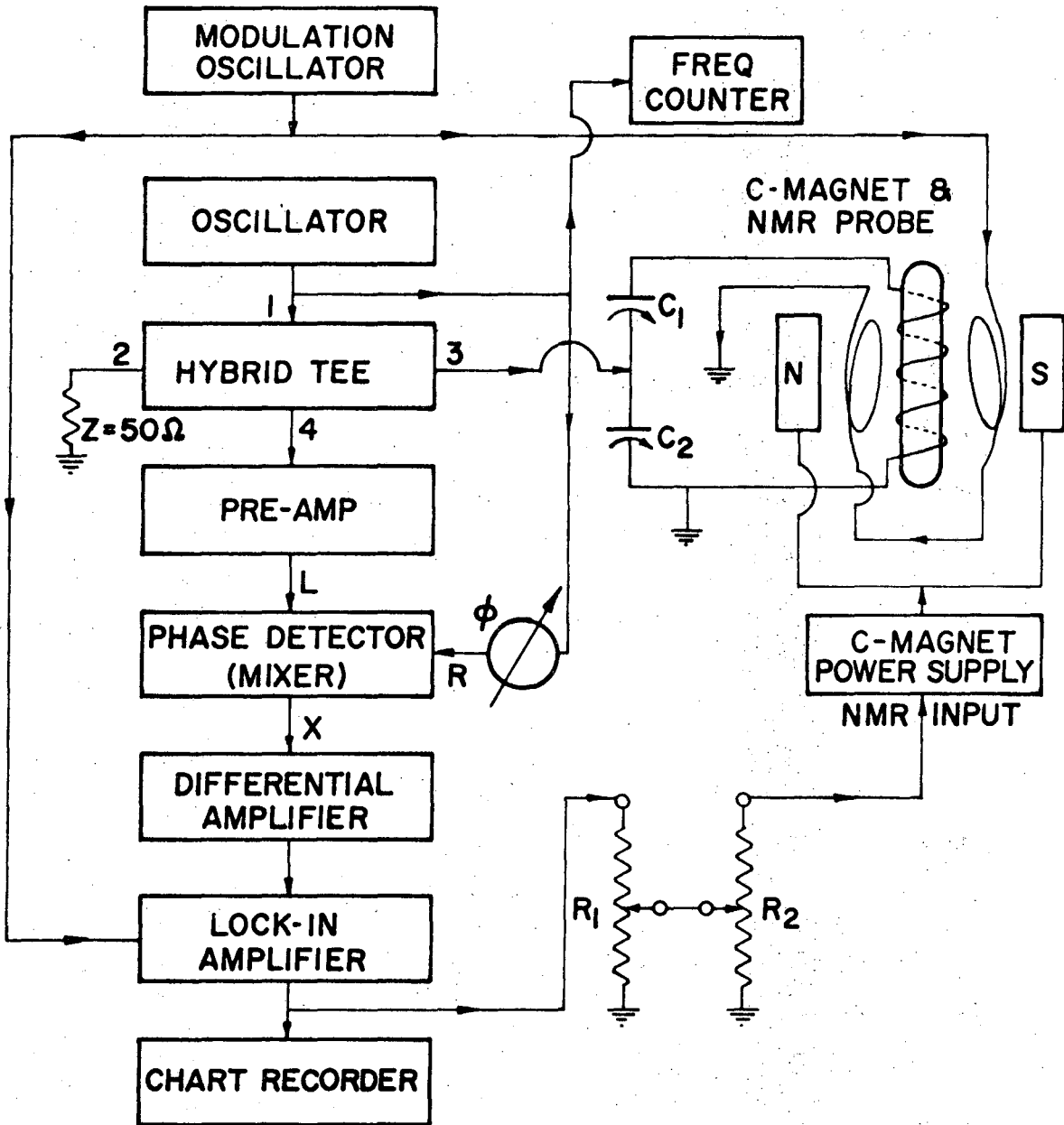
4. C-Field: Locking and Shimming:

In high precision resonance experiments, one requires a very homogenous magnetic field and a stable frequency source. A description of the latter will be left to the next section.

The C-field is provided by a Varian Associates V4012A electromagnet with 12" circular pole pieces. It is powered by a Varian V2100 regulated constant current power supply and further controlled by a nuclear magnetic resonance (NMR) field control system. In the early days of our experiment a Harvey-Wells FC-502 was used as the field control system, but due to instabilities and noise in the marginal oscillator, we replaced that system with a Klein-Phelps⁵⁴ type NMR system. We have constructed two Klein-Phelps type NMR systems, one for field locking and one for field mapping. The general principle of operation of these systems is the same; they convert the difficult problem of field measuring into a simpler problem of frequency reading.

We shall not discuss the detailed problems of NMR systems here because we are using them only as a tool in our experiment. Of course it was a struggle to put the two NMR systems into operation. The books by Andrew⁵⁵ and Abragam⁵⁶ were the principal sources used while encountering NMR problems.

Figure 18 shows the block diagram of a Klein-Phelps type NMR system which we used for the C-field locking. The system consists of a simple NMR spectrometer assembled around a hybrid junction. The NMR frequency is supplied from the OSC to the first arm of the HYBRID TEE. The second arm is terminated with 50Ω characteristic resistance. The sample coil L is resonated by the series combination C_1C_2 . To tune the circuit, an oscilloscope is connected to the fourth arm of the bridge and the



XBL 737-963

Fig.18. Klein-Phelps type NMR field locking system.

capacitance C_1 is changed to minimize the PRE-AMPL output. This resonates the LC circuit to the OSC frequency. At the instant of resonance the reflection from the probe is minimum. C_2 is adjusted to further minimize the reflected power. This procedure is repeated until no further reduction in reflected power can be achieved. This is called the balance condition of the hybrid bridge. Any deviation from the balance condition due to a change in C-field will unbalance the bridge, yielding a reflected power from the NMR probe. This reflected signal is amplified, phase detected first in the mixer with the OSC frequency, then in the LOCK-IN-AMPL at the modulation frequency. The signal is rectified, and then sent to the C-magnet power supply as a correction signal. R_1 and R_2 in Fig.18 are 10-turn helipot which divide the correction voltage to control the strength of the feed-back, so that any change in the C-field is fed back, and the long and relatively short term variations of C-field are eliminated.

To keep the rf region unaffected by the modulation current (amplitude modulation), the Harvey-Wells NMR probe is placed 2" away from the transition region. Of course the control of the magnetic field at a point (side-lock) far from the center has weaker control at the central region where variations interest us most. Later we built a frequency modulated NMR system and attached its probe to the hairpin. We first used this second system for field mapping and shimming, then switched the locking from the side to the center. We found that the instability of the calculated field is reduced from 1 part in 10^6 to 2 parts in 10^7 per run (5 hours) by this center locking procedure. We have checked that the switching from the side to the center does not disturb the field appreciably. This check is done by going back to the side-lock and reading the field again at the hairpin position with the center probe.

Besides the constancy of the C-field, the homogeneity over the rf region is another important factor. Whatever the shape of the field (dome or dish), it is kept constant by the locking system. But the spatial variations of the field strength broaden the resonance. This spatial variation is mapped with the second NMR system shown in Fig. 19. Very crude field measurement is done with the aid of a Hall-probe gaussmeter, but the accurate field measurement is accomplished with the aid of a hairpin-attached NMR probe. The proton probes we have used were homemade,⁵² except one which is already being used for the side-locking. For the homemade probes we used distilled water and FeCl_3 , and a few turns of #32 wire with formvar insulation. The function of the FeCl_3 is to broaden the line width.

Improving the homogeneity of a field is called shimming. This can be done mechanically, electrically, or with a combination of both. In mechanical shimming, either the parallelism of the pole faces is adjusted or some magnetic material is put in an appropriate place in the C-region. This method was tried at Berkeley by some experimenters. Hughes^{13, 15} and his-coworkers at Yale locked the C-field with an NMR system and tried to improve the homogeneity using the stray fields of the A and B magnets. They measured the field with an NMR probe and changed A and B currents slightly to get better homogeneity in the horizontal direction. For the vertical direction they adjusted the parallelism of the C-magnet pole faces with brass spacers. The inhomogeneity they obtained was 6 parts in 10^6 over a 3mm horizontal and 3mm vertical region.

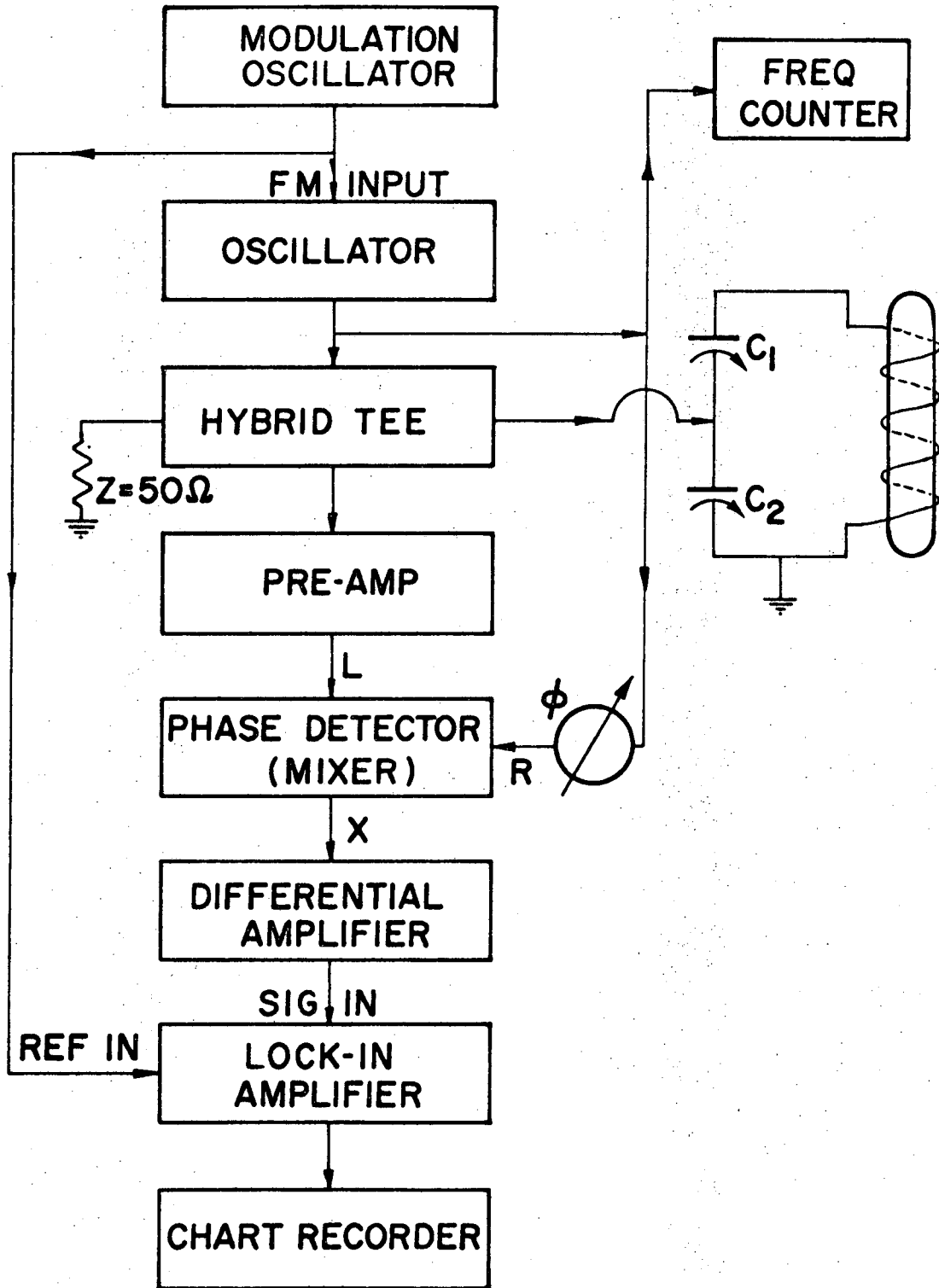
Electrical shimming techniques were used for the first time in the atomic beam laboratory at Berkeley for this experiment. The design criteria of electrical current shims are discussed by W. A. Anderson.⁵⁷

The principle is to arrange the windings in such a way so as to obtain a spatial gradient of the field in the desired direction. Then this gradient is used to cancel the spatial variations which are already present in the C-region. In the above paper, the various corrections to magnetic field gradient are classified as first, second, third and fourth orders. A first order correction produces a gradient in one direction. A second order correction controls the curvature, and so on.

In our system we have three sets of shim coils. One set of coils controls the field gradient along the direction of the beam. The second set controls the vertical gradient and a third controls the spatial curvature of the field. Each coil consists of 10 turns of #32 wire with formvar insulation. The resistance of each coil is about 3.5Ω .

The capability of shim coils is of course limited. It is important to have a starting field shape which can be flattened by the shim coils. A sharp dish or dome can not be flattened with the present shim coils. By driving the magnet in the normal or reversed direction and then returning it to the set point, one can greatly alter the shape of the field in the central region of the magnet because of hysteresis effects. By adjusting the direction, current and duration of saturation, one can partially flatten domes and dishes. In this way the starting field can be brought into the handling zone of the shim coils.

The probe in Fig.19 can be moved horizontally and vertically along two scales. The probe is attached to the bottom of the hairpins, and is $1\frac{1}{8}$ " below the beam axis. While mapping, the hairpin is raised by $1\frac{1}{8}$ " to bring the probe on the beam axis. Then the field is mapped and shimmed horizontally and vertically, using the NMR dispersion signal (here one has to be careful in identifying the central peak because we

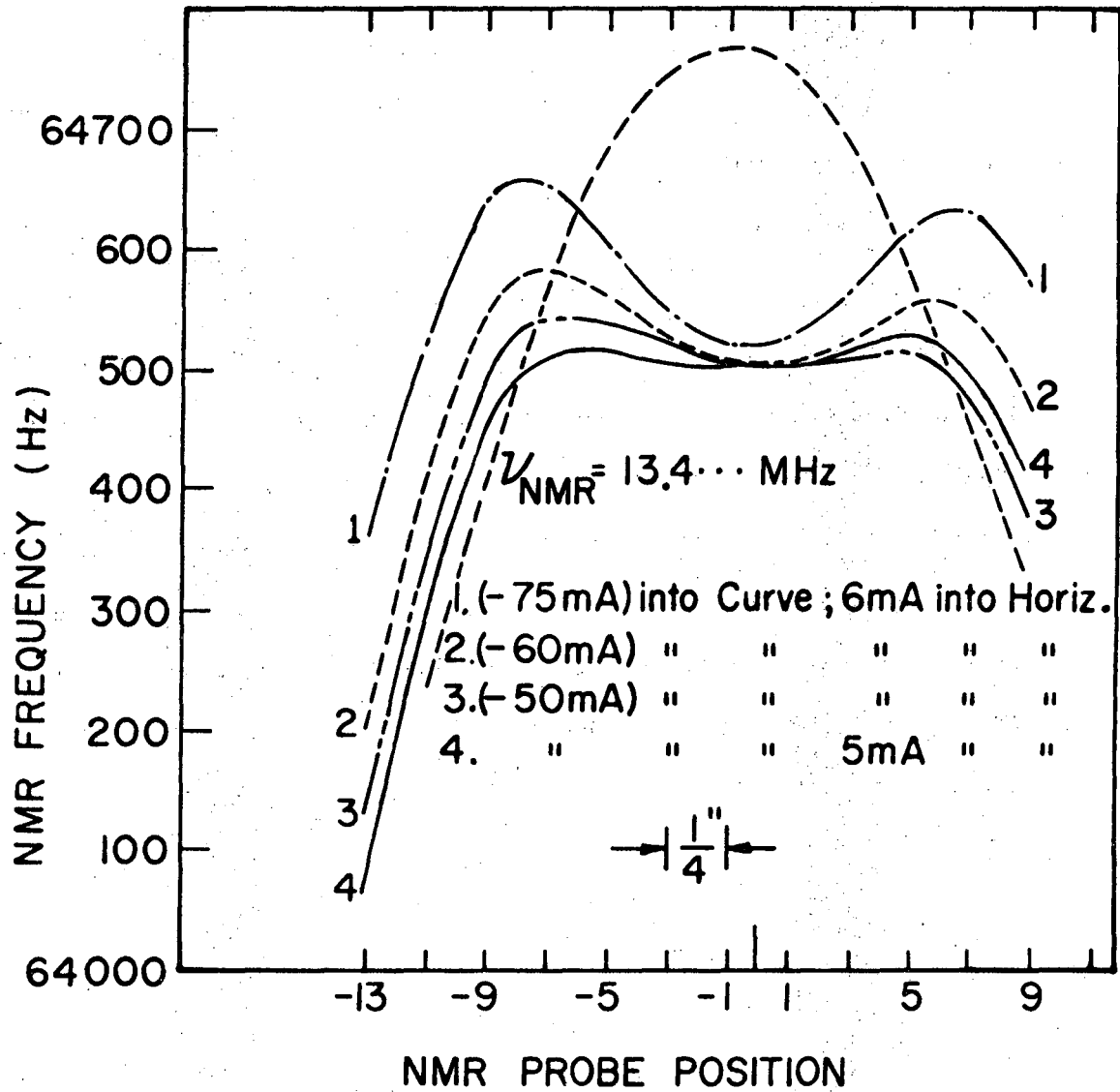


XBL 737-962

Fig.19. Klein-Phelps type NMR field mapping system.

have side bands due to the modulation frequency). A plot of the resonance frequency versus the NMR probe position shows us the detailed structure of the field in that region. We have shimmed the field, starting with a dome shape as well as a dish shape. Figure 20 shows a horizontal shimming of a dome shaped field. Figure 21 shows the vertical field leveling.

Once the field is homogenized to 1 part in 10^6 over a certain region (it was about 1.5" in the horizontal direction for our experiment), one can tune the resonance so the chart recorder output indicates a zero in the dispersion curve (a maximum of the resonance). Now, as the probe is moved, any variation in field is detected with high sensitivity. One has to continue the fine shimming in this way. With this electrical shimming technique we homogenized the field to 2 parts in 10^7 over the rf region. Increasing the sensitivities of the LOCK-IN amplifier and of the chart recorder results in an increase in the sensitivity of the system. Figure 22 shows the field variations over the rf region just before the start of a run.



XBL 737-958

Fig.20. Several stages in horizontal field leveling.

The dome shaped curve is the original form of the field to be leveled.

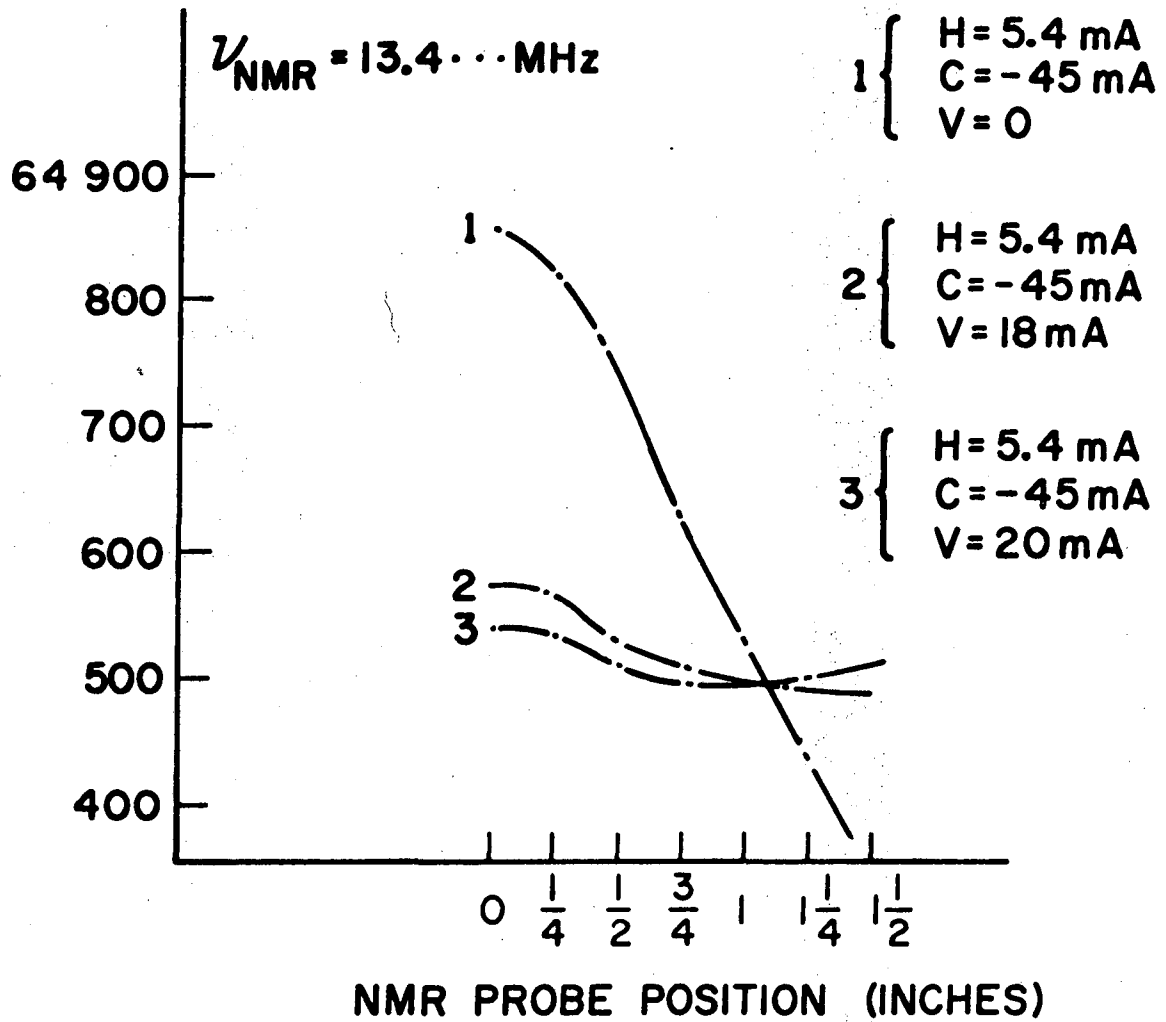
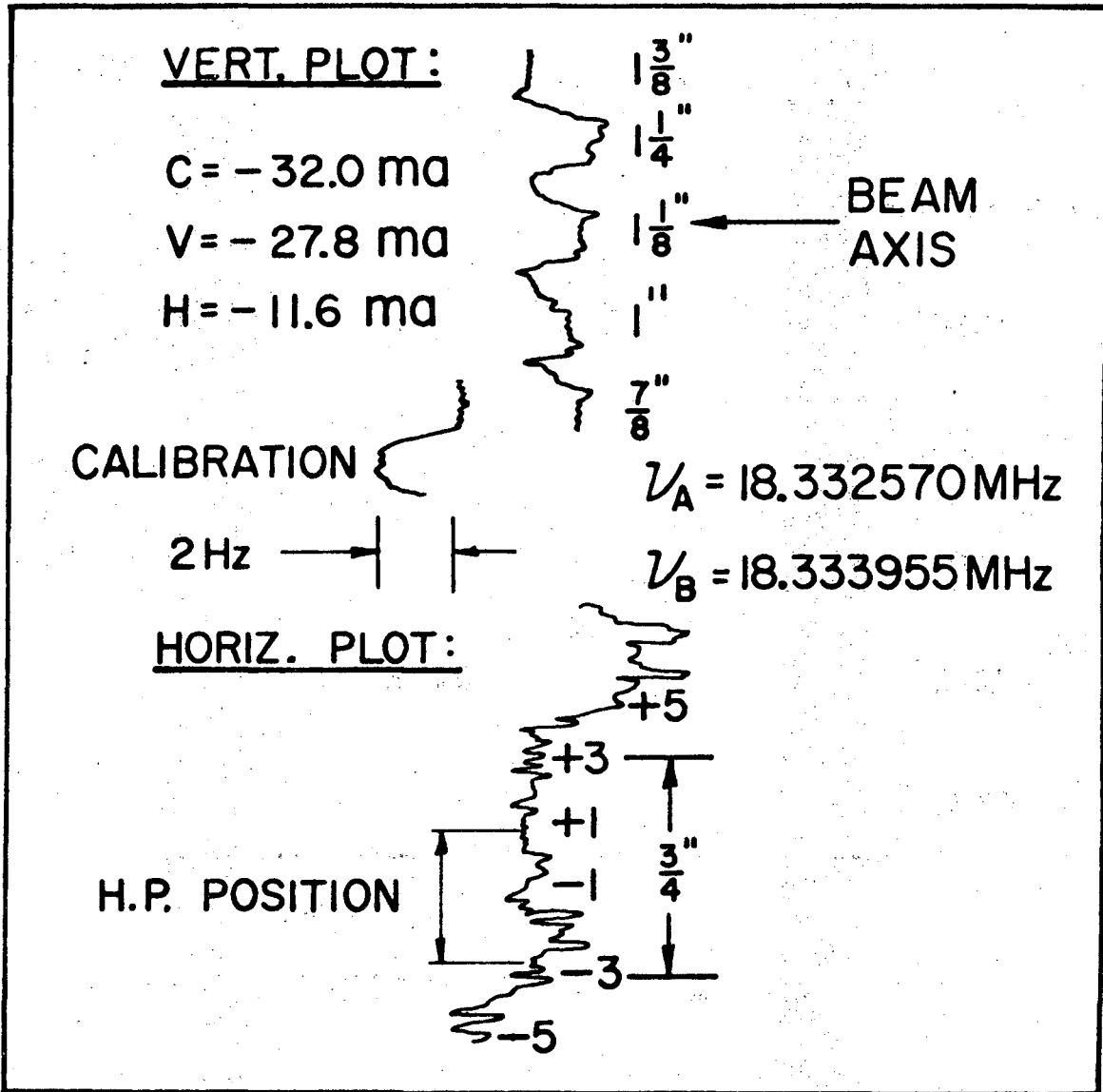


Fig.21. A few instants in vertical field leveling.

H, C, and V stand for horizontal, curvature, and vertical, respectively.



XBL 735-557

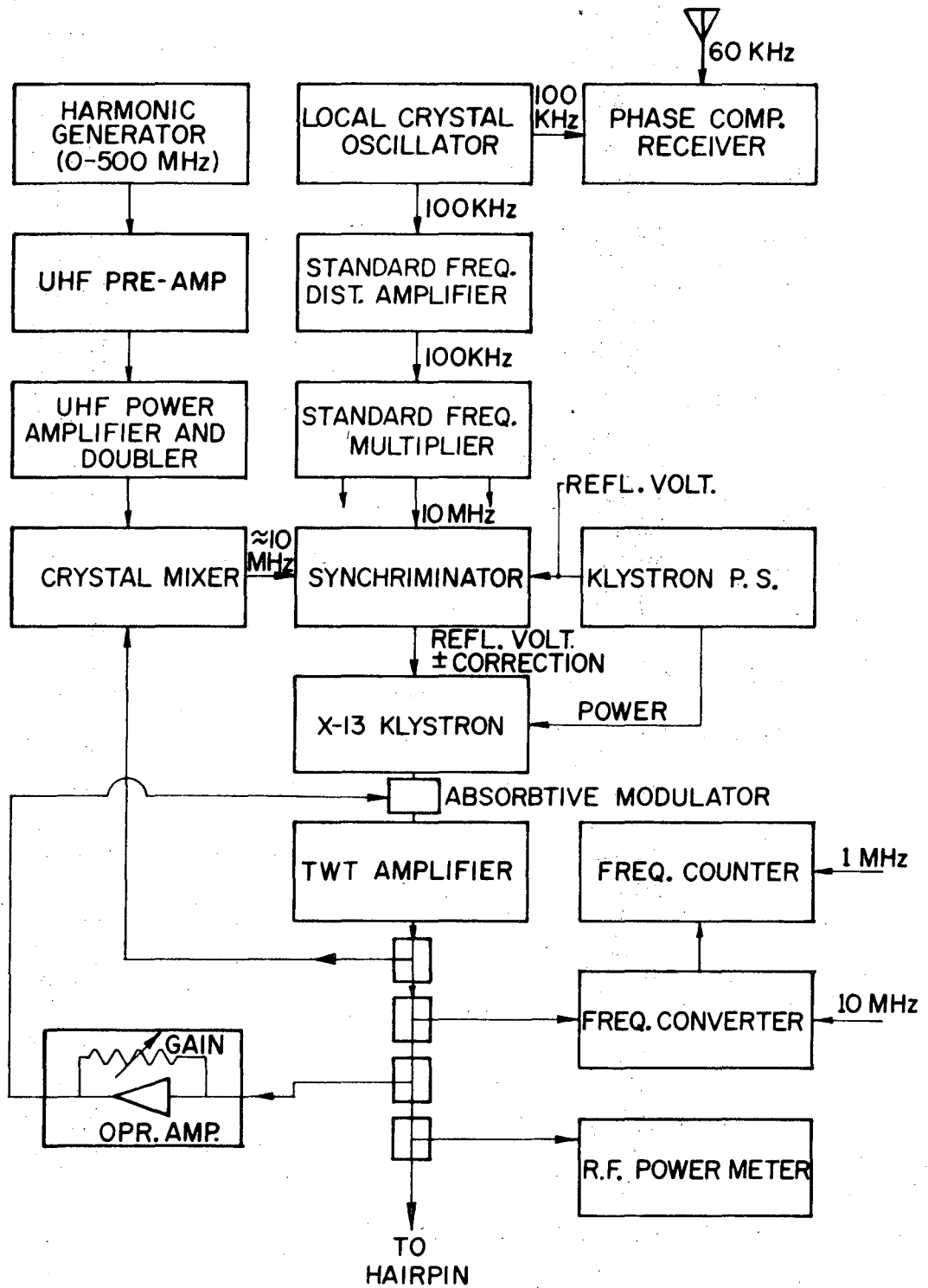
Fig.22. Chart recorder output of the fine field shimming.

The bumps between the flat portions of the trace are transient effects caused by motion of the NMR probe.

5. Radio-Frequency System

As we have mentioned earlier the radio frequency circuitry is a very important part of a high precision measurement. Figure 23 shows a block diagram of the frequency, power control, and measurement circuitry we have used.* The frequency source we used was an X-13 klystron which is a micrometer tuned, X-band reflex klystron manufactured by Varian Associates. The tuning range of the klystron is 8.1 to 12.4 GHz. It adequately covers the frequencies 8.859 GHz and 12.067 GHz at which we worked. The klystron is tuned to 8.859 GHz for the Rb^{85} calibration, and to 12.067 GHz for the Cs^{133} calibration. Tuning is done by changing the cavity dimension with the micrometer, and the reflector voltage on the klystron power supply. The output frequency of the klystron is locked on a harmonic of the reference oscillator. The reference oscillator is a Hewlett-Packard, model 5105A (0-500 MHz) frequency synthesizer. This device has provisions for both analog and digital remote frequency control, in addition to manual control. It has its own crystal reference, which is compared with the local standard periodically. The local standard oscillator puts out 100 kHz, which is compared with WWVB, a 60 kHz signal coming from the National Bureau of Standards at Fort Collins, Colorado. The 60 kHz signal originates from a Cs^{133} -standard and has an instability a few parts in 10^{13} per day. The frequency of the local crystal oscillator is continuously checked, and the drift rate was found to be less than 0.5 in 10^{10} per day. The harmonic, which is compared to the klystron, is set 10 MHz above (or below) the klystron

*It is very similar to the one used by Zak⁵⁸ and his coworkers for the previous experiment in the same laboratory.



XBL 737-959

Fig.23. Block diagram of the radio-frequency system.

frequency, that is, the frequency of the reference oscillator is so chosen that some particular harmonic is displaced 10 MHz from the klystron frequency. The klystron and harmonic generator outputs, after some necessary amplification and duplication, are applied to the inputs of a crystal mixer. The output of the mixer is the beat (difference of the input signals) frequency, which is near 10 MHz, but not exactly, due to the instability of the klystron oscillator. This beat frequency is compared with an exact 10 MHz standard frequency in the Schmandl FDS3 synchriminator. The synchriminator consists of two amplifying channels for amplification of the two 10 MHz inputs, and a discriminator circuit which can be operated either as a frequency discriminator or phase discriminator. In either case, the difference (in frequency or in phase) is converted into a DC voltage and added in series to the reflector voltage as a correction. The positive or negative value of this correction voltage corresponds either to the frequency deviation or phase deviation of the beat signal with respect to the 10 MHz standard, depending on the mode of operation. Since the klystron frequency is dependent on the reflector voltage any variation in the output frequency of the klystron is automatically fed back. We used the PHASE COMPARISON mode of operation of the synchriminator.

The frequency of the klystron is measured with a frequency meter via a frequency converter. The stability of the frequency was better than 1 part in 10^8 while the klystron was locked.

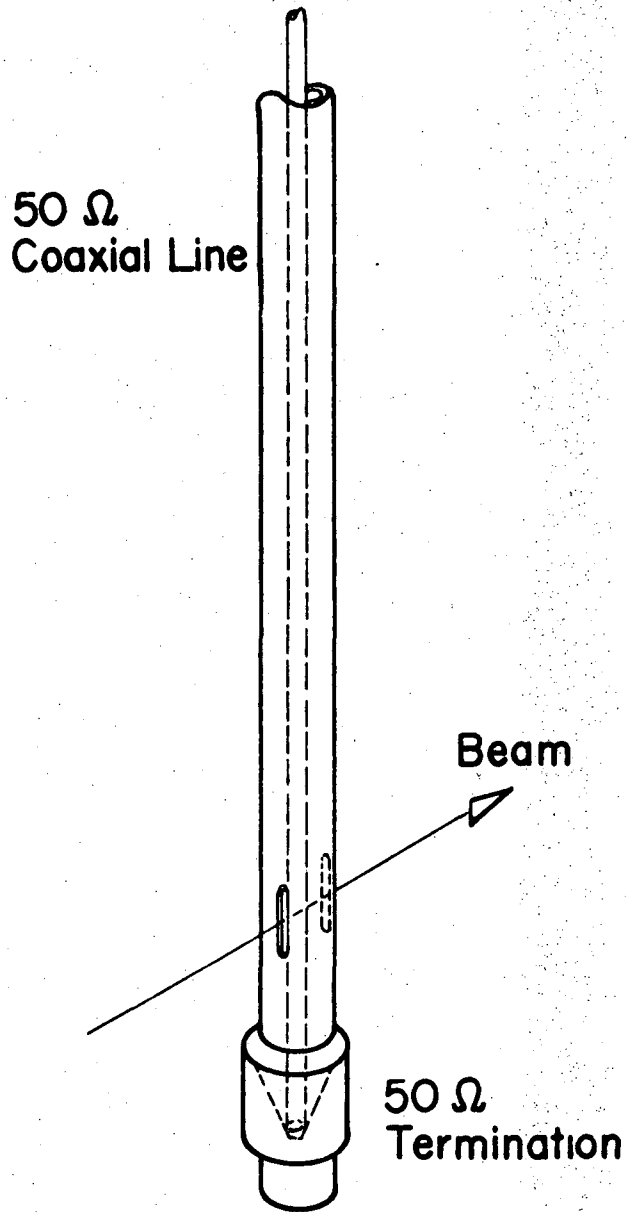
The rf power is leveled in a power leveling loop shown in Fig. 23. The power is controlled with the GAIN switches on the Operational Amplifier and on the TWT (Traveling-Wave-Tube amplifier). The rf power leveling loop consists of a rectifier, which is not shown in Fig. 23,

an operational amplifier and an absorptive modulator. The operational amplifier (which is a DC amplifier) picks up the variations in the signal level at the output of the TWT and feeds it back to the input after some amplification. The absorptive modulator levels the rf without frequency pulling, in this way, any change in the rf level is detected, amplified and fed back through the modulator, thus holding the level constant.

The power going to the hairpin is measured with an rf power meter just before the hairpin. A 20db (1% of the total power) directional coupler is used to measure the power. A 50Ω terminated hairpin was used in most of this work, but we also tried to construct a stripline hairpin for the first time in Berkeley. Figure 24 shows a sketch of the 50Ω terminated hairpin. A 50Ω termination (characteristic impedance of the line) reduces the reflected power from the end of the hairpin, and consequently eliminates standing waves in the rf region. If the termination is ideal, the wave pattern in the rf region has the traveling wave form.

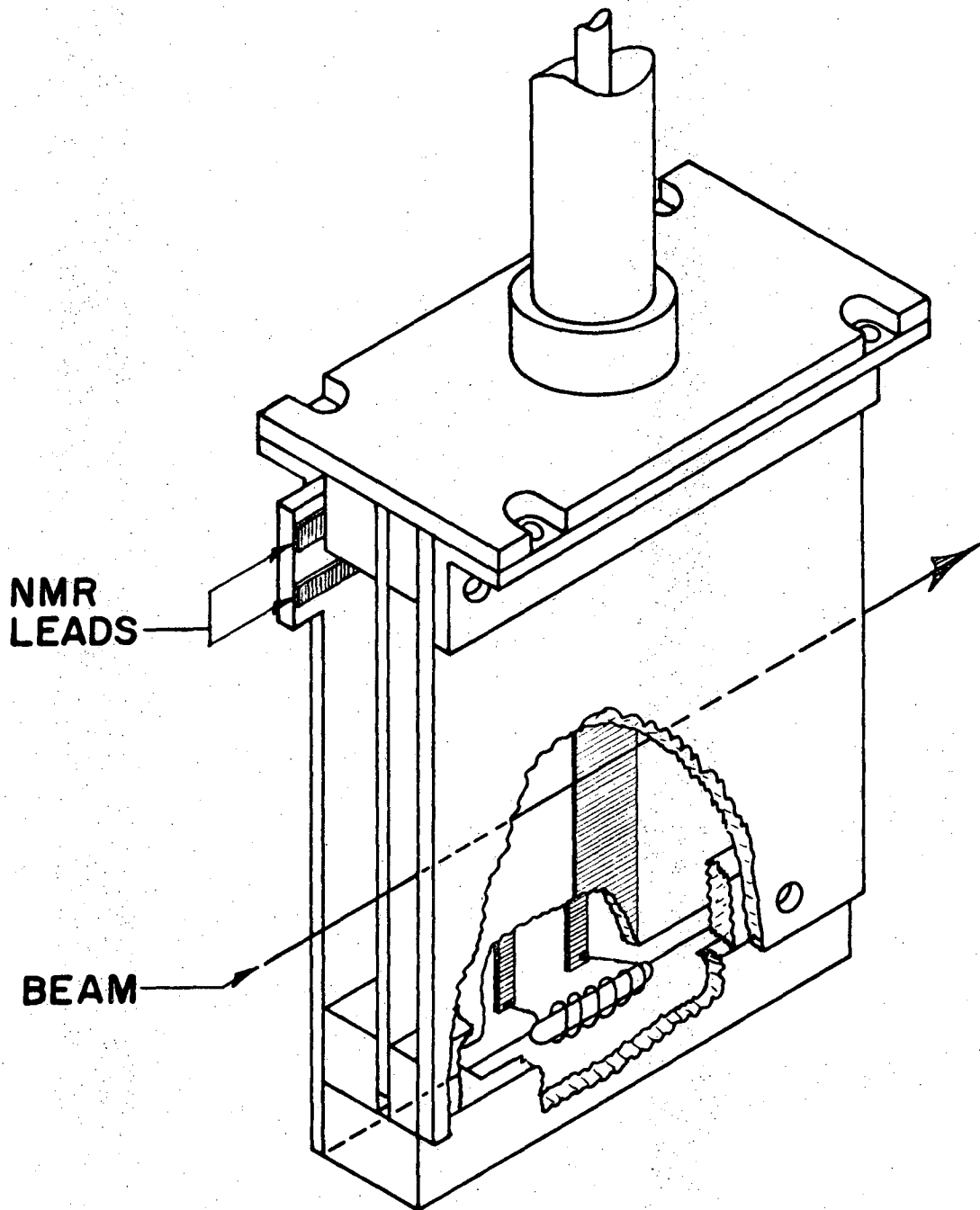
The stripline hairpin we constructed is shown in Fig.25. The reason for constructing such a hairpin was to obtain a better π -transition field configuration in the rf region and reduce the Millman effect, which is resonance asymmetry that occurs when the direction of the oscillatory field varies along the length of the rf region.

Striplines, microstrips, and slab lines are newly used electromagnetic wave propagation devices which are replacing the commonly used coaxial lines for the TEM propagation mode. The propagation losses in these lines proves to be smaller than those in commonly used coaxial lines.



XBL 718-1275

Fig.24. 50-ohm terminated hairpin.



XBL 737-928

Fig.25. The stripline hairpin with NMR probe. The scale is about twice that of the real construction, and some details are not shown to preserve the clarity of the figure.

The theory and application of this new circuit design technique is given in the microwave literature.^{59,60} The structure of a stripline consists of a very thin plate of conductor on a dielectric substrate. The thickness of the conducting copper plate goes down to a fraction of a mil. The substrates are alumina (Al_2O_3), rutile, or any other dielectric material. We used 1/32" substrates in our construction and assembled them with nylon screws in order not to disturb the magnetic field in an area so close to the rf region. The beam width and height are limited by a hairpin-attached collimator which is not shown on the figure. The height and the width of the collimator slit are 3/16" and 1/16", respectively. The thickness of the copper conductor is 2 mils. The copper is etched away in the shape required, using $FeCl_3$ baths for the etching process. The width of the center conductor is about 10mm. Unfortunately, an unexplained structure appeared in the stripline hairpin resonances. The structure seemed to be a satellite-line under the resonance peak, and the closer to the saturation power the more dominant the asymmetry. A probable reason may have been rf leaking out of the hairpin structure, so we wrapped the rf region with a copper foil containing slots for the beam, but it did not help much. The behavior of the asymmetry was such that it was difficult to see the effect of field orientation or hairpin alignment on the asymmetry. Altogether, the results of the stripline hairpin were in good agreement with the results of the 50 Ω terminated hairpin, which is the most trusted hairpin in the atomic beam group. This agreement means that the asymmetry did not pull the resonance frequency much.

Table III shows a comparison of the two hairpins in terms of resonance widths. By looking at the table, one sees that the stripline

hairpin resonance is about three times sharper than the 50Ω terminated hairpin resonance, while the rf region is doubled roughly. We think that this difference in factors is due to a better π -transition field configuration in the stripline hairpin.

Table III. Full Widths at Half Maximums (kHz) for the hairpins we used.

Hairpin	RF region	Rb ⁸⁵	He*	Cs ¹³³	He*
50Ω Coaxial	6 mm	40	100	25	80
Stripline	10 mm	15	35	-	-

Because of the asymmetry in the resonances, we did not carry out a study with the stripline hairpin using Cs¹³³ as calibration.

The stripline was a shorted hairpin, so the wave pattern in the rf region had a standing wave form, whereas the pattern was a travelling wave using the 50Ω terminated hairpin. The termination of the stripline hairpin in its characteristic impedance was another technical problem. In order not to slow down the course of the experiment, we postponed the termination problem to future studies. Perhaps the asymmetry will disappear after appropriate termination of the stripline.

A power dependence study for each hairpin was made separately before taking any "good" data. In these studies we changed the rf power from a minimum value, which is just enough to see the resonance, to a maximum value, which certainly saturates both resonances. Then we plotted the resonance amplitude as a function of rf power and saw the expected behavior of the power dependence. Using those plots, we chose the rf power for the

"good" data at a point below where saturation starts. Typical rf powers for the "good" data were 50 mW for the 50Ω terminated hairpin and 2 mW for the stripline hairpin.

6. Experimental Procedure

We preferred to take data after 6 o'clock in the evenings because the switching transients in the building and moving any magnetic piece in the laboratory affected the C-field. We tried not to move any metallic piece while counting was in progress. The C-field was monitored continuously with one of the two NMR systems while data were collected. Figure 26 shows a chart recorder trace of the monitored field during a run.

We performed a run using the following sequence of tasks:

- a) Field is shimmed coarsely (inhomogeneity: 1 part in 10^6). This takes about a day if everything goes well. (see Figs. 20 and 21).
- b) Diffusion pumps are turned on at least 5 hours prior to the assumed time of START, and liquid nitrogen traps are filled when the pressure is less than 10^{-3} torr.
- c) Frequency system is turned on about 3 hours prior to the assumed time of START.
- d) Calibration oven power supply is turned on about 30 min. prior to START.
- e) Fine shimming (inhomogeneity: less than 2 parts in 10^7 over rf region) is done and the FINAL form of the field homogeneity is recorded on the chart recorder output. The horizontal and the vertical fine plots (see Fig.22) are glued into the LOG-BOOK.
- f) He beam and the metastabilizing electron gun are turned on.
- g) If the vacuum is OK, the data collection system is turned on.

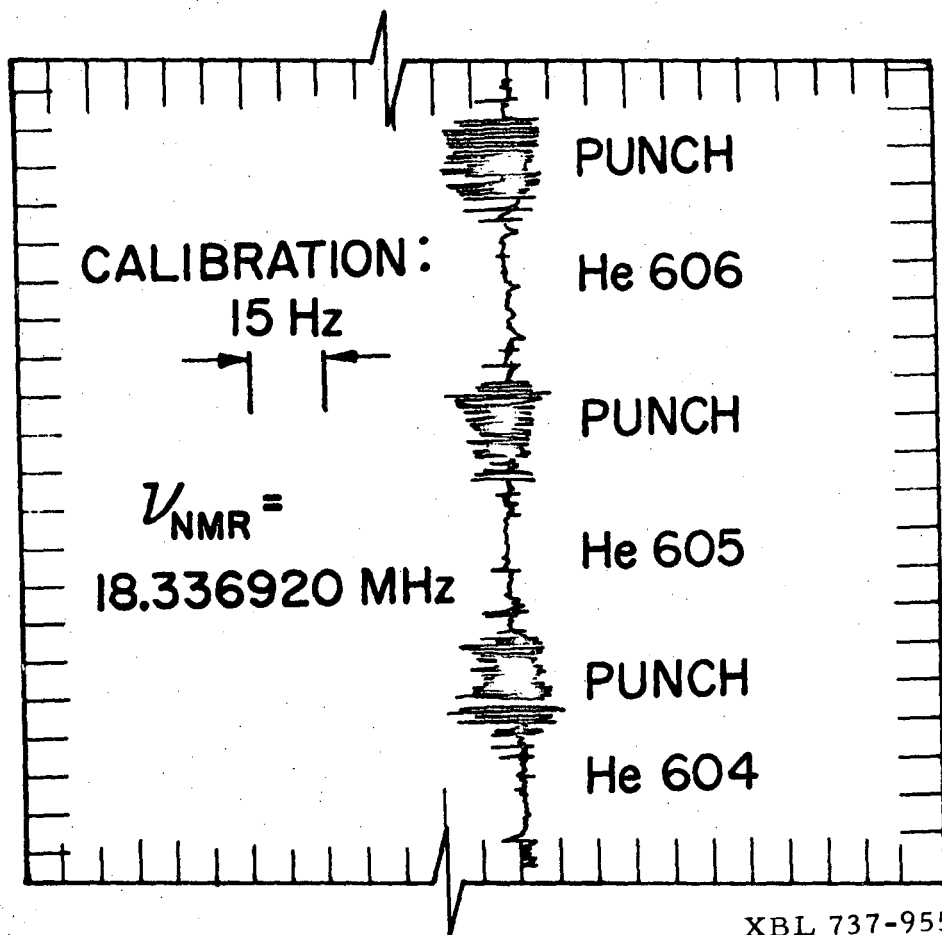
h) A run information table (see Table IV) is completed and glued into the LOG-BOOK.

i) The initial frequency and the increment (channel width) are entered into the computer (PDP11). In doing this one makes use of the field information, obtained from the NMR field reading system, for the chosen hairpin position.

j) And RUN is carried out, as explained in the section on Detectors and the Data Collection System.

Each run took about 5 hours if everything went well. In each run we made about 20 simultaneous recordings of the helium and the calibration resonances. Using the key-punch output with a computer program called LFIT, the g_J value was obtained. An outline of the computational program is given in Appendix B. A list of constants which are used in computation is given in Appendix C.

Systematic error is one of the important uncertainties that plague an experimenter. Although the discussion of the sources of systematic errors is left to the next chapter, it should be mentioned that under various run conditions the measurement was repeated 629 times in this experiment.



XBL 737-955

Fig.26. A chart recorder trace of the monitored field.

This monitor was done with the side-NMR probe while the field was locked with the central probe. The effect of the punching machine on the field locking system is seen here.

Table IV. A sample of RUN conditions.

$g_J(\text{He}, 2^3S_1) / g_J(\text{Rb}^{85}, 2S_{1/2})$ Measurement

Date: Feb. 27, 1973

Freq. Scan, low lock points:

Initial: 383.872136 MHz

Harmonic: 23

Final: 383.883640 MHz

Synthesizer Scan:

Initial: 492.7255000 MHz

Harmonic: 18

Final: 492.7402000 MHz

Magnet Currents:

A: 5 Amps.

B: 5 Amps.

C: 3-12-36 (setting)

Field Orientation:

Normal: Reverse:

" : " :

" : " :

Shim Currents: Hor. : 6 mAmps.

Vert. : 24.4 mAmp Curva. : 44 mAmps.

NMR Freq. Lock: Side: =13.459592 MHz

Center: =13.459766 MHz

Source Position: 2.00

Detector Position: 1.688

Source Dewar: Warm:

Cold:

Source Pressure: 95 torr

RF Power: 50 mW

Hot Wire Curr.: 2.8 Amps

Pressure Range: 10⁷ torr

He Count Rate: 20,000/.3 sec

Rb. Count Rate: 1200/.3 sec

Gun Emission Curr. : 60 mAmps

Gun Voltage: 100 V DC

Estimate of Field Stability (from NMR) : (See Figs. 20, 21, and 22)

Field Homogeneity (from field mapping) : (See Figs. 20, 21, and 22)

III. DATA, ANALYSIS, AND RESULTS

1. Introduction

The program LFIT computes the magnetic field from the calibration resonance and evaluates $g_J(\text{He})$ from Eq. (19a). Then the program finds the ratio of $g_J(\text{He})/g_J(\text{calibration})$, and combining this with $g_J(\text{calibration})/g_J(\text{H})$, which is supplied from references 1, 2 and 3 for Rb^{85} and Cs^{133} , then, obtains the $g_J(\text{He})/g_J(\text{H})$ ratio. This ratio is a number slightly less than unity. In the common literature the ratio is expressed in terms of its deviation from unity "a", as in Eq. (40). The computational program is directed to find out the value of "a". If one wants to work backwards from the final value of "a", one finds the numbers corresponding to $g_J(\text{He})/g_J(\text{Rb}^{85})$ and $g_J(\text{He})/g_J(\text{Cs}^{133})$. These results will be given later in this chapter.

In order to discover possible systematic effects, we worked at the four available orientations of the static magnetic field and the hairpin (++, +-, -+, --) where + and - represent the two possible orientations. Sources of error and the attempts to eliminate them will be discussed later.

2. 5-Parameter Analysis

We processed the data by a least squares fitting of a Lorentzian line shape. Firstly, the 5-parameter program (Math-5) was used, and secondly, we checked the results with a 4-parameter program (Math-4). The parameters

in the Lorentzian distribution function (see appendix B) are the amplitude $P(1)$, the width $P(2)$, the center $P(3)$, the background $P(4)$, and the slope of the baseline $P(5)$.

The computer output of the data for a particular measurement includes a Lorentzian fitted curve for both isotopes, the calculated magnetic field from the calibration resonance, and the results $g_J(\text{He})$ and "a", with the standard deviation and standard deviation of the mean for that group of data, taken under a specific set of conditions. When starting to analyse the results, we searched through all the computer outputs and examined each resonance one by one, using the following criteria.

- 1) Resonance symmetry
- 2) Least squares fitting
- 3) Counting statistics
- 4) Side-peak problem
- 5) Slope of the baseline
- 6) Obviously poor result (something grossly wrong).

Then we made a list of resonances, labeling each observation with the above criteria. Leaving out the ones which have at least one of the defects mentioned above, we obtained 322 "good" resonances for the 50 Ω terminated hairpin and 96 for the stripline hairpin, out of a total of 629 resonances, in the case of the 5-parameter fit. Then these good results were preprocessed with another program called g_J -STATISTICS. This short program, which produces average values and errors, is given at the end of appendix B. The results of the 5-parameter analysis are given in Table V and a histogram is given in Fig. 27. In this selection we eliminated all slopes greater than 50, with a few exceptions for which the slope was the only problem and the resonance looked good. The slope in counts per channel

measures the rate of growth of background counts along the baseline and gives an indication of transient fluctuations in beam intensity during a scan in one particular direction.

In order to be sure about the final average, we made another elimination for the 5-parameter fit results. This time we left out the ones that had a baseline slope greater than 25. This reduced the number of "good" resonances to 208 for the 50 Ω terminated hairpin, and 59 for the stripline hairpin. The averages of this elimination scheme are given in Table VI and a histogram is shown in Fig. 28.

As a final step for the 5-parameter analysis, we separated the dome-field and the dish-field results among the ones which had a baseline smaller than 25, and ran them with the g_J -STATISTICS program separately to search for any systematic change. The results are given in the first half of Table VII. Unfortunately, we did not study the dome-field case for the Rb⁸⁵ calibration because of time limitations, but we have good enough evidence that it would not change the results.

3. 4-Parameter Analysis

In order to gain further confidence in the final results, we changed the fitting routine in the program from Math-5 to Math-4. This omits the baseline slope, $P(5)$, from the fitting process. Then we ran all of the data with the new program. Comparing the results of the two analysis, we discovered that resonances which had a large slope (say $P(5) > 75$) in the 5-parameter analysis, gave very different results in the 4-parameter analysis. But among the resonances which we entitled "good", only two observations were so. Leaving out those two results, we averaged the 4-parameter fitted results with the g_J -STATISTICS program. These averages are given in Table VIII.

We also checked the dome-field and the dish-field resonances with the 4-parameter fitted program; the results are given in the second half of Table VII.

Table IX shows the summary of the results from all the analyses. Each line in that table includes all four permutations of field direction and HP position.

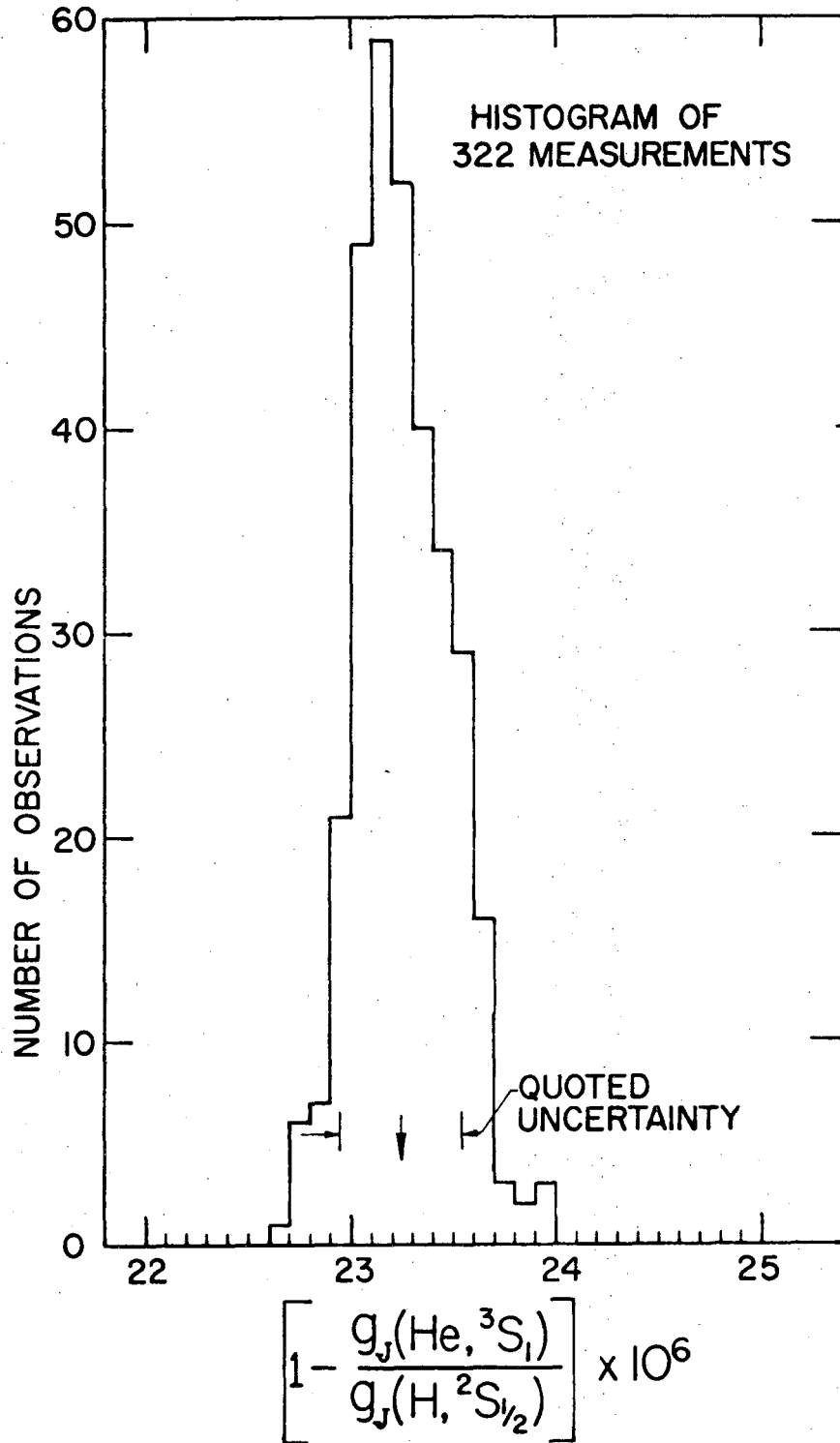
Table V. $g_J(\text{He}, ^3\text{S}_1)/g_J(\text{H}, ^2\text{S}_{\frac{1}{2}})$ measurement; 5-parameter analysis results for the 50 Ω terminated and stripline hairpins. The baseline slope is <50 in absolute value with a few-exceptions for which the resonances looked good.

50 Ω HP RESULTS

CALIB-RATION	NUMBER OF OBSERVATIONS	FIELD ORIENTATION	HP POSITION	a (ppm) AVG	SD	SD OF MEAN
Rb ⁸⁵	140	-	+	23.16	.20	.02
	22	-	-	23.33	.19	.04
	25	+	+	23.24	.14	.03
	10	+	-	<u>23.25</u>	.13	.04
				avg=23.25		
Cs ¹³³	22	+	+	23.34	.33	.07
	23	+	-	23.30	.37	.08
	58	-	+	23.19	.20	.03
	22	-	-	<u>23.14</u>	.21	.04
				avg=23.25		
TOTAL	322			$\bar{a} = 23.25$ ppm.		

STRIPLINE HP RESULTS

Rb ⁸⁵	11	+	+	23.42	.37	.11
	3	+	-	23.91	.04	.02
	67	-	+	22.95	.17	.02
	<u>15</u>	-	-	<u>23.16</u>	.09	.02
TOTAL	96			avg=23.36		



XBL 737-936

Fig.27. Histogram of the observations in Table V for the 50Ω terminated HP.

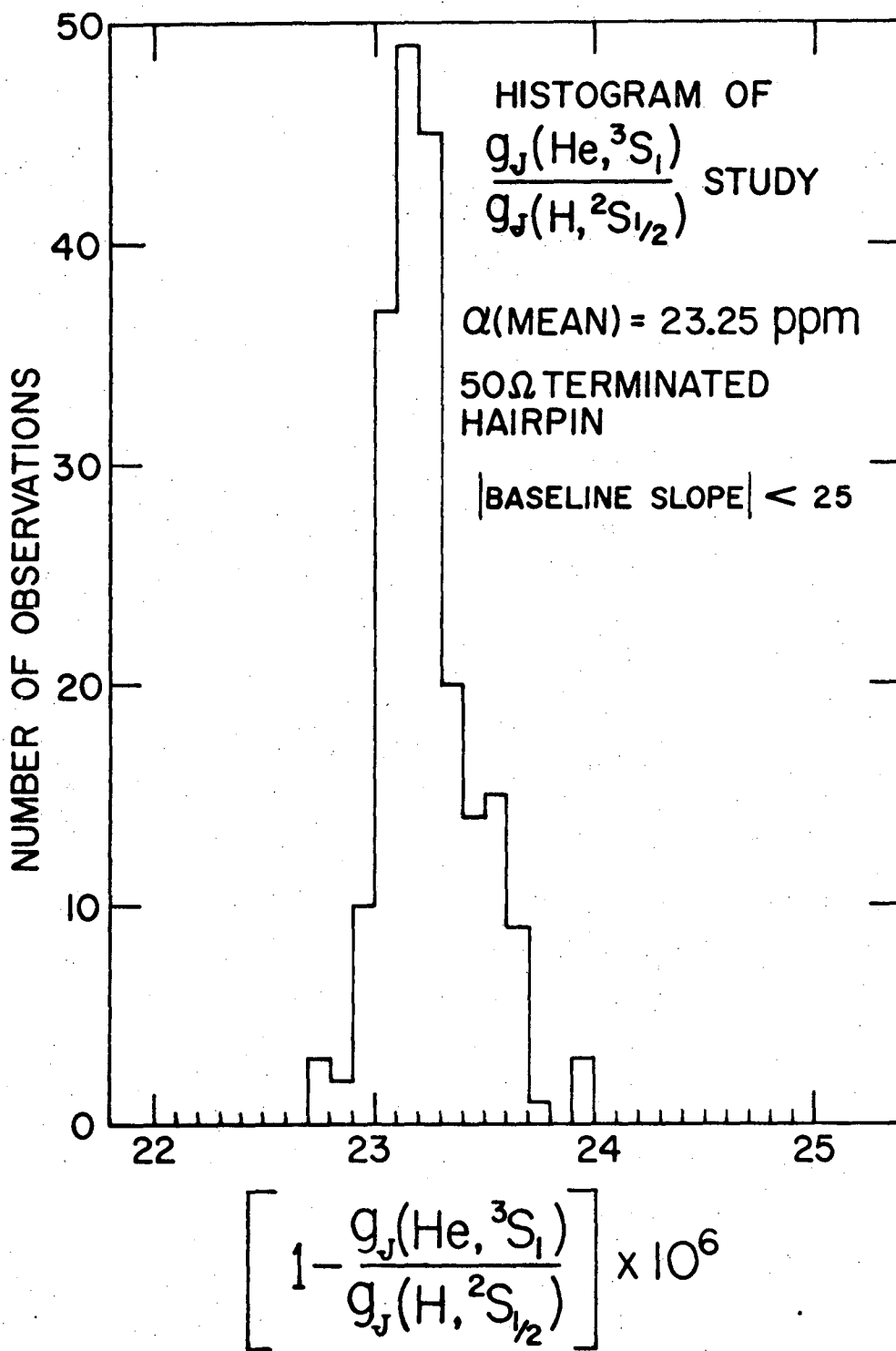
Table VI. $g_J(\text{He}, ^3\text{S}_1)/g_J(\text{H}, ^2\text{S}_{\frac{1}{2}})$ measurement; 5-parameter analysis results for 50 Ω terminated and stripline hairpins. The baseline slope is <25 in absolute value.

50 Ω HP RESULTS

CALIB- RATION	NUMBER OF OBSERVATIONS	FIELD ORIENTATION	HP POSITION	a (ppm) AVG	SD	SD OF MEAN
Rb ⁸⁵	64	-	+	23.10	.10	.01
	12	-	-	23.25	.17	.05
	16	+	+	23.24	.12	.03
	9	+	-	23.23	.12	.04
				avg=23.21		
Cs ¹³³	20	+	+	23.33	.33	.07
	20	+	-	23.29	.37	.08
	49	-	+	23.17	.16	.02
	18	-	-	23.18	.14	.03
				avg=23.25		
TOTAL	208			$\bar{a} = 23.23$ ppm		

STRIPLINE HP RESULTS

Rb ⁸⁵	3	+	+	23.15	.07	.04
	3	+	-	23.91	.04	.02
	50	-	+	22.96	.14	.02
	3	-	-	23.05	.01	.01
TOTAL	59			avg=23.27		



XBL 737-935

Fig.28. Histogram of the observations in Table VI for the 50 Ω terminated HP.

Table VII. $g_J(\text{He}, ^3S_1)/g_J(\text{H}, ^2S_{1/2})$ measurement; 500 terminated hairpin, dome and dish fields Cs^{133} calibration results for the observations which have baseline slope <25 in absolute value.

5-PARAMETER LORENTZIAN FIT

LEVELED FIELD	NUMBER OF OBSERVATION	FIELD ORIENTATION	HP POSITION	a (ppm)		SD OF MEAN
				AVG	SD	
D	12	+	+	23.56	.21	.06
O	12	+	-	23.57	.11	.03
M	34	-	+	23.19	.12	.02
E	9	-	-	23.11	.13	.04
				avg = 23.36		
D	8	+	+	23.00	.07	.03
I	8	+	-	22.86	.09	.03
S	15	-	+	23.14	.23	.06
H	9	-	-	23.24	.11	.04
				avg = 23.06		
TOTAL	107			$\bar{a} = 23.21$		

4-PARAMETER LORENTZIAN FIT

D	12	+	+	23.55	.20	.06
O	11	+	-	23.50	.05	.01
M	34	-	+	23.21	.17	.03
E	9	-	-	23.09	.10	.03
				avg = 23.34		
D	8	+	+	22.91	.06	.02
I	8	+	-	22.87	.11	.04
S	15	-	+	23.17	.20	.05
H	9	-	-	23.16	.11	.04
				avg = 23.03		
TOTAL	106			$\bar{a} = 23.18$		

Table VIII. $g_J(\text{He}, ^3\text{S}_1)/g_J(\text{H}, ^2\text{S}_{\frac{1}{2}})$ measurement; 4-parameter analysis results for the 50 Ω terminated and stripline hairpins. The baseline slope is <50 in absolute value, with a few exceptions for which the resonances looked good.

CALIB-RATION	NUMBER OF OBSERVATION	FIELD ORIENTATION	HP POSITION	a (ppm) AVG	SD	SD OF MEAN
Rb ⁸⁵	140	-	+	23.10	.14	.01
	22	-	-	23.22	.13	.03
	25	+	+	23.21	.15	.03
	10	+	-	23.19	.10	.03
				avg=23.18		
Cs ¹³³	22	+	+	23.27	.35	.07
	22	+	-	23.25	.32	.07
	58	-	+	23.24	.23	.03
	22	-	-	23.08	.21	.04
				avg=23.21		
TOTAL	321			$\bar{a} = 23.20$		
STRIPLINE HP RESULTS						
Rb ⁸⁵	10	+	+	23.49	.38	.12
	3	+	-	23.86	.09	.06
	67	-	+	22.93	.16	.02
	15	-	-	23.08	.04	.01
Total	95			avg=23.34		

Table IX. The summary of the results obtained by different analyses. This table is a summary of the tables V through VIII.

50Ω HP RESULTS

TYPE OF ANALYSIS	LEVELED FIELD	SLOPE	CALIBRATION	^a avg.
Math-5	DOME	<50	Rb ⁸⁵	23.25
"	DOME & DISH	"	Cs ¹³³	23.25
"	DOME	<25	Rb ⁸⁵	23.21
"	DOME & DISH	"	Cs ¹³³	23.25
"	DOME	"	"	23.36
"	DISH	"	"	23.06
MATH-4	DOME	-	"	23.34
"	DISH	-	"	23.03
"	DOME	-	Rb ⁸⁵	23.18
"	DOME & DISH	-	Cs ¹³³	23.21

STRIPLINE HP RESULTS

MATH-5	DOME	<50	Rb ⁸⁵	23.36
"	"	<25	"	23.27
MATH-4	"	-	"	23.34

4. Results

After the preceding analyses we quote the g_J ratio of helium in its $1s2s, ^3S_1$ metastable state to the g_J of hydrogen in its ground state as follows:

$$\frac{g_J(\text{He}, ^3S_1)}{g_J(\text{H}, ^2S_{1/2})} = 1 - 23.25(30) \times 10^{-6} \quad (59)$$

Combining this with the results given in refs. 4 and 5 we find the absolute value of $g_J(\text{He})$ in the 3S_1 state as follows:

$$g_J(\text{He}, ^3S_1) = -2.002\ 237\ 35(60) \quad (60)$$

As was mentioned earlier, the computer program was directed to evaluate the $g_J(\text{He})/g_J(\text{H})$ ratio which involves other numbers (see Appendix C) besides our $g_J(\text{He})/g_J(\text{calibration})$ ratios. Extracting those intermediate numbers from the final result (Eq.(59)), we find the measured ratios of $g_J(\text{He})/g_J(\text{calibration})$ as follows.

$$\frac{g_J(\text{He}, ^3S_1)}{g_J(\text{Rb}^{85}, ^2S_{1/2})} = 1 - 46.83(30) \times 10^{-6} \quad (61)$$

and

$$\frac{g_J(\text{He}, ^3S_1)}{g_J(\text{Cs}^{133}, ^2S_{1/2})} = 1 - 151.28(30) \times 10^{-6}. \quad (61a)$$

5. Sources of Errors and Attempts to Eliminate Them

a. Systematic Errors

The systematic error was the main thing we struggled with throughout the experiment. To eliminate it from the final result we took data under various run conditions, of which a sample was given in Table IV.

In our experiment, the things that might affect the accuracy of the result systematically are grouped and listed below:

- 1) Orientation of the C-field
- 2) Original form of the leveled field (dome, dish)
- 3) Hairpin position
- 4) Calibration isotope

and

- 5) Microwave power
- 6) Beam intensity
- 7) Temperature of the beam
- 8) Shim coils
- 9) Geometry
 - a) Source position
 - b) Detector position
 - c) Beam trajectory (A and B magnet currents)
 - d) Beam flag position

and so on.

The effects arising from the first four of the above list are reduced by reversing the conditions, that is, to change the direction of the magnetic field in the C-magnet, to turn the hairpin 180° around its axis, and to use another calibration isotope.

The systematic errors coming from the rest of the list are minimized by finding an optimum condition (at least a condition close to the optimum) of operation for the items in the list, varying them one by one. For example, an optimum rf power seemed to be 50mW for the terminated hairpin, 2mW for the stripline hairpin. Above those powers saturation

might start. An optimum intensity is that for which one has a beam good enough to see the resonance without exceeding the maximum count rate of the counter.*

The basic principles of gas-kinetics led us to use a cold (liquid nitrogen temperature) beam instead of a warm (room temperature) beam.

The presented geometry is determined by varying the factors under the topic Geometry. We looked at the He beam-profile by moving the detector across the beam and determined the He detector position from the profile. We were not able to put the He detector at the maximum of the profile because of the calibration beam and the physical size of the two MEMs.

Crosstalk Substraction

One more systematic error might be the crosstalk between beams. By the word crosstalk we mean the unwanted registration of calibration atoms by the helium detection channel or vice-versa. After setting up the geometry, we checked the crosstalk in both directions by shutting off one source at a time. At the end of this check we found out that no helium atoms were detected by the calibration detector but some calibration atoms were recorded by the helium detector. A typical crosstalk is 300 counts on a peak out of 45,000 counts of helium. Because of these unwanted counts we took crosstalk data at the end of each run, to be processed later. Crosstalk data consists of one more recording of a

*We used Hewlett-Packard 5202L and 5203L Scaler-Timers. The stated maximum count rate of these devices is 5×10^6 counts/sec. The counting rate for the He beam was 6×10^4 counts/sec, which is well below the limit of the scaler.

resonance while the helium beam is turned off, without changing any other condition. Later on we changed the 5-parameter fitted program in such a way as to subtract the crosstalk counts from the helium resonances. Then we executed each run data and its crosstalk with the crosstalk-processing program. We found out that the effect of the crosstalk correction on the result is less than 2 parts in 10^8 which is 15 times smaller than our final quoted error.

b. Random Errors

Some random errors were eliminated while the data were being taken. If something abnormal happened to cause an effect big enough to see on the displayed resonance, that particular observation was discarded immediately. If the effect was not big enough to see by the human eye, then it went into the data, of course. But the computer output tells us something about those events. For example, a large baseline slope means that the count rate (beam intensity) increased (or decreased depending on the sign of the slope) during one direction of the scan, resulting in a slope for that particular resonance. This is why we discarded quite a number of resonances with large slopes while we were analyzing the data and the results.

The "obviously poor" results were certainly due to the random effects.

6. Confirmation by Another Program

In order to check the sensitivity of the results to the computational technique, we ran some of the data with a new and different program in which the magnetic field cancels out analytically. This new program was developed by Prof. Howard A. Shugart. The computer output of the new computational technique confirms the LFIT technique well beyond the

Table X. Sensitivity of the result to any systematic effect which might cause a frequency pulling in one direction by an amount 1kz.

$\nu(\text{Rb})$ MHz	$\nu(\text{He})$ MHz	$\delta\nu(\text{Rb})$ kHz	$\delta\nu(\text{He})$ kHz	$1-g_J(\text{He}, ^3S_1)/g_J(\text{H}, ^2S_{1/2})$
8859.599873	8859.591744	0	0	23.15 ppm
8859.598873	8859.591744	1	0	23.03 "
8859.599873	8859.590744	0	1	23.26 "
8859.598873	8859.590744	1	1	23.14 "

precision of the experiment.

This new program takes much less execution time in the computer, and because of this feature we made a further test of sensitivity of the results for a frequency shift due to the asymmetry, side bands, crosstalk or any other reason. To observe this effect, we purposely changed the central frequency by an amount $\delta\nu$. Table X shows the effect of these possible frequency shifts on the result of a particular resonance. We chose $\delta\nu = 1\text{kHz}$, which is roughly 1/100 of the line width of He and 1/30 of the line width of Rb.

7. Discussion of the Results

The results we have quoted were obtained with a 50Ω terminated HP, the most trusted rf loop at Berkeley. For this reason we kept stripline HP results apart from the terminated HP results. But stripline HP results are another confirmation for our final result. The average of stripline HP results is 23.32 ppm. The disagreement of this number with our final result for terminated HP is 7 parts in 10^8 which is well beyond the precision of the experiment.

If we quoted the error as ± 0.20 ppm this would cover all the averages we have arrived at in different analyses (see table IX), including the stripline HP results. But, owing to our experience with systematic effects, we quoted it as ± 0.30 ppm, sacrificing some precision. With this uncertainty our result is still 5/3 and 8/3 times more precise than Leduc's¹⁶ and Drake's¹⁵ experimental results, respectively.

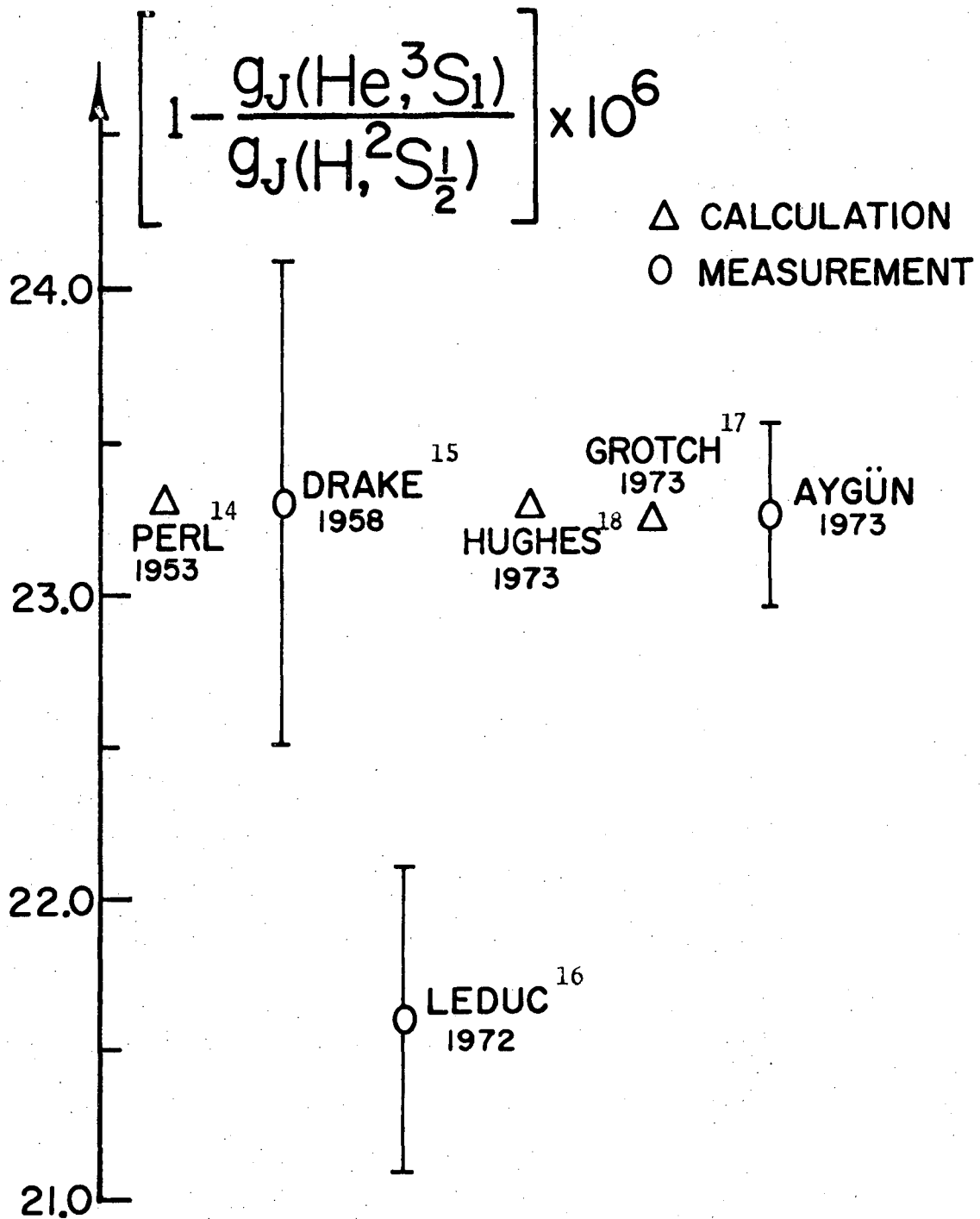
Our result resolves the discrepancy between the two previous experimental results in favor of the old atomic beam value. We heard from Prof. Brossel (see Appendix A2) that his group may attempt to improve

their result. The latest theoretical calculations have shown that the neglected terms in previous calculations are not large enough to eliminate the discrepancy as was speculated by the Paris group.

There is a perfect agreement between our result and three existing theoretical calculations. This agreement is an experimental test of the validity of quantum electrodynamic theory.

Figure 29 shows overlapping of error bars among the various $g_J(\text{He}, ^3S_1)/g_J(\text{H}, ^2S_{1/2})$ ratio studies both theoretical and experimental. The error bars of the theoretical studies are not shown in that figure, because they are less meaningful than the experimental error bars. The very first experimental result ($a=11 \pm 16$) by Hughes¹³ and his coworkers is not shown on that figure, but one can plot it in his mind on the figure roughly; its error bar does overlap Leduc's region, but the precision in that determination was very poor compared with later studies.

QED calculations of the metastable g_J -helium include the corrections of the order of α^3 . We believe that the second phase of this experiment in Berkeley may be accurate enough in precision to distinguish the effect of the α^3 terms.



XBL 737-929

Fig.29. Experimental and theoretical determinations of the helium-hydrogen g-factor ratio. This figure shows the discrepancy between the result of Ref. 16 and other results.

APPENDIX A1

THE PENNSYLVANIA STATE UNIVERSITY
104 DAVEY BUILDING
UNIVERSITY PARK, PENNSYLVANIA 16802

College of Science
Department of Physics

Area Code 814
863. 0007

Dr. B. D. Zak
Physics Department
University of California
Berkeley, CA 94720

Dear Bernard,

Roger Hestrom and I have just completed a preliminary calculation of $g_J(\text{He } 2^3S_1)$ which includes terms of relative order α^3 and $\alpha^2 m/\mu$. We find

$$g_J(\text{He } 2^3S_1) = g_0 (1 - 40.92434 \times 10^{-6})$$

This represents the result using the latest value of g_0 given in PRL 29, 1534 (1972). Based on this we

get

$$\frac{g_J(\text{He } 2^3S_1)}{g_J(\text{He } 1^3S_2)} = 1 - 23.220 \times 10^{-6}$$

Do you have any preliminary experimental results which either support or refute the above theoretical numbers? I'll send you a preprint as soon as we write things up in final form.

Yours truly,
Howard Grotch

APPENDIX A2

UNIVERSITÉ DE PARIS
ÉCOLE NORMALE SUPÉRIEURE
LABORATOIRE DE PHYSIQUE

PARIS (5^e), le March 12th 1973
24, RUE LOMOND
TEL : 328-07-25
707 42.00

Professor H. SHUGART
Department of Physics
University of California
California 94720
U.S.A.

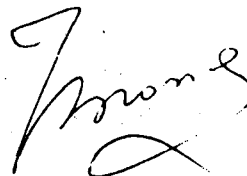
Dear Professor SHUGART,

I have just received a preprint by H. GROTCHE and R.A. HEGSTROM who made a new calculation of the Lande factor of (^4He , 2^3S_1) and find that the old theoretical value is essentially correct and that the neglected terms cannot explain the difference between our result and theory.

I am very anxious to know whether your own measurement has made a substantial progress and what is the result. Our own measurement is rather indirect, because it involves the measurement of the nmr frequency of ^3He . We might try to use as a field reference the ground state of hydrogen directly or the g.s of optically oriented rubidium, but before getting involved in this I would be very interested to know your own result.

I am planning to go to the meeting in VAIL, next June ; I hope to meet you there.

Very sincerely,



J. BROSSSEL

APPENDIX A3

UNIVERSITY OF CALIFORNIA, BERKELEY

BERKELEY • DAVIS • IRVINE • LOS ANGELES • RIVERSIDE • SAN DIEGO • SAN FRANCISCO



SANTA BARBARA • SANTA CRUZ

DEPARTMENT OF PHYSICS

BERKELEY, CALIFORNIA 94720

April 18, 1973

Prof. J. Brossel
Laboratoire de Physique
Ecole Normale Supérieure
24, Rue Lhomond
Paris (5^e) FRANCE

Dear Professor Brossel:

I have delayed answering your letter until I could report some definite results on our atomic beam g_J measurement of the $n = 2$ 3S_1 state of He^4 . Just today Erol Aygun, Bernard Zak and I have decided to end phase I of our work. This involves a one-hairpin measurement at two values of the magnetic field. Although a final analysis on more than 600 resonances is far from complete, we can report that our value is in essential agreement with the old atomic beam measurement and about twice as accurate. I hesitate to quote a number since it may change by a part in 10^7 depending upon how we finally treat the data. The final error bar will be ± 3 to 5 parts in 10^7 .

We plan to begin Phase II of our measurements within a month or two. This will involve an extended c-region and will employ the separated oscillating field method of averaging. We hope to improve the accuracy to the parts in 10^8 realm.

I believe it would be extremely useful to have more direct optical pumping measurements on this quantity. I am aware that Hugh Robinson and Charles Johnson have discussed the possibility of making an optical pumping comparison at Duke University. Also, the combination of your results and the atomic beam measurements also raises the question of possible problems with the two intermediate results you used to obtain the final g_J ratio.

We hope everything is progressing well with you and that you will have a pleasant trip to Vail.

Sincerely,

Howard A. Shugart
Howard A. Shugart

HAS/mn

APPENDIX A4

JOINT INSTITUTE FOR LABORATORY ASTROPHYSICS

UNIVERSITY OF COLORADO
BOULDER, COLORADO 80302



UNIVERSITY OF COLORADO

June 25, 1973



NATIONAL BUREAU OF STANDARDS

Dr. Erol Aygün
University of California
Department of Physics
Atomic Beam Group
Berkeley, California 94720

Dear Dr. Aygün:

I am replying to your letter of June 8.
The Physical Review Letter contains the best
number we have at present. The time scale for a
new number is 8-12 months.

This is probably too late for your needs.
However, if you need the number at that time, please
write to me at Hopkins.

Sincerely yours,

A handwritten signature in cursive script that reads "H. Warren Moos".

H. Warren Moos

HWM:ob

APPENDIX B. OUTLINE OF THE COMPUTER ROUTINE

Here we briefly outline the computational routine. The publications in Refs. 61, 62, and 63 are helpful in understanding it. In this measurement we have used three different programs, namely, *FREQ* for the field tables, *LFIT* for the computation of g_J , and *g_J-STATISTICS* for the statistical manipulation of the "good" results. *LFIT* is the main program we used, so we will outline it here essentially. A reprint of *g_J-STATISTICS* will be included. The program *LFIT* includes the following:

1. To fit the observed data to the Lorentzian line shape.
 2. To calculate the transition frequencies from the fitted curves.
 3. To calculate the magnetic field from the Breit-Rabi formula.
 4. To calculate the g_J , the ratios, and the statistics.
1. Least Squares Fitting to the Lorentzian Line-Shape.

Starting with the principle of least squares we define a function Q as follows:

$$Q = \sum_{i=1}^{50} R_i^2 w_i \quad (62)$$

where R_i is given by

$$R_i = (y_{\text{obs}} - y_L) \quad (63)$$

and w_i is the weight factor for the points on the resonance. We treat all

points equally, so $w_i = 1$. Here y_L is the Lorentzian distribution function defined as

$$y_L = \frac{P_1}{1 + P_2 (w_i - P_3)^2} + P_4 + P_5 w_i \quad (64)$$

where P_1 is the amplitude, P_2 is a parameter related to the width, P_3 is the center, P_4 is the background, P_5 is the slope in the background, w_i is the channel number ($i=1,2,3,\dots,50$).

The mathematics included here is to minimize the function Q of five parameters. The minimum of the function is called the best fit point (BFP) for which

$$\left[\frac{dQ}{dP_j} \right]_{\text{BFP}} = 0, J = 1, \dots, 5 \quad (65)$$

Here we did not take the partial derivative because the fitting routine starts with some initial values ($P_2 = 0.2$, $P_3 = 25$, $P_4 = 0$ and $P_1 = \text{Max.Counts} - \text{Min.Counts}$) which are guessed by the programmer. By changing one of the parameters at a time it tries to find a best fit value for that particular parameter. These iterations continue until the minimum of the function Q is found. The values of the parameters at the minimum of the function Q are the best fit values, and are printed out with the fitted curve. The value of the function itself at the minimum is denoted by χ^2 , which is a test of the goodness of fit, and printed out also.

$$\chi^2 = Q(P_1, \dots, P_5) |_{\text{BFP}} \quad (66)$$

In the form of the Lorentzian distribution function which we have used, the parameter P_2 is related to the width of the resonance as follows:

$$P_2 = \frac{4}{(\text{FWHM})^2}, \quad (67)$$

where FWHM stands for the full width at half maximum. This relation is obtained by assuming a resonance without a background and a slope ($P_4 = P_5 = 0$) and using a value of w_i which makes y_L/P_1 equal to 1/2 in the Lorentzian distribution function.

2. Calculation of Center Frequencies

Once the fitting routine is completed for both resonances separately, the program finds the center frequency by using the best fit position of P_3 in the following equation.

$$\nu_{\text{center}} = [\nu_i \cdot n + (P_3 - 1)\nu_{\text{int}} + 30]\text{MHz}, \quad (68)$$

where P_3 is the position of the resonance center in terms of point numbers, n is a harmonic of the klystron frequency which is determined by the frequency measuring system, ν_{int} is the frequency of one channel, 30MHz comes from the frequency reading system, and ν_i and ν_f are the initial and the final frequencies of the scanned frequency region of the klystron, respectively. The 30MHz is determined by the manner with which the frequency converter is operated. The converter gives us a frequency which is 30MHz below the actual frequency, so we have to add that much to find the actual frequency. In another mode of operation, the 30MHz term must be subtracted. The frequency of one interval (channel) is found from

$$\nu_{\text{int}} = \frac{(\nu_f - \nu_i) \cdot n}{N - 1}, \quad (69)$$

where N is the number of points. For our experiment, $N = 50$, $n = 23$ for

the Rb⁸⁵ calibration, and n = 32 for the Cs¹³³ calibration.

The calculations of the central frequencies are done separately for the calibration and the helium resonances, because the resonances are not exactly superimposed. That means that the field value is not set exactly at the crossing point. The observed frequency from the calibration resonance is used to evaluate the magnetic field in the Breit-Rabi formula Eq.(57), while the helium center frequency goes into the g_J formula Eq.(19a).

3. Calculation of the Magnetic Field

Using calibration constants (see Appendix C) in the Breit-Rabi function Eq.(57), the term values of the calibration atom are calculated. Taking the (+) and (-) signs for initial (F = I + J) and final (F = I - J) Zeeman levels, and using MHz as the unit, the transition frequency is the difference of the term values.

$$\nu_{BR} = X_i - X_f \quad (70)$$

The right hand side of this equation contains the magnetic field as an unknown. At this stage the program has two frequencies to be compared. One is the ν_{obs} from the fitted data; the other is the ν_{BR} from the Breit-Rabi formula. The program determines the magnetic field by comparing these two frequencies in an iterative procedure. From the Breit-Rabi formula we can not express the magnetic field as a simple analytic function of frequency, so we preferred to keep the form of the formula as it is and so the iterative comparison. The procedure is as follows:

First the program starts with a field value which is certainly below the crossing point. These values were 3161 gauss for the Rb⁸⁵ study and 4306 gauss for the Cs¹³³ study. (For the crossing point values see

Table II). Then the program looks at the absolute value of $(\nu_{\text{obs}} - \nu_{\text{BR}})$ and makes that value smaller than a number (0.000001 MHz) by changing the field with finer and finer steps. The starting step is 1 gauss and the stopping step is determined by the limiting number, so the value of the field which satisfies the condition

$$|\nu_{\text{obs}} - \nu_{\text{BR}}|_{\text{CALIB.}} < 1 \text{ Hz.} \quad (71)$$

is used in the g_J formula (Eq.(19a)) and also printed out on the computer output.

4. Calculations of g_J , g_J -Ratios and Statistics

The calculated field and the central frequency of the helium resonance are used in Eq.(19a) with the value of (μ_0/h) (see Appendix C) to evaluate $g_J(\text{helium})$ in its 3S_1 metastable state. Then the $g_J(\text{He})/g_J(\text{calibration})$ ratio is calculated; the $g_J(\text{calibration})$ is supplied as a constant. Finally, the ratio is combined with the $g_J(\text{calibration})/g_J(\text{H})$ ratio to form $g_J(\text{He})/g_J(\text{H})$. Consequently, this final ratio is expressed in terms of its deviations from unity as in Eq.(40).

The standard deviation and the standard deviation of the mean are found from

$$\sigma = \sqrt{\frac{\sum (a_i - a)^2}{N - 1}} \quad (72)$$

$$\sigma_m = \frac{\sigma}{\sqrt{N}} \quad (73)$$

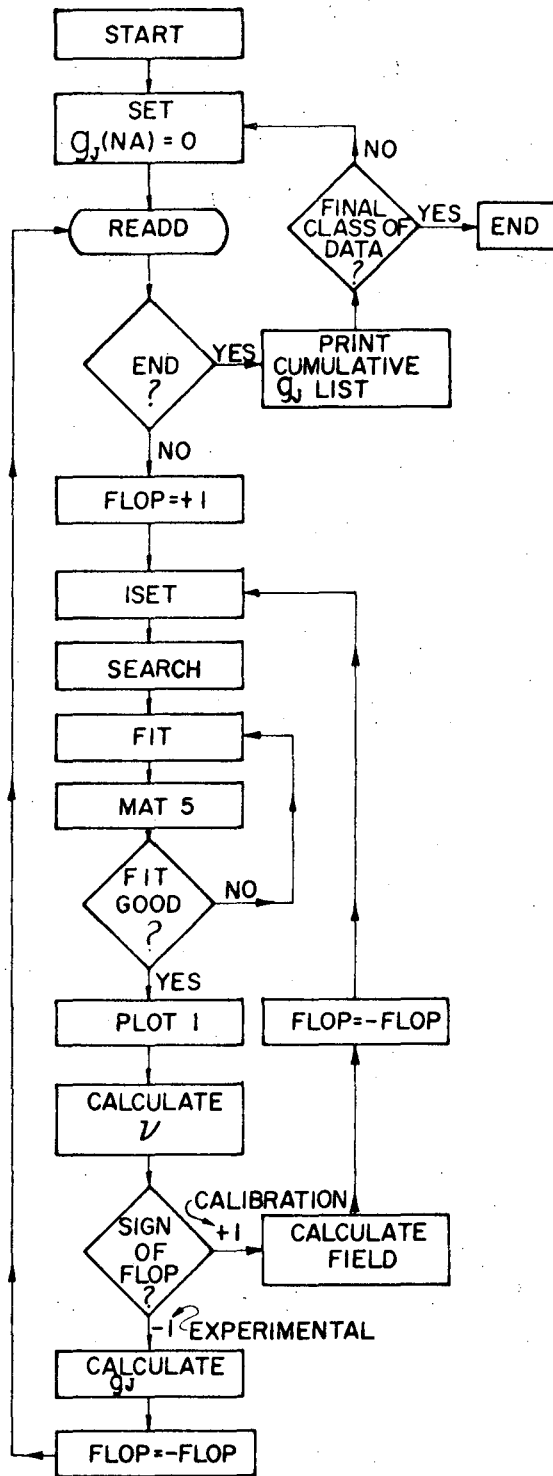
respectively, where N is the number of observations.

The output information of LFIT includes fitted curves, best fit values of the parameters, ν_i , ν_f , ν_{center} (or ν_{obs}), the calculated magnetic field,

$g_J(\text{He})$, $g_J(\text{He})/g_J(\text{H})$, and the deviation "a" with its statistics σ and σ_m .

The final phase of analysis is to process the statistics of the "good" results with another short program called g_J -STATISTICS.

A Flow-Chart of LFIT and the g_J -STATISTICS program are shown on the next two pages.



XBL 737-960

Fig.30. Flow chart of the program LFIT which was used for computing $g_J(\text{He}, 2^3S_1)$.


```
C      PROGRAM HELIUM GJ STATISTICS
C
C      THE FIRST CARD SHOULD BE A COMMENT CARD DESCRIBING THE SET
C      NEXT COME THE DATA CARDS
C      THE RUN NUMBER OCCURS IN COLS 1-6, A IS IN COLS 11-20
C      THE FINAL CARD IN THE SET SHOULD BE BLANK
C
      97 FORMAT (40A2)
      98 FORMAT (1H1, 40A2)
      99 FORMAT (1H0, 10X, 32HRUNS INCLUDED IN THE CALCULATION //)
100  FORMAT (      16,4X,F10.3)
101  FORMAT (1H , 5(1X, 3HHE ,13,F10.3,4X))
108  FORMAT(1H0, 1X, 5HAVG = F10.3,5X,4HSD = F10.3,5X,12HSD OF MEAN =
      1  F10.3)
      DIMENSION AGJ(200), ICOM(40), IRUN(200)
      READ 97, (ICOM(I), I =1,40)
      PRINT 98, ICOM
      PRINT 99
      DO 104 N = 1,200
      READ 100, IRUN(N), AGJ(N)
      IF(AGJ(N)) 103,103,104
103  NGV = N-1
      GO TO 105
104  CONTINUE
105  ANGV = NGV
      PRINT 101, ( IRUN(I), AGJ(I) , I =1, NGV)
      SA = 0.0
      DO 106 N = 1, NGV
106  SA = SA + AGJ(N)
      SAM = SA/ANGV
      SD = 0.0
      DO 107 N =1, NGV
107  SD = SD + (AGJ(N) - SAM)**2
      SD = SQRT(SD/(ANGV - 1.0))
      SDM = SD/SQRT(ANGV)
      PRINT 108, SAM, SD, SDM
      CALL EXIT
      END
```

APPENDIX C. CONSTANTS USED IN THE COMPUTATION

1) Rb⁸⁵ CALIBRATION, STATE: 1²S_{1/2}

$$g_J = -2.002332^{20}$$

$$g_I = 0.00029364 \text{ (in terms of Bohr magneton)}$$

$$a = 1011.910813 \text{ MHz}^{64}$$

$$\Delta\nu = 3035.732739 \text{ MHz}^{64}$$

$$\mu_I = 1.34788 \text{ (in terms of nuclear magneton)}$$

$$g_J(\text{Rb}^{85})/g_J(\text{H}) = 1.0000235851^{1,2}$$

$$I = 2.5$$

$$J = 0.5$$

$$F(1) = 3.0$$

$$M(1) = 0.0$$

$$F(2) = 2.0$$

$$M(2) = -1.0$$

2) Cs¹³³ CALIBRATION, STATE: 1²S_{1/2}

$$g_J = -2.002542^{20}$$

$$g_I = 0.00039900 \text{ (in terms of Bohr magneton)}$$

$$a = 2298.1579425 \text{ MHz}^{65}$$

$$\Delta\nu = 9192.631770 \text{ MHz}^{65}$$

$$\mu_I = 2.5641^{66} \text{ (in terms of nuclear magneton)}$$

$$g_J(\text{Cs}^{133})/g_J(\text{H}) = 1.000128062^{2,3}$$

$$I = 3.5$$

$$J = 0.5$$

$$F(1) = 4.0$$

$$M(1) = -1.0$$

$$F(2) = 3.0$$

$$M(2) = -2.0$$

3) HELIUM CONSTANTS

$$\text{STATE: } 2^3S_1$$

$$I = 0.0$$

$$J = 1.0$$

$$F(1) = 1.0$$

$$M(1) = 1.0$$

$$F(2) = 1.0$$

$$M(2) = 0.0$$

4) GENERAL

$$(\mu_0/h) = 1.399612 \text{ MHz/gauss}^{41}$$

$$M_p/M_e = 1836.12^{41}$$

$$g_J(\text{Rb}^{87})/g_J(\text{Rb}^{85}) = 1.000\ 000\ 004\ 1\ (60)^1$$

$$g_J(\text{Rb}^{87})/g_J(\text{H}^1) = 1.000\ 023\ 585\ 5\ (6)^2$$

$$g_J(\text{Cs}^{133})/g_J(\text{Rb}^{87}) = 1.000\ 104\ 473\ 7(44)^3$$

$$g_J(\text{H})/g_S(\text{e}) = 0.999\ 982\ 31\ (10)^4$$

$$g_S(\text{e}) = -2\ (1.001\ 159\ 656\ 7\ (35))^5$$

REFERENCES

1. C. W. White, W. M. Hughes, G. S. Hayne, and H. G. Robinson, Phys. Rev. 174, 23(1968).
2. W. M. Hughes and H. G. Robinson, Phys. Rev. Letters, 23, 1209(1969).
3. C. W. White, W. M. Hughes, G. S. Hayne, and H. G. Robinson, Phys. Rev. A 7, 1178(1973).
4. J. C. Tiedeman and H. G. Robinson in Atomic Physics 3, Proc. of the 3rd International Conference on Atomic Physics, edited by S. J. Smith and K. G. Walters (Plenum, New York, 1973).
5. S. Granger and G. W. Ford, Phys. Rev. Letters 28, 1479(1972).
6. Triebwasser, Dayhoff, and Lamb, Phys. Rev. 89, 98(1953).
7. E. Lipworth and R. Novick, Phys. Rev. 108, 1434(1957).
8. Koenig, Prodell, and Kusch, Phys. Rev. 88, 191(1952).
9. P. Kusch and H. M. Foley, Phys. Rev. 74, 250(1948).
10. T. Kinoshita and R. Cvitanovic, Phys. Rev. Letters 29, 1534(1972).
11. J. C. Wesley and A. Rich, Phys. Rev. A 4, 1341(1971).
12. Weinstein, Deutsch, and Brown, Phys. Rev. 91, 758(1954).
13. Hughes, Tucker, Rhoderick, and Weinreich, Phys. Rev. 91, 828(1953).
14. W. Perl and V. W. Hughes, Phys. Rev. 91, 842(1953).
15. C. W. Drake, V. W. Hughes, A. Lurio, and J. A. White, Phys. Rev. 112, 1627(1958).
16. M. Leduc, F. Laloe, and J. Brossel, J. Phys. (Paris), 33, 49(1972).

17. H. Grotch and R. A. Hegstrom, Private Communication, Pre-prints (to be published in Phys. Rev. A, August, 1973), see Appendix A1.
18. V. W. Hughes and M. L. Lewis, Bull. Am. Phys. Soc. 18, 120(1973) and pre-prints.
19. "g_J Determination of Na²³ with respect to that of K³⁹", master thesis by E. Aygün at METU, 1966.
20. P. A. Vanden Bout, E. Aygün, V. J. Ehlers, T. Incesu, A. Saplakoglu and H. A. Shugart, Phys. Rev. 165, 88(1968).
21. Powell and Craseman "Quantum Mechanics", (Addison Wesley, Mass. 1961).
22. E. Merzbacher, "Quantum Mechanics" (John Wiley and Sons, Inc. New York, 1970).
23. A. Messiah, "Quantum Mechanics" Vol. II, (North Holland Publishing Company, Amsterdam, 1962).
24. "Quantum Mechanics of One-And-Two-Electron Atoms", by H. A. Bethe and E. E. Salpeter (Academic Press Inc. 1957).
25. G. Breit, Phys. Rev. 34, 553(1929); 36, 383(1930); 39, 616(1932).
26. G. W. F. Drake, Phys. Rev. A 3, 908(1971).
27. W. Perl, Phys. Rev. 91, 852(1953).
28. A. Abragam and J. A. Van Vleck, Phys. Rev. 92, 1448(1953).
29. K. Kambe and J. H. Van Vleck, Phys. Rev. 96, 66(1954).
30. R. A. Hegstrom, Phys. Rev. A 7, 451(1972).
31. G. Breit, Nature, 122, 649(1928).
32. H. Margenau, Phys. Rev. 57, 383(1940).
33. L. I. Schiff, "Quantum Mechanics" (McGraw Hill, New York, 1955).
34. P. A. M. Dirac, "The Principles of Quantum Mechanics" (Oxford University Press, 1958).

35. D. R. Hartree, "The Calculation of Atomic Structure" (Wiley, New York, 1957).
36. J. C. Slater, "Quantum Theory of Atomic Structure" (McGraw Hill, New York, 1960, Vol. II).
37. E. U. Condon and G. K. Shortley "The Theory of Atomic Spectra" (Cambridge Univ. Press, Cambridge, 1964).
38. S. Eckart, Phys. Rev. 36, 878(1930).
39. E. A. Hylleraas and B. Undheim, Z. Physik, 65, 759(1930).
40. C. L. Pekeris, Phys. Rev. 112, 1649(1958), 115, 1216(1959), 126, 1470(1962).
41. B. N. Taylor, W. H. Parker, and D. N. Langenberg, Rev. Mod. Phys. 41, 375(1969).
42. H. Grotch and R. A. Hegstrom, Phys. Rev. A 4, 59(1971).
43. N. F. Ramsey, "Molecular Beams" (Oxford Univ. Press, London, 1956).
44. A. R. Edmonds, "Angular Momentum in Quantum Mechanics". (Princeton, U. P., Princeton, N. J. 1957) and D. M. Brink and G. R. Satchler, "Angular Momentum", (Clarendon Press, London, 1971).
45. B. R. Judd, "Operator Techniques in Atomic Spectroscopy", (McGraw Hill, New York, 1963).
46. E. Condon and O. Sinanoglu "New Directions in Atomic Physics", Vol. II: Experiment. Articles; 5 and 6 on pages 78 and 75 respectively.
47. P. Kusch and V. W. Hughes "Handbuch Der Physik", Vol. XXXVII/Article: "Atomic and Molecular Beams Spectroscopy".
48. W. J. Childs, "Case Studies in Atomic Physics" Vol. 3, Nr. 4, April 1973, Article: "Hyperfine and Zeeman Studies of Metastable States by Atomic-Beam Magnetic-Resonance". (North-Holland Publishing Company, Amsterdam, 1973).

49. R. S. Van Dyck, Jr., C. E. Johnson, and H. A. Shugart, Phys. Rev. Letters, 25, 1403(1970), Phys. Rev. A 4, 1327(1971).
50. G. W. F. Drake, A. A. Victor and A. Delgarno, Phys. Rev. 180, 25(1969).
51. G. W. F. Drake, Phys. Rev. A 3, 908(1971).
52. G. Breit and E. Teller, Astrophysics J. 91, 215(1940).
53. H. W. Moos and J. R. Woodworth, Phys. Rev. Letters, 30, 775(1973).
54. Melvin P. Klein and Donald E. Phelps, The Review of Scientific Instrument, Vol. 38, No. 10, 1967, page 1545.
55. E. R. Andrew, "Nuclear Magnetic Resonance" (Cambridge University Press, London, 1956).
56. A. Abragam "The Principles of Nuclear Magnetism", (Oxford Clarendon Press, 1961).
57. W. A. Anderson, The Review of Scientific Instruments, Vol. 32, No. 3, March 1961, page 241.
58. Bernard D. Zak and H. A. Shugart, Phys. Rev. A 6, 1715(1972).
59. Pucel, Massé, and Hartwig, IEEE Transactions on Microwave Theory and Techniques, Vol. MTT16, No. 6, June 1968, page 342.
60. M. V. Schneider, The Bell System Technical Journal, May-June, 1421(1969).
61. D. D. McCracken "A Guide To Fortran IV Programming" (Second Edition John Wiley and Sons, Inc., New York, 1972).
62. P. R. Bevington, "Data Reduction and Error Analysis for the Physical Sciences" (McGraw-Hill, New York, 1969).
63. H. D. Young, "Statistical Treatment of Experimental Data", (McGraw-Hill, New York, 1962).
64. S. Penselin, T. Moran, V. W. Cohen, and G. Winkler, Phys. Rev. 127, 524(1962).

65. Cs^{133} $\Delta\nu$ is the present frequency standard for other $\Delta\nu$ measurements.
66. V. S. Shirley, Table of Nuclear Moments, in "Hyperfine Structure and Nuclear Radiation" (North Holland Publishing Co., Amsterdam, 1968, Appendix C, page 985).

LEGAL NOTICE

This report was prepared as an account of work sponsored by the United States Government. Neither the United States nor the United States Atomic Energy Commission, nor any of their employees, nor any of their contractors, subcontractors, or their employees, makes any warranty, express or implied, or assumes any legal liability or responsibility for the accuracy, completeness or usefulness of any information, apparatus, product or process disclosed, or represents that its use would not infringe privately owned rights.

TECHNICAL INFORMATION DIVISION
LAWRENCE BERKELEY LABORATORY
UNIVERSITY OF CALIFORNIA
BERKELEY, CALIFORNIA 94720